Evaluation of an eddy resolving HYCOM simulation in the South Atlantic Ocean

Isabelle Sindiswa Giddy

Supervisors: Bjorn Backeberg, Isabelle Ansorge, Chris Reason and Edmo Campos

University of Cape Town

Faculty of Science

Department of Oceanography

This thesis is dedicated to my dog, Wizard, who teaches one about nature.

Contents

List of Figures

List of Tables

Preface

A $1/12^{\circ}$ resolution ocean model simulation of the South Atlantic Ocean has the potential for a great number of studies, across a wide range of topics. Because it was a large dataset, with which one could go down many avenues, I was set up for a challenge.

During my research, I presented my thesis work at two conferences, one international and one local. The level and range of ocean science being researched was impressive. At both of these events I met people that have influenced my thoughts on my career and on the work that I have presented here. It was also an absolute pleasure to meet some of the scientists whose papers I often read.

This study has, in my judgement, superficially evaluated a HYCOM model's success in representing the mean flow and hydrography in the South Atlantic. A few discrepencies between the model and observations are identified. Some of these are explained, in other cases an attempt is made to explain and yet others that could not be explained. In the process of my doing the research, the complexity of the Agulhas system became clear to me. The focus of my research on the Agulhas System came about for two reasons. First, it is arguably the most complex system in the South Atlantic and the least understood. This sparked my interest. It is also in close proximity to my home and in this abstract way feels more applicable to my life. Secondly, the region was chosen as it had the potential for me to develop an interesting skill set, in the analysis of eddies. Initially, I attempted to analyse all eddies in the South Atlantic, but when this study became too overwhelming and dispersed, I shifted my focus to the Agulhas system alone. Chapter 5 in the thesis is the result of this focus. In this way, I admit to approaching my thesis in a different order to the normal: hypothesis - experiment - results - conclusions, and rather: many explorations - results - hypothesis

- conclusions. I have learnt the difficulties associated with this approach, mainly that it becomes very challenging to focus one's study and draw out a question associated with a possible answer.

In undertaking this study, I have acquired a number of skills. I am now able to use Python, Matlab, Ferret and CDO fluently for data organisation, analysis and in the creation of scientific figures. I have dealt with the processing of a large range of observational datasets (e.g. Argo data, AVISO data, cruise data) as well as the processing of the model output. These skills are essential for modern day oceanographic research. Beyond the data analysis stage I have improved my presentation skills and scientific writing and thinking skills. Over all, I feel that it has been a great excercise in the process of scientific inquiry.

While doing my thesis I was based at the department of Oceanography at the University of Cape Town as well as having the opportunity to study as a visiting student for eight months at the University of São Paulo, where the model that I used was being run. This experience was challenging for a young scientist and for future planning a number of points may be noted. The most difficult aspect of my stay at the university was that I felt quite alone, partly because of the language barriers and partly because my visit was not explicitly planned and I was based in a quiet office, which did not lend itself to much interaction with other students or professors. I struggled to remain focused on answering a question using my model data and my ideas dispersed quite often. As a visiting student I completed a Portuguese course, an ocean modelling short course and participated in an atmosphere-ocean gaseous exchange course. The oceanography courses were difficult for me as they were given in Portuguese. Needless to say, my Portuguese improved quickly and it was a nice opportunity to meet other students. Being based at the university I was able to partake in other activities as well, such as the oceanography choir and capoeria. These were different and enjoyable experiences.

Finally, I would like to thank all my supervisors, especially Bjorn Backeberg who put the project together and has given me a lot of guidance. Thanks also goes to Edmo Campos who hosted my at his laboratory in São Paulo. Furthermore, I am very grateful for the funding received from SAMOC-SA, the Nansen-Tutu centre and the India-Africa-Brazil Fund.

Abstract

The South Atlantic Ocean acts as a key region of ocean teleconnections and water mass transformation, directly transporting waters from the Southern, Pacific and Indian Oceans towards the North Atlantic and feeding the upper branch of the Atlantic Meridional Overturning Circulation. To date, this region remains undersampled over long time periods. Models form useful platforms for the wholistic study of such regions where long term datasets are not available. However, it is important to first gauge to what extent the model deviates from available observations. In a detailed analysis, this study evaluates an eddy resolving $1/12^{\circ}$ HYbrid Coordinate Ocean Model simulation in the South Atlantic and Agulhas regions with reference to available observations and literature. The outcomes of this research contribute to improving the configurations of future ocean models by identifying the limitations of the model analysed. In addition, analysis of the 50 year (1960-2009) simulation reveals that, in this model simulation, mesoscale activity and sea surface temperature trends in the Cape Basin are not related to Agulhas Current transport changes. These findings highlights the need for long term observational databases and further research into climate related trends and interannual variability of the ocean, in particular around Southern Africa.

1 Introduction

1.1 The Meridional Overturning Circulation

The Meridional Overturning Circulaiton (MOC, Figure 1.1) is an ocean circulation pattern involving a large-scale exchange of water masses horizontally across oceans and vertically with depth (Wunsch, 2002). This global circulation scheme has been developed over the last two decades (Gordon, 1986; Broecker, 1991; Rintoul, 1991; Lozier, 2010). The horizontal mass exchange is driven by wind stress (force per unit area exerted by the wind on the ocean) in the upper ocean (surface-1500m) while the vertical movement of water is forced by a Meridional Overturning Circulation (MOC). The MOC is the result of a subduction of water masses at high latitudes (e.g. Nordic Seas, see Figure 1.1), where a sudden drop in temperature, coupled with high salinity concentrations results in an increase in the density of the water, which then sinks. This consequent downward flux of mass and subsequent lateral flow at depth is driven by heat/freshwater exchanges with the atmosphere as well as mixing within the ocean which alter the characteristics of the water masses supplying the deep water formation sites.

The predominant sites of deep water formation are along the Antarctic continental shelf in the Weddell and Ross seas and in the subpolar North Atlantic. These circulation patterns influence the global movement of water properties such as heat, salt, oxygen and carbon. The whole circulation system is important in the global climate system as it couples the global ocean to the atmosphere, creating a global circulation network of mass and heat transport (Schmitz, 1995; Lumpkin and Speer, 2007; Cunningham and Marsh, 2010). The MOC is also recognised as having an important role in

climate change (Clark et al., 2002), where the potential for the MOC to slow down in response to increased greenhouse gases has been demonstrated in model simulations.

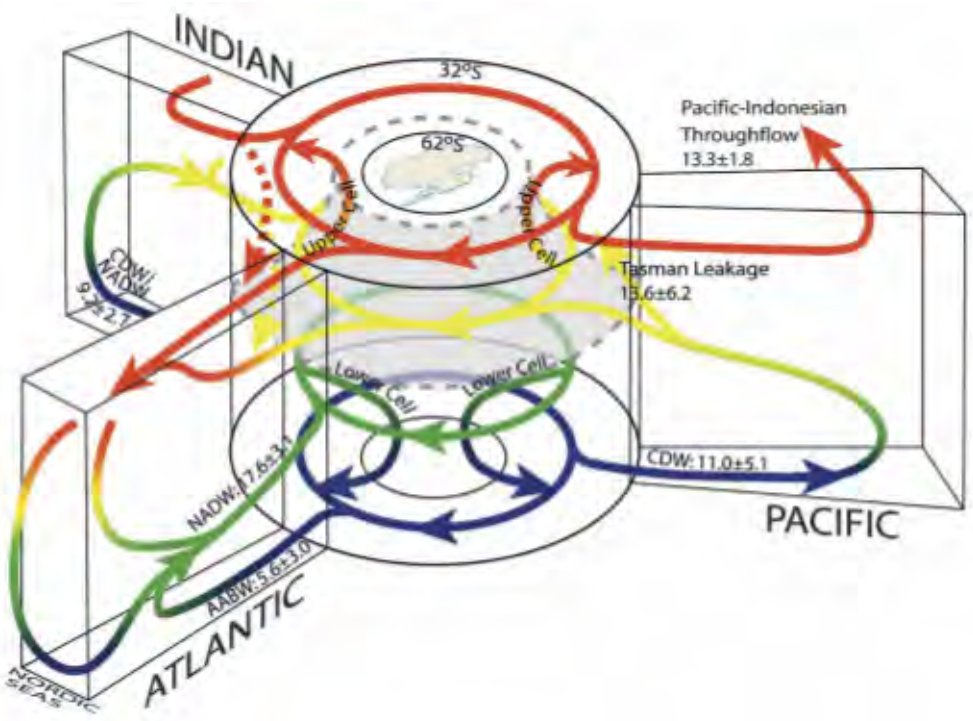

Figure 1.1: Schematic of the Global Overturning circulation. Color indicates approximate density ranges. Red: upper, $\gamma < 27.0$; yellow: intermediate, $\gamma \approx 27.0 - 27.6$; green: deep, $\gamma \approx 27.6 - 28.15$; blue: bottom, $\gamma > 28.15$. Gray surface with dashed edges is $\gamma \approx 27.6$ at 32°S, separating upper and lower cell transformation in the Southern Ocean. Dashed arrows indicate Indian-to-Atlantic westward exchange between Africa and the ACC. Shallow subtropical cells not included. Figure taken from Lumpkin and Speer (2007).

Circulation in the upper ocean of the Atlantic Ocean is forced by an interplay between winds and buoyancy forcing. Wind driven upper ocean gyre circulation is set up by the opposing directions of the trade winds and the westerlies, bordered on the east by Europe and Africa and on the west by the Americas (Munk, 1950).

As the South Atlantic sub-tropical gyre circulates, there is an ocean basin exchange of heat and salt with the atmosphere. The result of this is that the Brazil Current transports warm and salty water towards the South Pole and the northward branch of the South Atlantic Current, along with the Benguela Current, transports cooler and fresher water. Variations in the strength and position of the trades and westerlies created by atmospheric variability cause variations in the circulation patterns. In the North Atlantic the main mode of atmospheric variability is the North Atlantic Oscillation (Hurrell et al., 2003) while in the South Atlantic the main modes of atmospheric variability are known as the Southern Annular Mode (Marshall, 2003) and the El Niño-Southern Oscillation (ENSO; Philander,

1985).

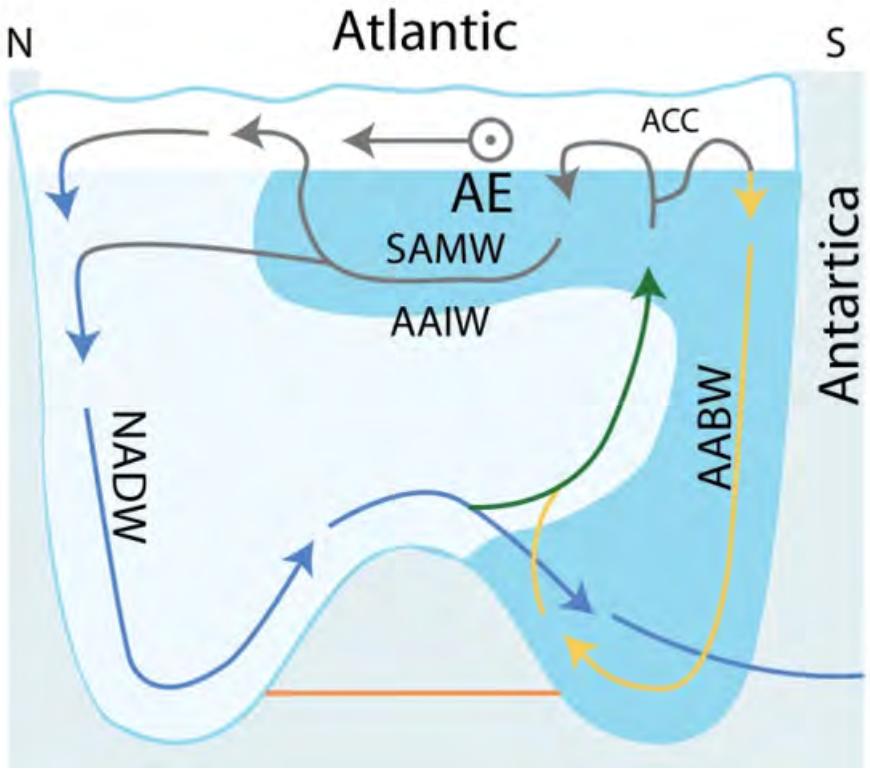

Figure 1.2: Idealised diagram of the Atlantic Meridional Overturning Circulation (MOC) taken from Sigman et al. (2010). Subantarctic Mode Water (SAMW), Antarctic Intermediate Water (AAIW) and Agulhas Eddies (AE; *also Agulhas Leakage*) move northwards in the surface (above 1500m). In the north this water sinks and forms North Atlantic Deep Water (NADW). ACC: Antarctic Circumpolar Current; AABW: Antarctic Bottom Water.

While wind forcing affects the gyre circulation in the Atlantic, the net upper ocean transport in both the South and North Atlantic Oceans is northwards. The counterintuitive net northward heat transport by the South Atlantic results because of the MOC. Deep waters form the lower arm of the MOC. Deep water formation occurs along the Antarctic continental shelf and in the Actic and subpolar North Atlantic. Bottom and deep water of the Arctic exits the northern passages and mixes with North Atlantic waters, contributing to North Atlantic Deep Water (NADW). The formation of North Atlantic Deep Water is a key, but not exclusive, driver in the Atlantic Meridional Overturning Circulation (AMOC), which itself is part of the MOC. NADW forms when warm, salty surface waters from the Gulf Stream reach the North Atlantic (see Figure 1.1 and 1.2), where the waters cool as a result of stong heat fluxes and freshen through fresh-water fluxes. When evaporation or ice formation takes place in the north, only fresh water is removed, leaving salt in the ocean and increasing the local surface salinity, and therefore the local surface water density. This dense, cold water sinks to depths of between 1000-4000m and becomes NADW. Once formed, NADW flows southwards across the north and south Atlantic to the Southern Ocean afterwhich it is transported to the Indian and

Pacific Oceans via the Antarctic Circumpolar Current (ACC). This southward flow is not only forced by the formation of NADW and the driving mechanism of this flow is still to be understood as more observational data is collected, (Rintoul et al., 2010).

In order to compensate for this southward flow of water at depth (Figure 1.2), warm, saline thermocline and surface waters are drawn to the northern North Atlantic, fuelling new NADW formation and resulting in a net northward transport in the Atlantic. The resultant surface and thermocline water circulation in the South Atlantic, driven by the need to compensate for NADW formation and the overall large negative bouyancy flux of the North Atlantic being much greater than that of the Southern Ocean, gives the South Atlantic its unique role in the climate system - in that it has a net northward heat flux, transporting heat northwards and across the equator (e.g., Macdonald and Wunsch, 1996).

1.2 The South Atlantic Ocean

The circulation in the South Atlantic is well described by Stramma and England (1999). A schematic of the surface circulation in the South Atlantic Ocean can be seen in Figure 1.3. The subtropical gyre of the South Atlantic is bounded in the north by the tropical Atlantic and in the south by the northern limit of the Antarctic Circumpolar Current. The anticyclonic subtropical gyre is driven by wind stress curl associated with the midlatitude westerly winds and tradewinds.

The gyre is formed by the northward flowing Benguela Current on the east, the westward flowing South Equatorial Current, the southward flowing western boundary current, the Brazil Current, and the eastward flowing South Atlantic Current. When the South Equatorial Current reaches the South American continent, two currents are formed: the Brazil Current flowing southwards and northwards flowing current which becomes the North Brazil Current. Water is transferred from the South Atlantic to the North Atlantic mainly through the North Brazil Current (Lumpkin and Speer, 2003). The regions linking the Pacific to the South Atlantic and the Indian Ocean to the South Atlantic are highly energetic (Chelton et al., 2011) and consist of the Malvinas Current and associated Brazil/Malvinas Confluence and Agulhas Leakage.

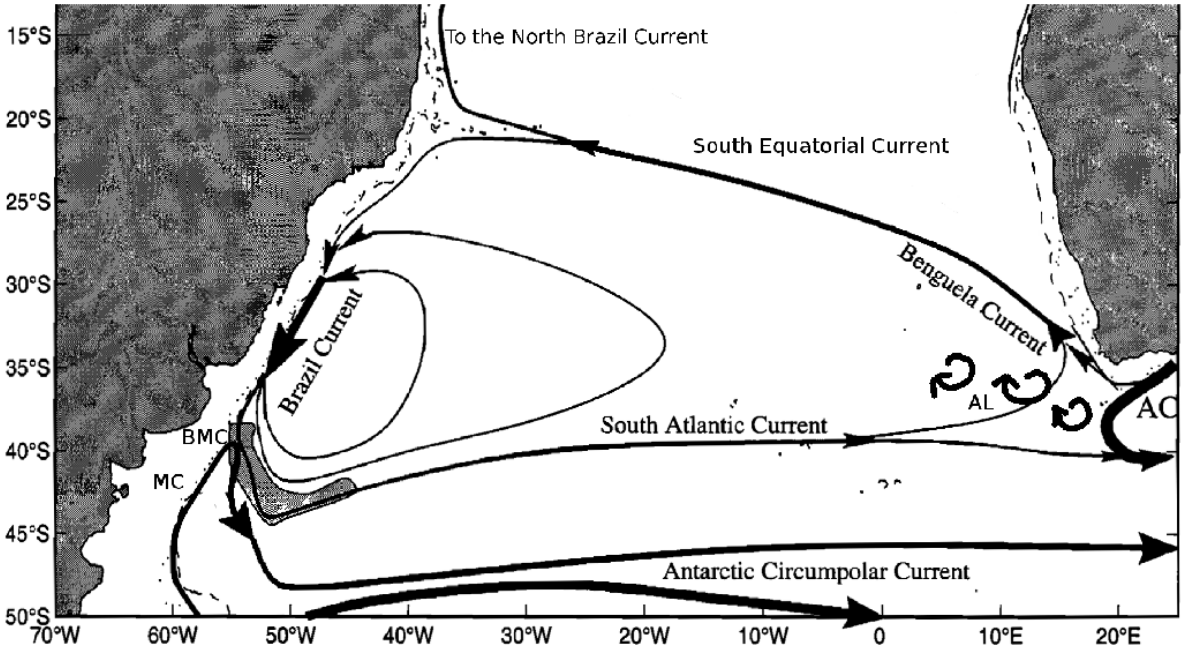

Figure 1.3: Simplified surface circulation in the South Atlantic (Adapted from Stramma and England (1999)). AC: Agulhas Current; AL: Agulhas Leakage; MC: Malvinas Current; BMC: Brazil/Malvinas Confluence.

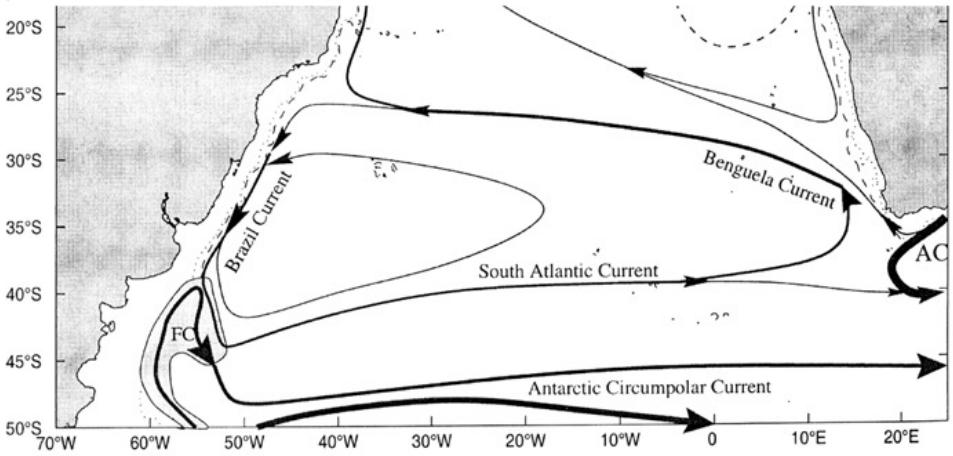

Figure 1.4: Diagram of intermediate water circulation in the South Atlantic. Taken from Stramma and England (1999)

Intermediate water circulation is illustrated in Figure 1.4. The circulation at intemediate depths is situated further south than at the surface, with the northern limb of the subtropical gyre reaching the South American continent south of 20°S. It is also notable that water from the Indian Ocean enters the intermediate water layer south of Africa, while in the deep waters no Indian ocean to South Atlantic leakage exists (Gordon et al., 1992).

The circulation in the South Atlantic at depth is illustrated in Figure 1.5. North Atlantic Deep Water (NADW) flows mainly along the South American continent, but also crosses the South Atlantic and

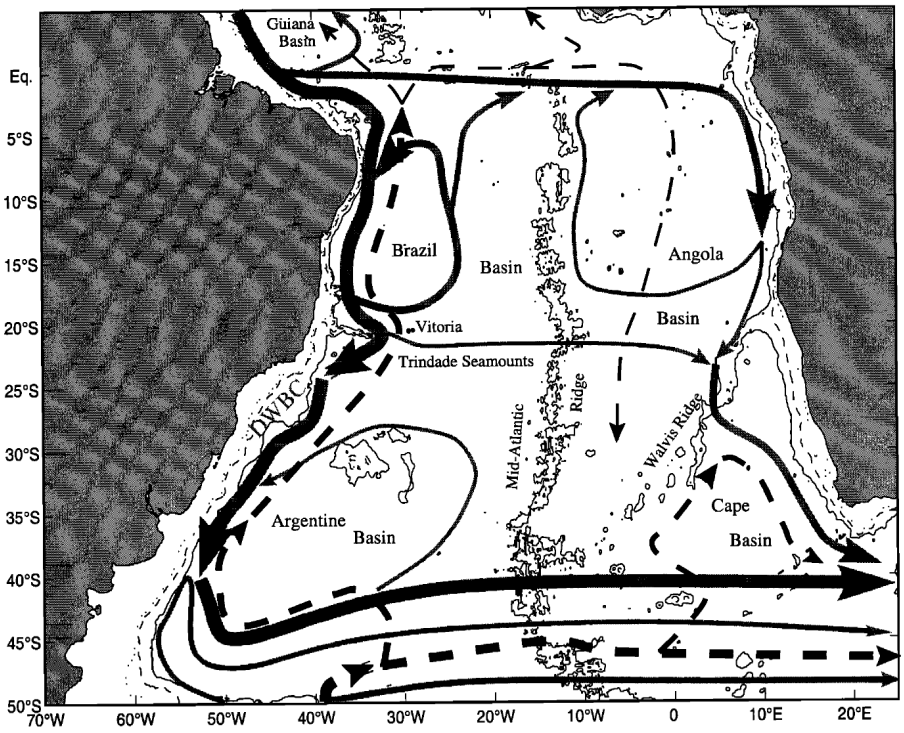

Figure 1.5: Deep water circulation in the South Atlantic, taken from Stramma and England (1999)

moves south along the eastern boundary of the South Atlantic basin, as can be seen by the black arrows in Figure 1.5. Dense Antarctic Bottom Water flows out of the Weddel Sea and enters the Atlantic via the southeastern side of the Argentine Basin and flows to the western boundary in the deep Argentine Basin. The spreading of this water is strongly influenced by bottom topography. Most of the AABW flows north, eventually crossing the equator along the western boundary of the basin. At the equator, AABW also spread eastwards to fill the Angola Basin from the North. The Cape Basin receives AABW from the south. This AABW then returns south into the Agulhas Region due to the presence of the Walvis Ridge which impedes its movement (e.g., Saunders and King, 1995).

1.3 The importance of the South Atlantic Ocean in global circulation

The South Atlantic Ocean plays a key role in establishing oceanic teleconnections between ocean basins whereby oceanic properties can be exchanged, mixed and redistributed (Garzoli and Matano, 2011; *see* Figure 1.3). Its unique role as the only large ocean transporting warm water from the

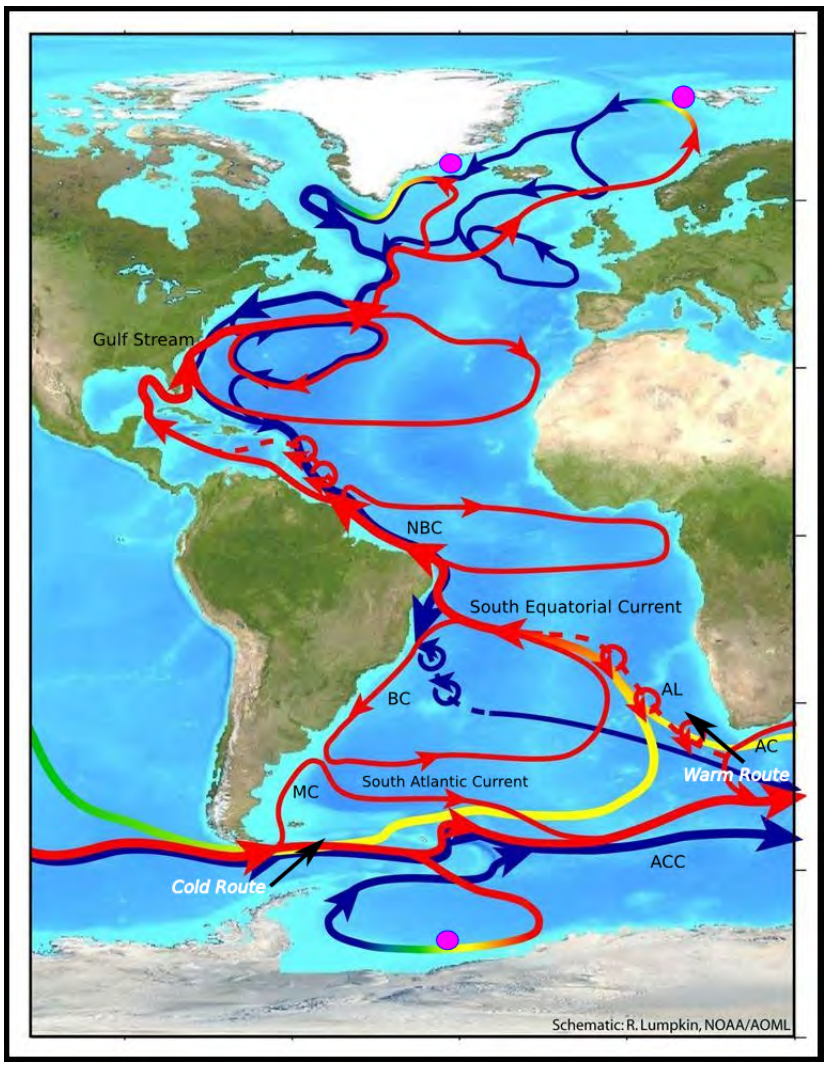

Figure 1.6: Schematic of the Atlantic Meridional Overturning Circulation. The surface currents (red) in the South Atlantic are labelled. MC: Malvinas Current; BC: Brazil Current; NBC: North Brazil Current; AC: Agulhas Current; AL: Agulhas Leakage; ACC: Antarctic Circumpolar Current. The pathways of the warm and cold water routes into the South Atlantic are identified. Deep currents are drawn in blue. Sites of deep water formation are identified by purple circles. Image adapted from Lumpkin (2007).

poles towards the equator (e.g. Gordon, 1986; Talley, 2003) is a result of the need to compensate for water that is subducted in the subpolar North Atlantic to form North Atlantic Deep Water (NADW).

In the upper 1500m of the South Atlantic gyre, water originating from the Pacific, Indian and Southern Oceans is transported along the upper arm of the global thermohaline circulation, northwards, by means of two paths, referred to as the cold-water route and the warm-water route (Speich et al. (2001); refer to Figure 1.3). The cold water route is defined as the inflow of Pacific and Southern Ocean water into the South Atlantic via the Drake Passage (Friocourt et al., 2005). The warm water route is the flow into the South Atlantic from south of Africa, transporting water masses from the Pacific via the Indonesian Throughflow (Speich et al., 2001; Friocourt et al., 2005; Sprintall et al., 2009) and Tasman leakage (Speich et al., 2002); from the Southern Ocean, indirectly from

the Drake Passage (Speich et al., 2001; Friocourt et al., 2005); and via recirculation within the Indian-Atlantic section of the Southern Hemisphere supergyre (Speich et al., 2007; Ridgway and Dunn, 2007). It is in this region that the Agulhas Current System lies (Lutjeharms, 2006) which is the primary conduit for the Indo-Atlantic inter-ocean exchange (Gordon, 1986; Gordon et al., 1992).

1.4 Variability in the South Atlantic Ocean

Modes of variability are are oceanic or climatic patterns with identifiable characteristics, usually identified through Sea Surface Temperature anomalies or Sea Level Pressure anomlies once the seasonal cycle has been removed. They are region dependent and often oscillatory. The main modes of variability in the South Atlantic are the Southern Annular Mode (SAM; Marshall, 2003), the El Niño-Southern Oscillation (ENSO; Philander, 1985) and the South Atlantic Subtropical Dipole (Hermes and Reason, 2005).

The Southern Annular Mode is the dominant mode of atmospheric variability in the high latitudes of the Southern Hemisphere. It has been found to contribute significantly to climate variability in the Southern Hemisphere on both high and low frequency timescales. This large-scale oscillation in atmospheric masses, between the polar cap region poleward of 60°S and the midlatitudes (centred near 45°S) is essentially a zonally symmetric structure, with synchronous anomalies of opposite signs in Antarctica and the midlatitudes. The SAM is said to be in its positive phase when there is an increase in geopotential height over the midlatitudes, a decrease in geopotential height at high latitudes and a strengthening and poleward shift of the storm track over the Southern Ocean (Thompson and Wallace, 2000). The positive phase is associated with an increase in the strength and poleward shift in the midlatitude westerlies and a decrease in strength of the polar easterlies. The SAM has been observed to be increasingly in its positive phase since the 1950s (Marshall, 2003), with the Southern Ocean experiencing a stronger atmospheric circumpolar flow and a weaker westerly flow in the midlatitudes (Thompson et al., 2000).

ENSO is a phenomenon that is inherently due to the coupling of the atmosphere and the ocean. During the El Niño phase, large scale warming of the Pacific Ocean is associated with a relaxation of the trade winds, shoaling of the thermocline and a displacement of the atmospheric convection

into the central Pacific from the East (Philander, 1985). Atmospheric Rossby and Kelvin wave propagation from the tropical Pacific forms an atmospheric bridge, connecting the Pacific ENSO to the Atlantic and Indian oceans (Alexander et al., 2002). These ENSO-driven large scale circulation changes alter the near-surface air temperature, humidity, and wind, as well as the distribution of clouds far from the equatorial Pacific. The resulting variations in the surface heat, momentum, and freshwater fluxes can induce changes in sea surface temperature, salinity, mixed layer depth and ocean currents.

There is also rubust evidence that ENSO has impacts of SST variability in the South Atlantic with numerous studies correlating modes of Sea Surface Temperature-Sea Level Pressure variability to ENSO (e.g., the third SVD mode isolated by Venegas et al. (1997), the second SVD mode isolated by Sterl and Hazeleger (2003)).

The most dominant mode of interannual variability in the South Atlantic has been identified as the South Atlantic Subtropical Dipole (SASD; Hermes and Reason, 2005; Morioka et al., 2012). The SASD is a northeast-southwest oriented SST dipole, forced by shifts in the anticyclone high pressure system. A positive (or, alternatively, negative) event is defined when there is a significant warm (or cool) SST anomaly evident in the southwest of the South Atlantic and a cool (or warm) anomaly in the eastern subtropics.

A further influence on the South Atlantic is that of the input of warm and salty water which enters the South Atlantic through Agulhas Leakage, forming the upper thermohaline connection between the Indian and Atlantic Oceans (Weijer et al., 1999). This process will be discussed in the following section.

1.5 The Agulhas Current System

The Agulhas Current System (*see* Figure 1.7) lies between two major wind belts, the southeast trades, between the Equator and about 30°S, and the Southern Hemisphere westerlies, over 35° – 65°S. The Agulhas Current is the strong western boundary current that makes up a major part of this system, and carries heat and salt to the poles. It is fed by recirculating subtropical gyre waters, waters from the Red and Arabian seas, from the Indonesian Throughflow and from the equatorial

Indian ocean via Mozambique channel eddies and the East Madagascar Current (Beal et al., 2006). The Agulhas Current has a mean transport of 70Sv at 32°S (Bryden et al., 2005). There has been some indications that the current has a peak in geostrophic velocity, derived from altimetry, during austral summers (Krug and Tournadre, 2012), but its variability on longer timescales remains largely unknown.

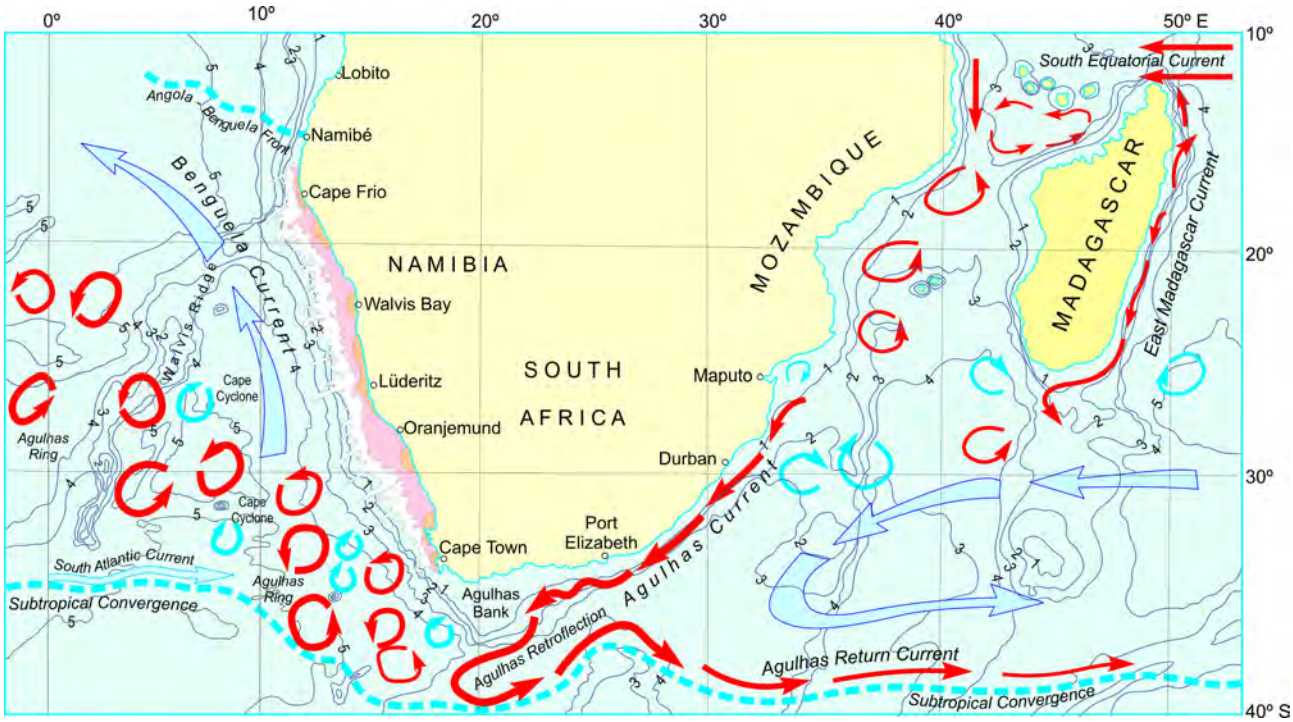

Figure 1.7: Schematic portrayal of the flow in the Agulhas System, taken from Ansorge and Lutjeharms (2007).

The Agulhas Current is fed by waters from the Indian and Southern Oceans. The properties of the water masses found in the Agulhas Current are sumarised in Table 1.1, below. The surface and thermocline layers are composed of Tropical Surface Waters (TSW) and Subtropical Surface Waters (STSW). The light, low salinity TSW is formed in the central Indian Ocean basin, near the equator (Beal et al., 2006) and enters the Agulhas via the Mozambique Channel (de Ruijter et al., 2002). Below TSW lies STSW at the salinity maximum (>35.55). STSW enters the Agulhas via the East Madagascar Current (Gründlingh et al., 1991). South Indian Central Water sits between a neutral density of $\gamma = 26.4$ and the base of the thermocline at ~9°C and $\gamma = 27.0$. Below the thermocline, at intermediate depths is fresh Antarctic Intermediate Water (AAIW) and relatively saline Red Sea Water (RSW). RSW forms in the Red Sea Basin, where it sinks as a result of excess evaporation. RSW enters the Agulhas Current most directly via the Mozambique channel (Beal et al., 2000). AAIW forms a salinity minimum < 34.7. It originates in the southeastern Pacific to the west 55°S,

80°W (Saekno et al., 2003). AAIW reaches the Indian ocean by way of the Drake passage and enters the South Indian Ocean gyre at about 60°E (Fine, 1993). The bottom waters of the Agulhas Current consists of North Atlantic Deep Water (NADW), which flows northwards within the Agulhas Undercurrent (Beal and Bryden, 1997).

Water Mass	Temperature [^{o}C]	Salinity	Neutral density [kg.m^{-3}]	Depth [m]
TSW	24.7-26.3	34.9-35.3	25.5-26.5	0-200
STSW	8.0-25.0	>35.5	25.8	200-500
SICW	7-15	34.6-35.8	26.6-26.8	300-500
RSW	7.0-23.0	34.8-40	27.3-27.7	500-1500
AAIW	2-10	33.8-34.6	27.2-27.4	800-1200
NADW	<2.0	34.8	28.0-28.1	>2500

Table 1.1: Characteristics of the major water masses found in the Agulhas Current. Values are composed of the studies from Beal et al. (2006); You (1997); Donohue and Toole (2003). TSW: TSW: Sub-tropical Surface Water; SICW: South Indian Central Water; RSW: Red Sea Water; AAIW: Antarctic Intermediate Water; NADW: North Atlantic Deep Water.

The Agulhas Current is unique in that it abruptly retroflects on itself, returning approximately 75% of its water back to the Indian Ocean (Lutjeharms and Van Ballegooyen, 1988). The rest of the water enters the South Atlantic through the Cape Basin in the form of Agulhas rings (Gordon, 1986), filaments (Lutjeharms and Cooper, 1996), smaller cyclonic and anticyclonic eddies (Schouten et al., 2000; Boebel et al., 2003), direct leakage of predominantly intermediate waters (de Ruijter et al., 1999) and as a coastal jet at the shelf edge (Bang and Andrews, 1974; Gordon et al., 1995). This inter-basin flux is termed Agulhas Leakage. Estimates of Agulhas Leakage are uncertain, ranging between 2 and 15Sv (Gordon et al., 1992; Garzoli et al., 1996; de Ruijter et al., 1999; Richardson, 2007). Similarly, there have been no direct observations taken of Agulhas Leakage on long timescales. The warm and salty water that enters the South Atlantic is advected northwards over 2-4 decades (Weijer et al., 2002; van Sebille et al., 2011; Rühs et al., 2013), influencing the formation of deep water at the poles, contributing to the buoyancy balance of the AMOC and, therefore, the regulation of global climate (Beal et al., 2011).

It is the phenonmenon of the Agulhas Retroflection that results in Agulhas Leakage. The Agulhas Retroflection can be defined by the point where the southwestward flowing Agulhas Current turns back on itself and returns towards the Indian Ocean as the Agulhas Return Current. Primarily, it is the interaction of the latitude of maximum westerlies and the southward inertia of the Agulhas Current when it separates from the African continent that results in the Agulhas Current partially

turning back on itself, "leaking" warm and salty water into the South Atlantic in the process. A number of theoretical and numerical modelling studies suggest five factors that influence the retroflection: inertia and planetary vorticity (the β-effect), vortex stretching, coastline geometry, bottom topography, and the wind field structure over the higher latitudes of the Indian Ocean. These are explained in detail in the review paper by de Ruijter et al. (1999).

The resultant transfer of warm and salty water from the Indian ocean to the Atlantic ocean is known as Agulhas Leakage (de Ruijter et al., 1999; Pichevin et al., 1999; Dijkstra and de Ruijter, 2001). Anticyclonic and cyclonic eddies, rings and filaments in the Cape Basin are thought to be actively implicated in the Indian-Atlantic interocean exchange (Gordon, 2003; Richardson et al., 2003), which form at the turbulent retroflection region (Boebel et al., 2003). Agulhas rings, produced at an average rate of 5 $\pm$ 1 year^{-1} (Gordon et al., 1992; de Ruijter et al., 1999; Schouten et al., 2002), are warm core, anticyclonic eddies with diameters of 200-400km and exceeding depths of 2000m. Agulhas rings are known to decay rapidly in the Cape Basin (Schouten et al., 2000; Schmid et al., 2003; van Sebille et al., 2010). In particular, they lose their anomalous surface heat content quickly to the atmosphere (van Aken et al., 2013), while the remaining salt anomaly persists for longer, increasing the salinity of the South Atlantic (Biastoch et al., 2008a; Biastoch and Böning, 2013).

1.6 The importance of the Agulhas Current System in the South Atlantic Ocean

In our current changing climate, an increasing trend in Agulhas Leakage (Rouault et al., 2009; Biastoch et al., 2009) may result in an overall salinification of the South Atlantic (Biastoch and Böning, 2013). Furthermore, this buoyancy forcing associated with warm and saline Agulhas Leakage waters that enter the South Atlantic may act to strengthen the Atlantic Meridional Overturning Circulation (MOC) by enhancing the Atlantic meridional pressure gradient, increasing the salinity of waters reaching the North Atlantic and priming the water for deep water formation (Weijer et al., 2002; Biastoch et al., 2008a). This process could play a role in stabilising the Atlantic MOC (Zahn, 2009) at a time when anthropogenic warming and accelerated Greenland ice-sheet melting is predicted to weaken it (Gregory, 2005; Stammer, 2008; Hu et al., 2009). This theory is strengthened

when taking into account that paleorecords show that the Atlantic MOC has previously responded to changes in the warm-water route of the MOC. Paleooceanographic studies suggest that increased input of relatively warm, saline Agulhas Current waters in the South Atlantic are associated with late Pleistocene deglaciations (e.g. Peeters et al., 2004; Martínez-Méndez et al., 2010). Using an ocean circulation model, Knorr and Lohmann (2003) showed that the gradual warming of the Southern Ocean during a deglaciation period induced a resumption of the interglacial mode of the thermohaline circulation, triggered by increased mass transport via the warm and cold water routes. In the other direction, Bard and Rickaby (2009) have also shown that a decrease in Agulhas Leakage due to the northward migration of the subtropical front, may have caused climate to cool beyond typical ice age temperatures.

1.7 Variability in the Agulhas Current System

Observations have shown that the westerly winds in the Southern Hemisphere have strengthened and shifted polewards, alongside an intensification of the trade winds in the last 50 years (Thompson and Solomon, 2002; Gillett and Thompson, 2003; Toggweiler, 2009; Backeberg et al., 2012; Swart and Fyfe, 2012). The strengthening and poleward migration of the southern hemisphere weterlies has intensified the supergyre linking the South Indian, South Atlantic and South Pacific oceans (Cai, 2006). Recently, it was shown that the eddy kinetic energy and propagation velocities of the surface signature of eddies in the Retroflection Region of the Agulhas System have also intensified in association with the intensification of the Indian Ocean trade winds (Figure 1.8; Backeberg et al., 2012).

Through model hindcasts and observations derived from altimetry, there is general consensus that the Agulhas Leakage is increasing (Biastoch et al., 2008a; van Sebille et al., 2009; Biastoch et al., 2009; Rouault et al., 2009; Le Bars et al., 2014). A recent paper explained how this increase in Agulhas Leakage is linked to the anthropogenically forced climate change seen in the wind systems (Biastoch and Böning, 2013). However, as mentioned previously, there are no direct observations of Agulhas Current transport and Agulhas Leakage on long timescales. The longest timescale available is that derived from altimetry by Le Bars et al. (2014). Although they did not succeed is computing the absolute Agulhas Leakage, they were able to infer an increasing trend over the last two decades.

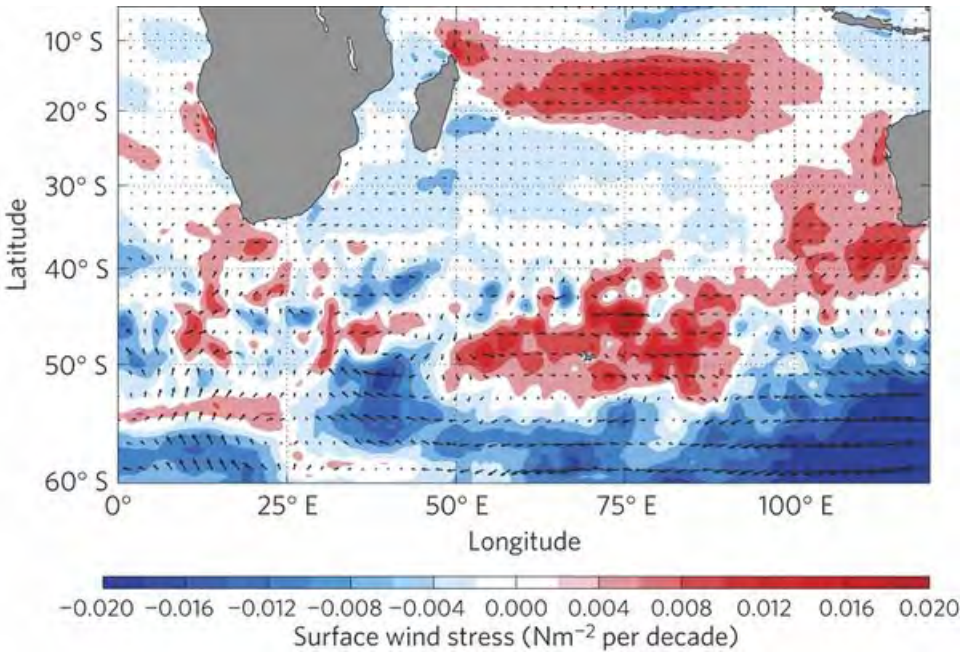

Figure 1.8: Decadal trend of surface wind stress magnitude from 1993-2009 (CFSR data; Saha et al. (2010)) over the subtropical Indian Ocean, (Backeberg et al., 2012). Vectors represent direction and magnitude of the change.

All other studies on the trends in Agulhas Current transport and Agulhas Leakage have been based on model simulations. The forcing mechanisms behind the trends seen in Agulhas Leakage have been under debate.

Rouault et al. (2009) and van Sebille et al. (2009) found that the increase in Agulhas Leakage is linked with the upstream strength of the Agulhas Current associated with changes in the wind stress curl in the Indian Ocean; however they disagreed on the effects that the changes in the wind system may have on Agulhas Leakage. Van Sebille et al. (2009) argued that a decrease in the Agulhas Current strength leads to an increase in leakage. Rouault et al. (2009) argued that the increase in Agulhas Leakage was caused by an increase in the strength of the Agulhas Current (a result from an increase in easterly winds over the subtropical Indian Ocean). Rouault et al. (2009) found that this change is portrayed in the Sea Surface Temperature (SST) signal at the retroflection region, which also increased.

Loveday et al. (2014) continue the discussion in a model study on the relationship between the Agulhas Current and Agulhas Leakage, finding that leakage is not sensitive to changes in Agulhas Current transport at 32°S, contradicting both the theories put forward by Rouault et al. (2009) and van Sebille et al. (2009). Other authors - de Ruijter et al. (1999), Biastoch et al. (2009) and Bard and Rickaby (2009) - propose that the variability of the leakage is associated especially with

the position of the maximum Southern Hemisphere westerly winds; where a southward (northward) shift in the westerlies induces increased (decreased) leakage. However, Durgadoo et al. (2013), in a numerical experiment, demonstrated that a northward shift in the westerly wind belt acts to increase Agulhas Leakage by strengthening the wind stress curl between the latitudes 35°-45°S and reducing it over the core of the Antarctic Circumpolar Current. Moreover, Durgadoo et al. (2013) show a strong Agulhas Leakage response controlled by the strength of the Southern Hemisphere westerlies and argue that the current increase in Agulhas Leakage is related to the increase in strength of the westerlies. However, at very strong westerly winds, the turbulent choking regime (Le Bars et al., 2012) comes into play. This occurs at very strong winds, where the increased volume transport of Agulhas Leakage is lost due to an enhanced interaction between the Agulhas Return Current and the Antarctic Circumpolar Current.

That there is still much uncertainty in the forcing mechanisms and trends in the Agulhas Region emphasises the need for more observational platforms to be put in place. While there is progress being made in increasing in situ observations, with the Argo project (http://www.argo.ucsd.edu, http://argo.jcommops.org), SAMOC (Garzoli et al., 2010; Speich et al., 2010; Meinen et al., 2013; Ansorge et al., 2014), the Agulhas Current Time-Series (ACT) experiment (http://act.rsmas.miami.edu) and the GoodHope Line (Ansorge et al., 2005), these data sets are still not available at sufficient timescales for long term variability analysis. For this purpose, a model simulation is needed.

1.8 Aim of this thesis

The Agulhas system impacts on the South Atlantic and further downstream through Agulhas Leakage. It is highly complex with multiple factors acting to force variability and trends. The lack of long term observations has obliged studies of trends and processes in the Agulhas system to rely on model simulations as seen in the previous discussion where most of the studies mentioned above have all been based or partly based on model simulations. However, many models struggle to reproduce this region with sufficient accuracy (Barnier et al., 2006; Penven et al., 2011). The contradictory results of Rouault et al. (2009) compared to van Sebille et al. (2009) highlight the lack of understanding of this key region.

This thesis aims to analyse the representation of firstly the South Atlantic gyre and secondly the Agulhas Region in 1/12° configuration of the Hybrid Coordinate Ocean Model (HYCOM; Bleck, 2002).

Two key questions are addressed:

1. ***How well does this HYCOM model represent the South Atlantic Ocean?***

2. ***How well does this HYCOM model represent the Agulhas System?***

2.1 How accurate is the model, ATlb0.08, in representing the Agulhas region in comparison with available observations?

2.1 How do the trends produced by the model in the Agulhas region compare with the available literature?

Section 2 describes the model configuration and forcing, Section 3 describes the data and methodology used in the analysis, in Section 4 the model in the full South Atlantic domain is analysed and compared to observations and climatologies. In Section 5 the model representation of the Greater Agulhas System is assessed and the long term trends are compared with trends seen in observations and other model simulations.

2 Model Description

2.1 Overview

Ocean models are an ideal platform that can be used to study ocean processes in time and space where in situ data is insufficient or where one wants to exclude, simplify or simulate ocean circulation in order to further our understanding of the dynamics associated with regions in the ocean.

One of the main challenges of realistically replicating the complicated dynamics of the ocean lies in the need to account for varying processes that occur in different locations of the ocean which are dominated by varying physical, chemical and biological processes. The HYbrid Coordinate Ocean Model (HYCOM; Bleck, 2002) is a primitive equation ocean general circulation model. HYCOM is based on the Miami Isopycnic-Coordinate Ocean Model (MICOM; Bleck and Smith, 1990) and takes advantage of the best features of isopycnic-coordinate and fixed-grid ocean circulation models within one framework (Bleck, 2002). HYCOM interchanges between three coordinate systems according to the environment. In the open ocean, HYCOM implements isopycnal coordinates, retaining water mass characteristics over time. In the surface mixed layer, HYCOM implements z-level coordinates in order to maximise the representation of thermodynamical and biochemical processes, maintaining sufficient vertical resolution in unstratified, weakly-stratified or convectively unstable regions of the ocean. On the ocean bottom and in coastal regions, HYCOM implements terrain-following coordinates, maintaining high vertical resolution in these regions.

In situ hydrographic observations in the South Atlantic and Agulhas Region, while improving with the Argo project (http://www.argo.ucsd.edu, http://argo.jcommops.org), SAMOC (Garzoli et al.,

2010; Speich et al., 2010; Meinen et al., 2013; Ansorge et al., 2014), the Agulhas Current Time-Series (ACT) experiment (http://act.rsmas.miami.edu) and the GoodHope Line (Ansorge et al., 2005), are still not available at sufficient timescales for long term variability analysis. A HYCOM model is chosen for analysis as the isopycnic-coordinate biased configuration is appropriate for long term studies (Bleck, 2002). In Section 2.2 the general features of HYCOM simulations are described. In Section 2.3 the 1/12° resolution simulation of the Atlantic domain (ATIb0.08) that is used as the basis of this thesis is described. In Section 2.4 the atmospheric forcing and time integration of the model is discussed.

2.2 HYCOM

HYCOM was initially described by Bleck (2002). In the following section the vertical coordinate system, governing equations and mixing processes implemented in HYCOM are summarised.
For more detailed information one can refer to the HYCOM documentation
(https://hycom.org/hycom/documentation).

2.2.1 The vertical coordinate system

The vertical movement of water masses in ocean models is simulated in two forms: Lagrangian and Eulerian motion. Isopycnic models are based on Lagrangian motion. They allow the coordinate surface to move with the respective water masses in the vertical, giving isopycnic layers the ability to retain water mass characteristics over long time periods. Z-level and sigma-coordinate models are based on the Eulerian approach. They utilise a fixed vertical coordinate system, where water is allowed to pass through a coordinate surface, thereby better resolving processes in regions of instability and in shallower waters.

HYCOM smoothly interchanges the vertical coordinates between isopycnic, in the stratified open ocean, to z-level coordinates in the weakly stratified upper-ocean mixed layer, and to terrain-following coordinates in shallow water coastal regions. This system of vertical coordinates can be visualised in Figure 2.1 below.

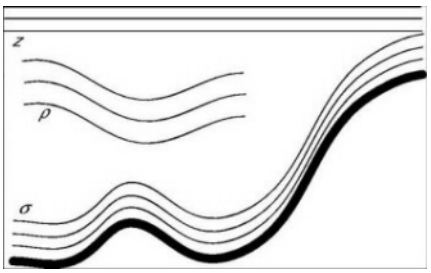

Figure 2.1: The vertical coordinate scheme implemented in HYCOM simulations. Z-coordinates in unstratified and shallow waters, isopycnic coordinates in the open ocean and terrain following sigma coordinates along the bathymetry.

2.2.2 Governing Equations

HYCOM contains five prognostic equations, two for the horizontal velocity components, a mass continuity or layer thickness tendency equation, and two conservation equations for a pair of thermodynamic variables such as salinity and temperature or salinity and density. Complementing the five prognostic equations are several diagnostic equations, including the hydrostatic equation, an equation of state linking potential temperature, salinity and pressure (Brydon et al., 1999) and an equation describing the vertical mass flux, $\dot{s}dp/ds$, through an s surface.

Below is the equation of continuity, which best describes the primary dynamics of the HYCOM model:

$$\frac{d}{dt_s}\left(\frac{dp}{ds}\right) + \nabla_s \bullet \left(V\frac{dp}{ds}\right) + \frac{d}{ds}\left(\dot{s}\frac{dp}{ds}\right) = 0 \tag{2.2.1}$$

Where $V = (u, v)$ is the horizontal velocity vector; p is the pressure and s the vertical coordinate.

The equation of the vertical mass flux, determines the spacing and movement of layer interfaces, and the algorithm built on this equation is referred to as the "grid generator" (Bleck, 2002), which forms the fundamentals of hybrid coordinate modelling.

Effectively, the "grid generator" allows coordinate layers to maintain a finite thickness, by becoming non-isopycnic, wherever lack of stratification would cause isopycnic layers to collapse to zero thickness. The result is that isopycnic grid points, which would otherwise be deactivated in a pure isopycnal model, are put to use in improving vertical resolution. While the "grid generator" acts to maintain this minimum layer thickness in the upper part of the water column, by changing coordinate systems it also attempts to restore the grid to isopycnic coordinates wherever possible.

2.2.3 Mixing Processes

When HYCOM is run with isopycnic vertical coordinates, horizontal advection/diffusion is performed in the same manner as in MICOM. Temperature and salinity are advected and diffused in layer 1. Only salinity is advected and diffused in deeper layers, with temperature diagnosed from the equation of state to maintain constant density in these layers. When HYCOM is run with hybrid vertical coordinates, temperature and/or salinity are advected and diffused within the layers that have been declared as hybrid layers.

Vertical mixing is simulated through a combination of cabbeling, restoration processes and explicitly prescribed physical mixing. HYCOM allows for a number of vertical mixing schemes to be employed. The vertical mixing scheme employed in the HYCOM run for this study is the K-Profile Parameterization (KPP; Large et al., 1997). KPP mixes the entire water column by matching the surface boundary layer mixing parameterization to that of the ocean interior, and takes into account mixing processes that result from wind and mixed layer turbulence. Additional mixing parameterizations for internal wave breaking, vertical current shear, salt fingering and double diffusion processes are defined, and a background vertical mixing coefficient ensures diapycnal diffusion in the deep ocean.

2.3 The ATIb0.08 Configuration

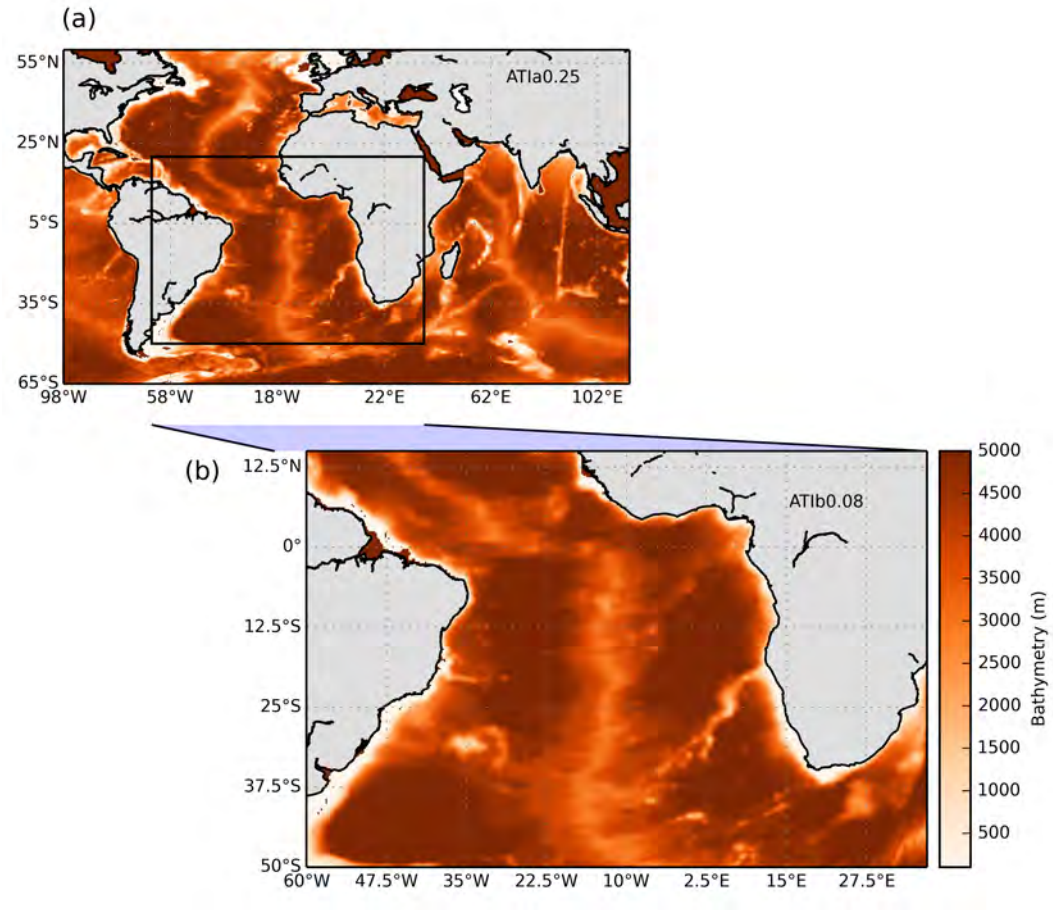

Figure 2.2: Diagram of the model domain of ATIb0.08, nested within the model domain of ATIa0.25. Bathymetry is shown in orange.

To simulate the upper (>2000m) circulation in the Atlantic Ocean, the Laboratory of Numerical Modelling at the Oceanographic Institute of the University of São Paulo (LABMON), ran a 1/12°, high resolution HYCOM simulation (ATIb0.08), which is one-way nested within the semi-global coarser resolution 1/4° simulation (ATIa0.25). The densities in this model simulation are calculated according to a sigma-t algorithm in which only temperature and salinity and not pressure is taken into account, thus making the model appropriate for upper layer studies (upper 2000m) of the ocean. The domain of the simulation is shown in Figure 2.2. The parameterizations used for both the ATIa0.25 and ATIb0.08 simulations are summarised in Table 2.1, below.

Parameter		ATIa0.25	ATIb0.08
Horizontal Resolution	km	27.8	9.3
Number of grid points (ixjxk)	x10^6	13.09	28.102646
Integration time step	Baroclinic	270	720
Barotropic	9	24	
Max viscocity due to shear instability	$m^2.s^{-1}$	0.005	0.005
Max diffusivity due to shear instability	$m^2.s^{-1}$	0.005	0.005
Internal wave viscosity	$m.s^{-1}$	0.0001	0.0001
Internal wave diffusivity	$m^2.s^{-1}$	0.00001	0.00001
Salt fingering diffusivity factor	$m^2.s^{-1}$	0.001	0.001
Diffusion velocity for Laplacian momentum dissipation	$m.s^{-1}$	0.03	0.03
deformation-dependent Laplacian viscosity		0.05	0.05
Diffusion velocity for biharmonic thickness diffusivity	$m.s^{-1}$	0.005	0.005
Diffusion velocity for Laplacian temp/saln	$m.s^{-1}$	0.005	0.005

Table 2.1: Parameterization values for the model simulation ATIa0.25 and ATIb0.08

The domain of ATIa0.25 spans across the Atlantic and Indian Oceans, 98°W-114°E, 65°S-60°N. The domain of the ATIb0.08 spans the South Atlantic Ocean, from 80°W-40°E; 50°S-20°N. ATIa0.25 and ATIb0.08 have eddy-permitting horizontal resolutions on a Mercator projection, 22 hybrid vertical layers, and use the K-profile parameterization (KPP) mixed layer formulation. On the western boundary, 148Sv (where 1Sv = 1x$10^6 m^3.s^{-1}$) volume inflow is fixed between 45° and 65°S and on the eastern boundary, 148Sv volume outflow is fixed in the region of south Australia. 148Sv transport is chosen as an approximate volume transport of water that flows across the Drake Passage (Renault et al., 2011). The Indonesian straits are closed with no Indonesian Throughflow. At the open lateral boundaries the temperature and salinity are relaxed to Levitus climatology, using a two-degree wide buffer zone and 120 days relaxation time. The northern and southern boundaries are closed (no barotropic inflow or outflow), with temperature and salinity relaxed to Levitus climatology. The Sea Surface Salinity (SSS) is weakly relaxed to climatology. No restoring towards observed Sea Surface Temperature (SST) is performed. The bathymetry is defined by non-smoothed ETOPO 5 (NOAA, 1986). The models are not coupled to an ice model. ATIb0.08 is one-way nested within ATIa0.25, with the variables relaxed to ATIa0.25. The relaxation on the boundaries uses a newtownian relaxation approach, with a 2-degree buffer zone on the inner model and relaxation times of 1-24 days.

2.4 Atmospheric forcing and integration strategy

The choice of atmospheric forcing is crucial for ocean modelling. Atmospheric forcing from the National Centres for Environmental Prediction/National Center for Atmospheric Research (NCEP/NCAR; http://www.esrl.noaa.gov/psd/) reanalysis monthly mean products were used to force the model simulations, which provides an adequate time and space resolution, although the data set has some known biases (Smith et al., 2001).

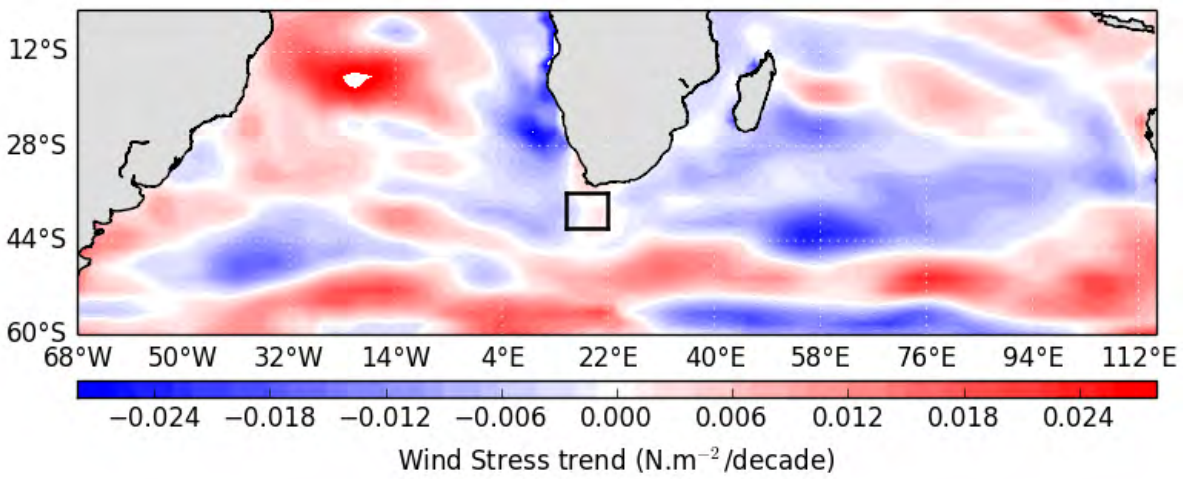

Figure 2.3: Decadal trend of surface wind stress magnitude from 1983-2009 (NCEP/NCAR monthly mean products) over the subtropical Indian and Atlantic Oceans.

The dataset provides monthly means of wind stress, long-wave radiation, short wave radiation, precipitation and humidty. The models compute evaporation and sensible heat from the precipitation and air temperature respectively.

Starting from rest, the simulation was span-up for 10 years, forced with inter-annually varying NCEP/NCAR monthly mean fields (1948-2010). The model was allowed to adjust to the introduced conditions for 12 years until 1960. ATIb0.08 is thus assessed from the period 1960-2009. Figure 2.3 shows the westerly wind stress, zonally averaged from 20°-118°E and meridionally averaged from

35°-50°S. A significant ($p<0.001$) increasing trend in westerly wind stress from 1983-2009 is shown. That there has been an intensification of trades and westerlies has been previously documented by Backeberg et al. (2012) using CSFR data for the period 1993-2009. The NCEP/NCAR wind product shows a similar pattern although not exactly the same, highlighting the differences that models could encounter due to different wind products.

2.5 Limitations

The outstanding limitations of the configuration are noted here, to be kept in mind during the rest of the analysis.

1. The model is closed to Indonesian throughflow: this excludes signals in the model output that might be transported through this region such as the ENSO (van Sebille et al., 2014), however the model will respond to atmospheric changes as a result of ENSO due to the monthly atmospheric forcing. A link between Agulhas Leakage and the Indonesian Throughflow has also been documented (Gordon, 1986; Gordon et al., 1992; Le Bars et al., 2013), which will not be resolved in the model. This link was also quantified in models in its fraction transmitted to the North Atlantic by Speich et al. (2001) and Speich et al. (2007).

2. Similarly, the model is not coupled with an ice-model and does not extend across the entire Southern Ocean. Thus signals transferred through the ocean as a result of SAM will not be entirely resolved in the model. However, the atmospheric changes will affect the model as the model is forced by atmospheric observations.

3. The model is relaxed to salinity. Because of the large uncertainties in estimated precipitation, evaporation and river runoff, most models restore salinity to climatological values. This results in the underestimation of salinity (Stammer et al., 1996). The restoration of model simulations to climatological salinity values has been found to constrain density driven circulation, affecting the temporal evolution of the Atlantic Meridional Overturning Circulation (Behrens et al., 2013).

4. The bathymetry used in the model is low resolution ETOPO5 bathymetry. This will have consequences to regions that are sensitive to or strongly affected by bathymetry.

5. The use of monthly wind products, rather than daily wind products, may have the effect of decreasing the variance resolved by the model, which may have consequences for meso-scale processes (Maltrud et al., 1998).

2.6 Summary

The setup and configuration of the $1/12^{\circ}$, high resolution HYCOM simulation (ATIb0.08), nested within the semi-global coarser resolution $1/4^{\circ}$ simulation (ATIa0.25) have been described. The primary advantage of HYCOM is that is it mainly isopycnic, preserving water properties over time and making the model ideal for long term studies. The limitations of the model configuration have been noted. In the Chapters that follow the $1/12^{\circ}$ resolution configuration will be assessed in comparison to available observational and climatological datasets in the South Atlantic Ocean. In Chapter 5, particular attention is paid to the Agulhas Region.

3 Data and Methodology

The model simulation ATIb0.08 was evaluated in the South Atlantic and Agulhas regions. This model simulation is being run in LABMON, Ocean Modelling Laboratory at the Oceanography Institute of the University of São Paulo (IOUSP). The aims of this study are to determine to what extent of accuracy the HYCOM configuration described in Chapter 2 represents the South Atlantic and what trends are evident in relation to the forcings of the model. This analysis contributes towards the understanding and modelling of the region.

In Chapter 4, the model is evaluated against a number of observational datasets, climatologies and published literature. In Chapter 5, a detailed analysis of the Agulhas Region is performed. The analysis uses observational datasets and an automatic eddy detection algorithm is implemented as a tool to analyse the eddies in the Cape Basin. The datasets used, and calculations and statistics performed in both Chapters 4 and 5 are described in this chapter.

3.1 Observational Datasets and Climatologies

In order to perform a thorough analysis of the model simulations accuracy in representing the South Atlantic and Agulhas regions, various observational data sets were used. The data sources used for various aspects of model-observation comparisons are summarised in Table 3.1. In the following sub-sections the datasets are described in detail.

Variable	Region	Dataset
Sea Surface Height	South Atlantic Agulhas	AVISO Ssalto/Duacs (http://www.aviso.oceanobs.com/duacs/)
Sea Surface Temperature	South Atlantic	WOA09 (http://www.nodc.noaa.gov/OC5/WOA09/woa09data.html) MOI SST OSTIA SST (www.myocean.eu)
Sea Surface Salinity	South Atlantic	WOA09 Aquarius CAP Level 3 product (http://podaac.jpl.nasa.gov/dataset/AQUARIUS_L3_SSS_SMID_7DAY_V3)
Temperature	South Atlantic	WOA09 CARS09-ARGO only product (http://www.marine.csiro.au/~dunn/cars2009/)
	Agulhas	Bonus GoodHope Cruise Argo floats (http://www.argo.ucsd.edu/) WOA09
Salinity	South Atlantic	WOA09 CARS09-ARGO only product
	Agulhas	Bonus GoodHope Cruise Argo floats (http://www.usgodae.org/cgi-bin/argo_select.pl) WOA09
Agulhas Transport	Agulhas	Moorings (Bryden et al.,2005)

Table 3.1: Observational datasets used in the model verification of the South Atlantic and of the Agulhas regions in ATIb0.08.

3.1.1 Satellite Altimetry Data

Sea Surface Height (SSH) observations are used in order to compare general geostrophic flow characteristics and variability in the South Atlantic and in comparisons of the eddy characteristics in the Agulhas Region in the HYCOM model using an automatic eddy detection algorithm.

The gridded satellite altimetry data used in this study are produced by Ssalto/Duacs and distributed by Archiving Validation and Interpretation of Satellite Oceanographic data (AVISO, http://www.aviso.oceanobs.com/duacs/). The absolute dynamic topography gridded product that was used for this study is derived from a combination of sea level anomaly observations based on two satellites (Jason-2/Envisat or Jason-1/Envisat or Topex/Poseidon/ERS) with the same groundtrack. The output from these satellites is merged with the corrected Rio09 mean dynamic topography (Rio et al., 2011).

Absolute Dynamic Topography represents the elevation of the ocean caused by water movements, calculated as the difference between the SSH measurements and a model of the Earths geoid (the slope of the ocean if only the Earth's rotation and gravity are considered), after removing the effects of tides and the inverted-barometer effect.

The product quality is homogenous with time and thus suitable for comparison over longer timescales. The data grid has a spatial resolution of ¼ x ¼ degrees, and a temporal resolution of 7 days.

3.1.2 Microwave Optimally Integrated Sea Surface Temperature

Microwave radiometers provide a valuable source of sea surface temperature measurements as they can take measurements regardless of cloud cover. The optimally interpolated SST product at ¼° resolution, monthly means from 2002-2009 was used as a SST comparison with HYCOM. The SST data includes data from the following satellite radiometers: TMI, AMSR-E, WindSAT, MODIS Terra and MODIS Aqua.

Monthly means of Global Ocean OSTIA Sea Surface Temperature and Sea Ice Reprocessed (1985-2007) at a ¼° resolution was used to compare long terms trends of SST in the Agulhas Region with the model. This product provides the foundation SST refered to as an L4 product, composed of *in situ* and satellite data from infra-red and microwave radiometers.

3.1.3 Aquarius Sea Surface Salinity

Salinity varies due to evaporation and precipitation over the ocean, as well as river runoff and ice melt. Along with temperature, it is a major factor in contributing to changes in density of seawater and therefore ocean circulation. It is therefore of importance to ensure a good representation of salinity distribution when using an ocean circulation model.

A version 2.0 Aquarius CAP Level 3 product (gridded product) is used to compare the Sea Surface Salinity (SSS) output of the HYCOM model. This product is based on the Combined Active Passive (CAP) algorithm. The CAP algorithm utilizes data form both the onboard radiometer and scatterometer to simultaneously retrieve salinity, wind speed and direction by minimizing the sum of

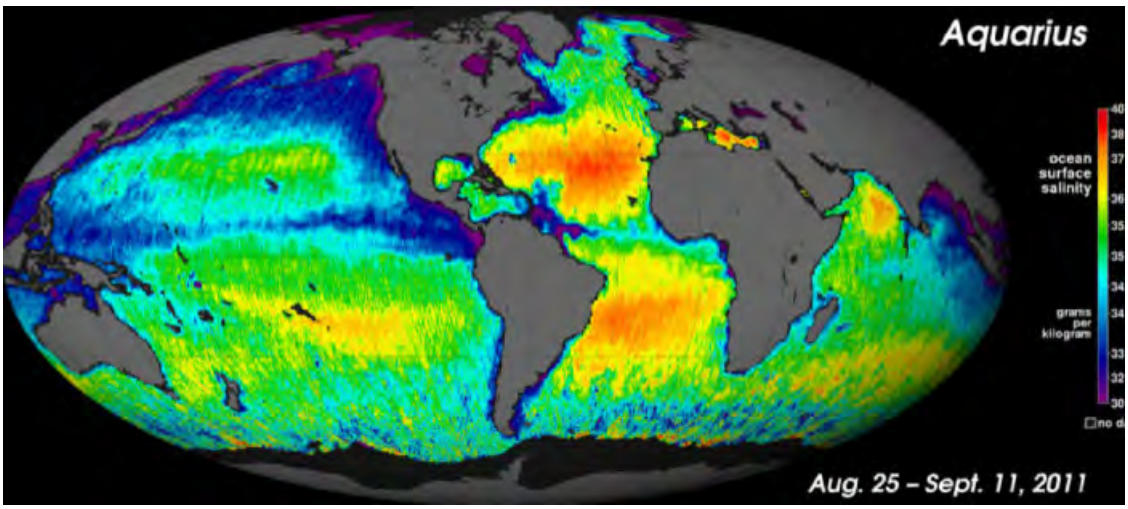

Figure 3.1: Time mean (25/08/2011-11/09/2011) Sea Surface Salinity derived from the satellite, Aquarius.

squared differences between model and observations. The satellite's global output can be visualised in Figure 3.1. In Aquarius output, SSS is measured in grams per kilogram. In the model output SSS is measured in PSU. In line with the new TEOS10 regulations, no SI units will be reported in this study when referring to salinity.

CAP Level 3 standard mapped image products derived from Aquarius Sea Surface Salinity satellite measurements (Lee et al., 2012) were used in this study in comparison with a HYCOM climatology of the sea surface salinity field in the South Atlantic. This product is a gridded (1 degree spatial resolution) salinity and wind speed data and was averaged over monthly timescales, from 24-August 2011 to 31-December 2012.

With the release of the Aquarius/SAC-D satellite, observations of SSS have been greatly augmented. Measurements of salinity are derived from surface microwave emissions which change as the conductivity of the ocean surface waters changes. In order to pick up these changes in microwave emissions (in the band of 1.4 GHz), the satellite needs to be technically sensitive to minute changes. The challenges of measuring SSS from space are augmented by significant errors which can be introduced by the sea surface temperature and roughness, the intervening atmosphere and ionosphere, and galactic signals reflected off the sea surface.

On board the Aquarius satellite is an instrument which consists of three radiometers in push broom alignment at incidence angles of 29, 38 and 46 degrees incidences angles relative to the shadow side of the orbit. Footprints for the beams are: 76km (along-track) x 94km (cross-track), 84km x 120km and 96km x 156km, yielding a total cross-track swath of 370km. The radiometers measure

brightness temperature at 1.413 GHz in their respective horizontal and vertical polarizations. A scatterometer operating at 1.26 GHz measures ocean backscatter in each footprint that is used for surface roughness corrections in the estimation of salinity.

3.1.4 World Ocean Atlas 2009

Temperature and salinity products from WOA09 were used in various comparisons in this study. The model field was initialised by Levitus World Ocean Atlas and thus comparisons with the model output are expected to be similar.

The temperature and salinity data used in the WOA09 dataset are extracted from a 1° latitude-longitude grid at standard depth levels from the surface to a maximum depth of 5500m. The data was processed by the National Oceanic and Atmospheric Administration (NOAA), and archived at the National Oceanographic Data Center (NODC), identically to the methods used in World Ocean Atlas 2005 (WOA05) series (Locarnini et al., 2006).

The temperature and salinity datasets are derived from historical oceanographic temperature and salinity profile data. These datasets are composed of bottle samples (Reversing thermometers), Mechanical Bathythermograph (MBT), ship-deployed Conductivity-Temperature-Depth (CTD) package, Digital Bathythermograph (DBT), Expendable Bathythermograph (XBT), profiling floats, moored and drifting buoys, gliders, and the undulating oceanographic recorder (UOR). Profiles used in this project were obtained from the NODC/WDC archives and include all data gathered as a result of the GODAR and WOD projects (Locarnini et al., 2010; Antonov et al., 2010).

For more details the World Ocean Atlas product documentation can be accessed at ftp://ftp.nodc.noaa.gov/pub/WOA09/DOC/woa09documentation.pdf.

3.1.5 CSIRO Atlas of Regional Seas

CARS09-Argo only product was used as an alternative observationally derived climatological comparative data set.

CARS09 is an atlas of seasonal ocean water properties. It comprises of gridded fields (½° resolution) with 79 levels to 5500m with the mean ocean properties over the period of modern ocean measurement, and average seasonal cycles for that period (Ridgway et al., 2002). It is derived from a quality controlled archive of all available historical subsurface ocean property measurements – research vessel instrument profiles and autonomous profiling buoys (Argo). The Argo data is updated every few months. Argo floats measure the temperature and salinity in the upper 2000m of the ocean and are not restricted to shipping routes. All available Argo data is used and the dataset is subjected to extra local screening before use. CARS is different to WOA09 as it employs extra stages of in-house quality control of input data, and uses an adaptive-length scale scheme to maximise resolution in data-rich regions and takes into account topographic barriers, resulting in an excellent definition of oceanic structures and accuracy of point values. It is also of a higher resolution and as such adds to the comparison with the model output. The temperature and salinity datasets used in this study is the CARS Argo-only version which were updated in January 2013. The dataset was restricted to Argo so as not to be repetitive in comparison with WOA09.

3.1.6 Argo floats

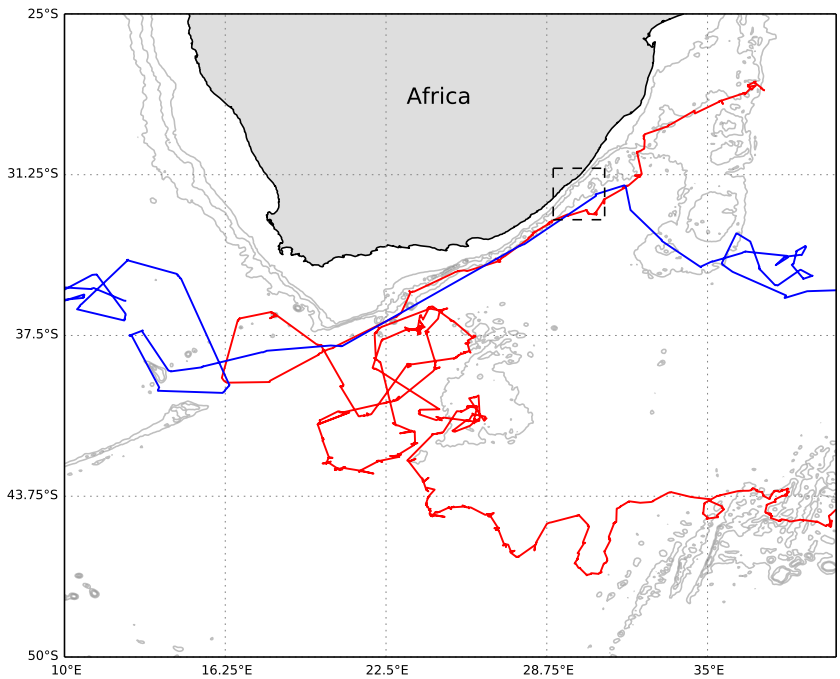

Figure 3.2: Trajectories of the Argo floats used in this study. The box (31°S-33°S, 29°E-31°E where profiles were meaned is outlined.

ARGO floats that passed through the region of 31°S-33°S, 29°E-31°E, over the time period 2000-

2005 were identified with the IDS D1900222 and D1900223 (*see* Figure 3.2). The outputs were averaged and used in a comparison with the model's representation of water properties with depth in the Agulhas Current. Argo is an international program which collects high quality temperature and salinity profiles from the upper 2000m of the ice-free global ocean. Argo floats are battery powered autonomous floats that spend most of their life drifting at a depth of 1000m where they have neutral buoyancy to the ambient water. The Argo data was collected and made freely available by the International Argo Program and the national programs that contribute to it (http://www.argo.ucsd.edu, http://argo.jcommops.org). The Argo Program is part of the Global Ocean Observing System.

3.1.7 Bonus GoodHope Cruise 2008

Temperature and Salinity transects along the GoodHope line (Figure 3.3; Swart et al., 2008) in HYCOM over February-March 2008 are compared with the Bonus GoodHope Cruise that was undertaken from 7 February – 18 March 2008 on the R/V Marion Defresne (Speich and Dehairs, 2008). The GoodHope line has been repeatedly sampled since 2004 (Ansorge et al., 2005) by high resolution XBT lines and CTDs. The transect lies in an important region of inter-ocean exchange (Beal et al., 2011).

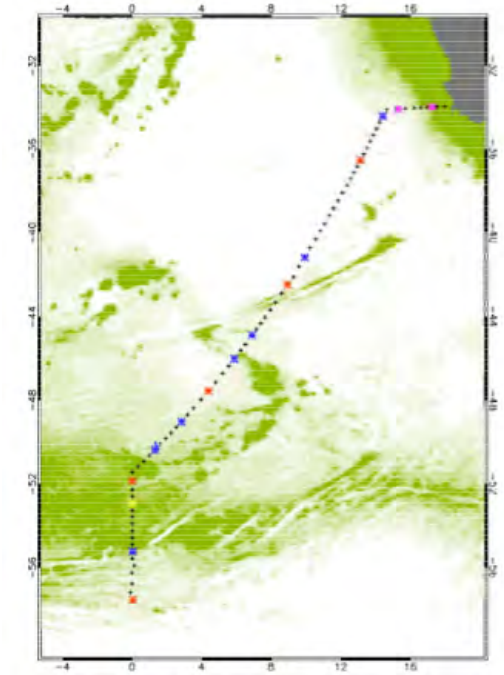

Figure 3.3: Map of the Bonus GoodHope cruise transect (Speich and Dehairs, 2008). Each cross indicates the position of a station. Bathymetry is shaded.

Full depth CTD data were acquired at 79 stations occupied in the region 33° 58'S – 57° 33'S, 17°

13'E – 0°E, from February 13, 2008 and March 17, 2008. Measurements were made at all stations from the surface to within 15 to 30 meters from the seafloor. The station spacing was varied from 7-8 nm on the continental slope, to 20 nm across frontal regions and strong topographic slopes, and, because of time delays and the tight ship-time, the spatial resolution was lowered to 30 nm in the deep abyssal planes and away from mesoscale structures and sharp topography. The stations were made with a SEABIRD 911+ probe mounted on a 24- bottle SEABIRD Rosette.

3.2 Methods

A number of computations were performed in the diagnostics of the HYCOM simulations representation of the South Atlantic and Agulhas Region. The methodology of these computations is described in the following sub-sections.

3.2.1 Geostrophic velocity

Geostrophic velocity was used to compare the circulation in the South Atlantic represented in the model to observations from satellite altimetry.

The balance between the coriolis force and the horizontal pressure gradient is known as the geostrophic balance. It is described by the following geostrophic equations which are derived from the equations of motion, assuming that the flow has no acceleration, the horizontal velocities are much larger than vertical and that the only external force is gravity, and that friction is small:

$$u = \frac{-1}{fp}\left(\frac{dp}{dy}\right) \tag{3.2.1}$$

$$v = \frac{1}{fp}\left(\frac{dp}{dx}\right) \tag{3.2.2}$$

where $f = 2\Omega sin\theta$, the coriolis parameter with $\Omega = 7.29x10^{-5}rad/s$, the rotation rate of the earth and θ, the latitude.

The horizontal pressure gradient relies on two terms, the slope of the sea surface and pressure gradients due to horizontal density differences. By applying the geostrophic approximation at z=0; which assumes that density is constant at the surface, the surface geostrophic currents can be

calculated from SSH using the following equations:

$$u = \frac{-g}{f}\left(\frac{d\zeta}{dy}\right) \tag{3.2.3}$$

$$v = \frac{g}{fp}\left(\frac{d\zeta}{dx}\right) \tag{3.2.4}$$

where f is the coriolis parameter; g is the gravitational force; ζ is the sea surface slope; y is the latitudinal distance and x is the longitudinal distance.

3.2.2 Eddy Kinetic Energy

Eddy kinetic energy is representative of the mesoscale activity in the ocean. Mesoscale processes are important in regions such as the Agulhas Region, where the mesoscale activity dominates over the mean flow. Surface Eddy Kinetic Energy (EKE) was calculated in the Agulhas Region from surface velocities in ATIb0.08.

EKE is defined by the following equation:

$$EKE = \frac{U'^2 + V'^2}{2} \tag{3.2.5}$$

where the velocity anomalies $U' = U - \bar{U}$ and $V' = V - \bar{V}$, with $\bar{U}$ and $\bar{V}$ being the mean annual zonal and meridional velocities respectively.

3.2.3 Agulhas Retroflection Position

The retroflection extent is explicitly derived through a sea-surface height (SSH) contour, tracked through the 4 daily fields in ATIb0.08 and 7 daily fields in AVISO (following Backeberg et al.,

2012). The method used is similar in theory to that of Dencausse et al. (2010b), however the exact determination of the retroflection point differs. The retroflection is identified as the point where the outermost SSH contour in the Agulhas Current turns back on itself and flows eastward. The contour value is determined from the mean SSH spanning 30°S-32.5°S, 28°E-32.5°E, capturing the upstream Agulhas Current where the flow is less turbulent and therefore a more realistic value can be determined. To capture the inshore current edge, the mean value is considered where 200m $<$ h $<$ 1500m. The westernmost value of this upstream contour value is taken as the maximum loop extent, i.e. the point where the Agulhas Current retroflects. Figure 3.4 shows a snapshot from HYCOM of the algorithm as it identifies the point of retroflection, shown by a blue marker. Retroflection positions are spatially binned into $1/2^{\circ}$ longitudinal boxes, producing a zonal proabability density function.

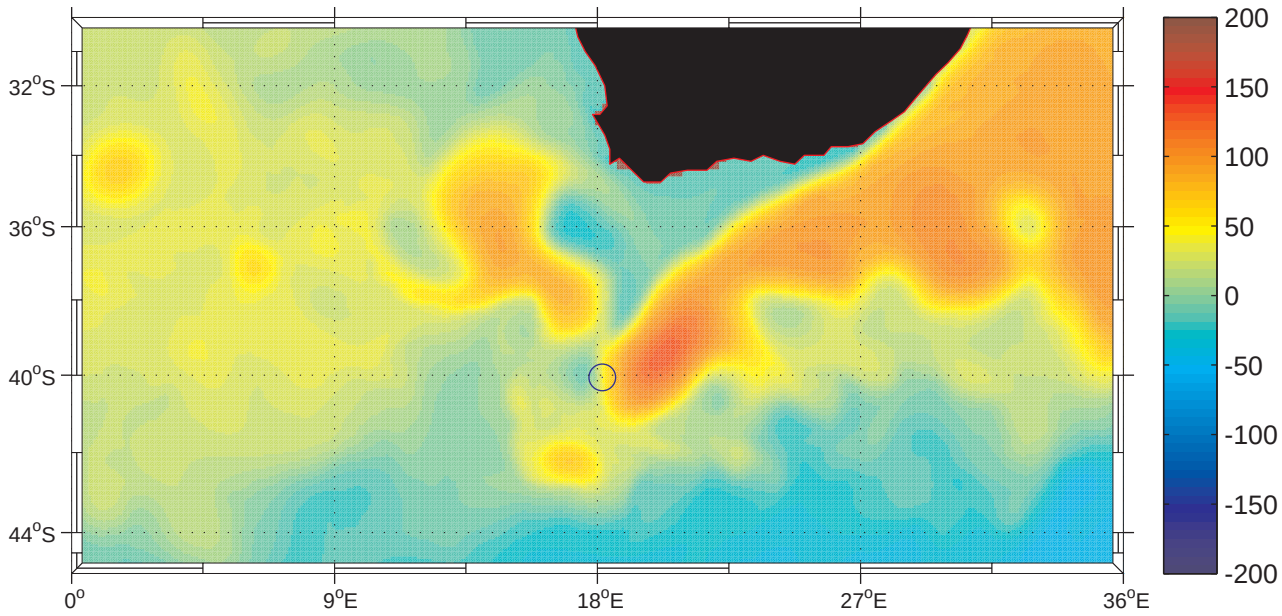

Figure 3.4: Snapshot of ATIb0.08 showing the identification of the retroflection position using contours of SSH. SSH is shaded. The point where the retroflection is identified is circled.

3.2.4 The automatic eddy detection algorithm

The advantage of using an automatic eddy detection algorithm is that it allows for a consistent and easy comparison of model output with altimetry observations.

There are various methods in which to automaticaly detect and track eddies, the most common being wavelet analysis (Siegel and Weiss, 1997; Doglioli et al., 2007; Dencausse et al., 2010a),

deformation (Okubo, 1970; Weiss, 1991), and geometry (Chelton et al., 2007, 2011). More recently Beron-Vera et al. (2013) suggested a new method based on geodesic transport theory (geodesic eddy detection). Each method has its advantages and an inter-comparison between the first three methods was recently executed by Souza et al. (2011b) who found the geometric method the most effective.

A hybrid automatic eddy detection and tracking algorithm, which defines vortices based on a mixture of geometric properties of the flow field (closed contours of SSH; Chelton et al., 2011), and dynamical properties of the flow (Okubo-Weiss criteria; Okubo, 1970; Weiss, 1991) was chosen for this study.

The algorithm was initially applied to the entire South Atlantic Basin as a validation method and then focused in on the Agulhas Region.

3.2.4.1 Eddy identification

Eddies were detected using the automatic eddy detection algorithm. Surface eddy velocities and relative vorticity was estimated from Sea Surface Height (SSH) through the geostrophic approximation, as follows:

$$u = \frac{-g}{f}\left(\frac{d\zeta}{dy}\right) \qquad v = \frac{g}{fp}\left(\frac{d\zeta}{dx}\right) \tag{3.2.6}$$

where f is the coriolis parameter; g is the gravitational force; ζ is the sea surface slope; y is the latitudinal distance and x is the longitudinal distance.

The relative vorticity ω can be calculated with the normal (s_n) and shear (s_s) components of strain:

$$\omega = \frac{dv}{dx} - \frac{du}{dy} \qquad s_n = \frac{du}{dx} - \frac{dv}{dy} \qquad s_s = \frac{dv}{dx} + \frac{du}{dy} \tag{3.2.7}$$

The Okubo-Weiss parameter aims to identify regions in a flow where the relative vorticity dominates over the strain tensors, defined as the center of the eddy. The parameter is computed from

geostrophic velocities and is defined as

$$W = s_n^2 + s_s^2 - \omega^2 \tag{3.2.8}$$

The eddy core is defined as a region of negative W (vorticity dominates over strain) surrounded by a region of positive W (strain dominates over vorticity). In this study, the threshold $W_0 = -2 \times 10^{-12} s^{-2}$ defines the contours of the eddy cores as used by Chelton et al. (2011). Two Hanning pass filters were then applied to the Okubo-Weiss parameter in order to overcome noise interference, which is primarily important in the altimetry data.

Firstly the Okubo-Weiss parameter is computed, secondly closed contours are detected. Eddies are then identified by the multiplication of the fields which satisfy the Okubo-Weiss parameter and the closed contours field. Effectively, this hybrid method defines a geostrophic eddy as the flow contained in a closed loop of SSH (as in the geometric method, Chelton et al., 2011), where the vorticity dominates the strain as in the Okubo-Weiss method (Okubo, 1970; Weiss, 1991). Following this, eddies were identified and selected, based on predefined criteria which is summarised in Table 3.2. The interval between SSH contours for closed loop detection was chosen as 2cm (the approximate accuracy of altimetry products) and the maximum size of a closed loop defined at 300km to avoid the selection of a gyre as an eddy.

Eddy Selection Criteria	
Minimum Radius	20km
Maximum Radius	300km
Minimum Amplitude	2cm
Minimum Lifetime	60 days
Maximum Speed	0.3m/s

Table 3.2: Eddy criteria used in the automatic eddy detection algorithm for eddy identification

In using this hybrid method, the detection of eddies is improved by reducing the sensitivity of the Okubo-Weiss algorithm which is highly sensitive to the threshold, W_0, and filtering process (Chelton et al., 2007). Chelton et al. (2007) have shown that while smaller values of W_0 result in a larger number of eddies tracked in regions of small SLA variance, it reduces the number of eddies tracked in regions of high SLA variance, such as the Cape Basin (Boebel et al., 2003). Combining the

Okubo-Weiss algorithm with the geometric method thus allows for a more accurate detection of coherent eddy cores. The filtering process reduces the number of false identifications caused by noisy structures but also reduces the capability of the method to keep track of the structures for a long period of time, which is then counter-balanced by mixing the Okubo-Weiss SSH fields with SSH fields of closed contours.

The algorithm has been found to be a suitable method for the investigation and comparison of eddies derived from both altimetry and ocean models and has been successfully implemented in a study on the Mozambique Channel eddies by Halo et al. (2013) and in the greater Agulhas system by Backeberg et al. (2012).

An example of all the anticyclonic and cyclonic eddies (with a lifetime greater than 8 weeks) detected by the algorithm (superimposed on the field of SSH values used to detect the eddies) on one timestep (27 February 2002) in ATIb0.08 is shown in Figure 3.5. Agulhas Rings are large, anticyclonic eddies (Lutjeharms, 1996).

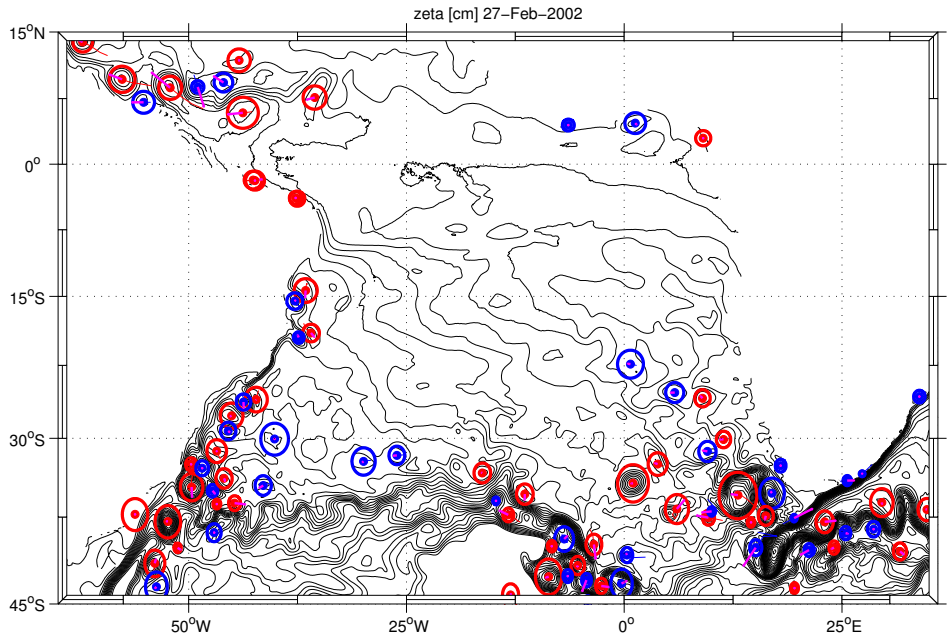

Figure 3.5: Snapshot (27 February 2002) of eddies detected in the South Atlantic by the eddy detection algorithm in ATIb0.08. Anticyclonic eddies in red, cyclonic eddies in blue. Lines show the track of the eddies in their lifetime. Contours of SSH are drawn and the bathymetry is shaded.

3.2.4.2 The eddy tracking algorithm

The eddy-tracking algorithm implemented in this study is that used by Penven et al. (2005). The algorithm considers an eddy, which minimises a generalized distance in parameter space, radius and

vorticity from one frame to the next frame, the same eddy.

The algorithm works as follows: an eddy (e_1) detected in a first frame is assumed to be the same eddy (e_2) in the subsequent frame if a generalised distance in a non-dimensional property space is minimum according to the following equation:

$$X_{e_1,e_2} = \sqrt{\left(\frac{\triangle X}{X_0}\right)^2 + \left(\frac{\triangle R}{R_0}\right)^2 + \left(\frac{\triangle \xi}{\xi_0}\right)^2} \tag{3.2.9}$$

where $\triangle X$ is the spatial distance between $e_1$and e_2; $\triangle R$ is the variation in diameter; $\triangle \xi$ is the variation in vorticity; X_0 is the characteristic length scale (50km); R_0 is the characteristic radius scale (100km, allowing for eddy splitting) and ξ_0 is the characteristic vorticity (1x10^{-5}s^{-1}). X_{e_1,e_2} is considered infinite if there is change in the sign in vorticity to ensure that no cyclone becomes an anticyclone, ensuring that the eddy polarity is preserved. All eddies are assigned a unique identifier, that the eddy retains throughout its lifetime. Where eddy splitting occurs, new identifiers are issued to each of the daughter eddies. Where no subsequent eddy is found the track is terminated.

3.3 Statistics

The differences between the model and observations were quantified in some cases by calculating the mean error:

$$bias = \bar{Y} - \bar{X} \tag{3.3.1}$$

where $\bar{Y}$ is the observational mean and $\bar{X}$ is the model mean.

Correlation coefficients of selected variables between HYCOM and observations were also computed

according to the following equation:

$$corr(y,x) = \frac{Y(t,y,x) - \bar{Y}(y,x)}{\sigma_Y(y,x)} \times \frac{X(t,y,x) - \bar{X}(y,x)}{\sigma_X(y,x)} \tag{3.3.2}$$

4 Model verification

A 1/12° resolution HYCOM simulation (ATIb0.08) in the South Atlantic is evaluated. The boundary conditions of the simulation are set by a 1/4° resolution HYCOM simulation (ATIa0.25) that spans the Atlantic and Indian oceans. Firstly, the Atlantic Meridional Overturning Circulation in ATIa0.25 and ATIb0.08 are evaluated. Secondly, the surface circulation and hydrology of ATIb0.08 are evaluated, followed by an evaluation of the vertical hydrography.

4.1 The Meridional Overturning Circulation (MOC)

The 1/4° configuration (ATIa0.25) forms the base model of the 1/12° configuration (ATIb0.08) that is analysed in detail in this study. It was therefore imperative to determine whether this base model was representative of the large scale circulation. The Meridional Overturning Circulation (MOC) is a large scale ocean ventilation process, whereby surface currents transport warm waters to the poles, and cold waters are transported by deep currents to the tropics. This circulation acts to regulate the climate (Wunsch, 2002; *see* Figure 4.1). The representation of the MOC in ATIa0.25 was computed.

The MOC is defined as the time-varying streamfunction in the vertical-meridional plane (Cunningham and Marsh, 2010).

$$\psi(y,z,t) = \int_{-z}^{0} \int_{x_{east(y,z)}}^{x_{west(y,z)}} v(x,y,z,t)dxdz \tag{4.1.1}$$

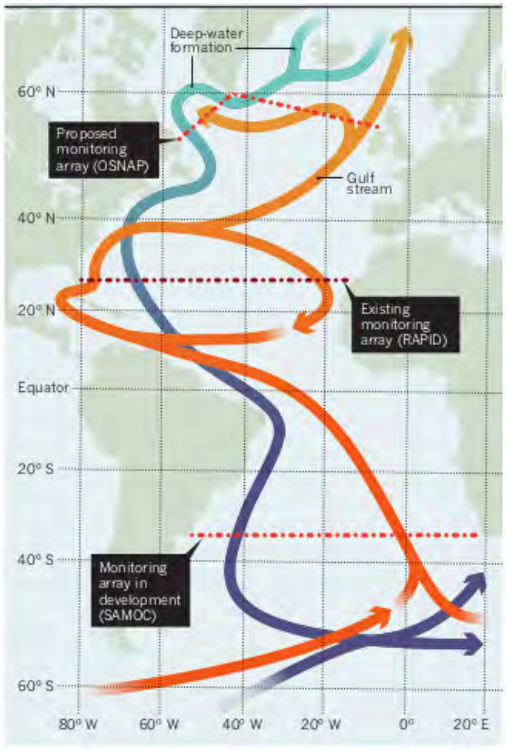

Figure 4.1: Schematic of the Atlantic Meridional Overturning Circulation (MOC) taken from Schiermeier (2013). The upper limb of the MOC is identified in orange. The lower limb of the MOC is identified in blue. The deep water formation sites in the North Atlantic are marked. Dashed lines represent existing and proposed monitoring arrays.

where $v(x, y, z, t)$ is the meridional velocity at longitude x, depth z, time t, latitude y and $x_{east}(y, z)$ and $x_{west}(y, z)$ are the eastern and western intersections with the seabed at a given latitude and depth. In the northern hemisphere, there is a northward flowing upward branch (with a thickness of ~1km in depth), and a southward flowing lower branch (with a thickness of ~1-3km). Together, these flows comprise the upper cell of the MOC. At depth there is a flow of Antarctic Bottom Water. For a schematic of the flow of water masses in the Atlantic, see Figure 1.2.

The meridional MOC as resolved by ATIa0.25 is displayed in Figure 4.2. The surface water flow below the Ekman layer is northward (positive transport), roughly between 400m-1000m. In the high latitudes of the North, convective sinking of surface water that has been transported north mostly with the Gulf Stream occurs, and the return flow of North Atlantic Deep Water between 1000m-4000m is equatorward. The deep Antarctic Bottom Water (AABW) cell that fills the abyssal plains is not fully resolved in this configuration, most likely attributed to the spin-up time (10 years) not being long enough for the establishment of AABW, the part exclusion of the Southern Ocean, and the sigma-t configuration.

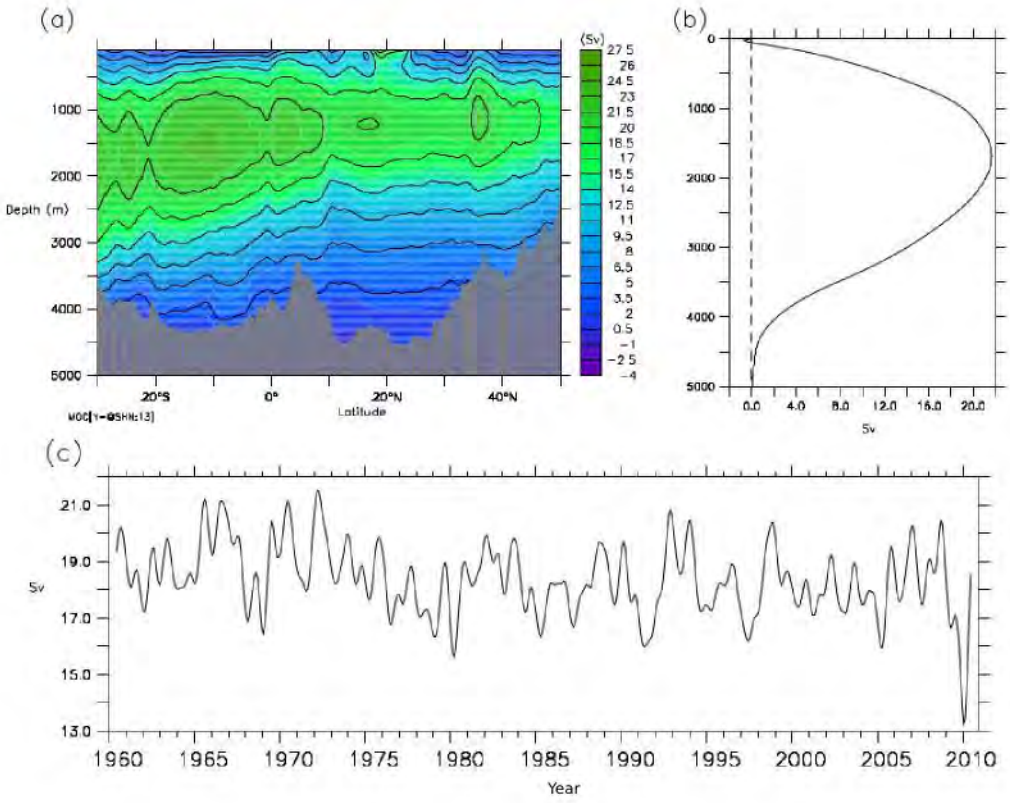

Figure 4.2: (a) Time mean (1960-2010) of the Atlantic Meridional Overturning Circulation in ATIa0.25. (b) Time mean (1960-2010) of the cumulated transport with depth averaged between 20°S-30°S (c) Yearly time series (1960-2010) of the Atlantic Meridional Overturning Circulation in ATIa0.25 at 26.5°N. The mean MOC is 18.35Sv±8.04Sv.

Results from the RAPID/MOCHA array suggest that the overturning circulation can vary enormously (Cunningham et al., 2007), with AMOC strength being recorded to vary over sub-seasonal to inter-annual timescales (Cunningham et al., 2007; Kanzow et al., 2010; Chidichimo et al., 2010; McCarthy et al., 2012). At 26.5°N, the MOC is represented as defined by equation 4.1.1, with a mean of 18.33Sv±8.04Sv (where 1Sv = $1x10^6 m^3.s^{-1}$), which is within the range of observations from the RAPID/MOCHA array (Cunningham et al., 2007).

From April 2009, a large decrease in transport (from a mean of 17.5Sv to a mean of 12.8Sv) was recorded in the AMOC transport at 26.5°N (McCarthy et al., 2012). It should be noted that this decrease in transport is also evident in the model simulation, ATIa0.25 (see Figure 4.1). It has further been observed that since 2004, the AMOC transport at 26.5°N has been decreasing (Smeed et al., 2014).

As the South Atlantic is linked to the North Atlantic it is assumed that there is some teleconnection

between changes in the North Atlantic and South Atlantic components of the MOC. However, it is not yet understood how these changes lead, lag or are different to the South Atlantic ocean and how the global transports of mass, heat and freshwater vary in time. In Figure 4.2b the mean cumulative transport averaged between 20°-30°S has a maximum of 21.5Sv, which is within range of MOC observations recorded in the region (at 24S: 21.5Sv - Bryden et al., 2011; at 35°S: 18.1Sv - Garzoli et al., 2013). This further emphasises the need to study the changes in these variables within the South Atlantic by improving observations (e.g., the SAMOC array soon to be put in place; Ansorge et al., 2014) and through the use of model simulations.

The MOC transport was subsequently computed for a section across 34.5°S (the latitude of the proposed SAMOC array; *see* Figure 4.1) in ATIb0.08 (Figure 4.4), similarly to the calculations made of the MOC at 26.5°N. The mean of 26.5Sv is higher than 18.1Sv, the mean MOC transport derived from XBT (Expendable Bathythermograph) data at 35°S (Garzoli et al., 2013), as well as higher than the values obtained from other observations and inverse models in the South Atlantic (*see* Table 4.1; Lumpkin and Speer, 2007; Dong et al., 2009; Bryden et al., 2011). The same can be said about the transport computed at 24°S (Figure 4.5).

Study	**Dataset**	**Volume Transport [Sv]**
Observations		
Bryden et al., (2011)	24^0S; James Cook Cruise in 1983 Discovery Cruise in 2009	16.5 21.5
Dong et al., (2009)	35^0S; AX18, 17 transects	17.9 $\pm$2.2
Garzoli et al., (2013)	35^0S;AX18, July 2002-Apr 2007; 24^0S Oct 2007-June 2010; 35^0S June 2010-Feb 2011 (27 transects)	18.1$\pm$2.3
Model Simulations		
Perez et al., (2011)	OFES and POCM	15-16.5
Dong et al., (2011)	OFES at 34^0S	
ATIb0.08		
	34.5^0S	26.5$\pm$ 4.6
	24^0S	27.64$\pm$ 3.2

Table 4.1: Table comparing observational and model simulations of the MOC in the South Atlantic

That ATIa0.25 computed a cumulative transport averaged between 20°-30°S with a maximum of 21.5Sv, which is closer to observations and this indicates that the ATIa0.25 configuration may be

better simulating this region than the higher resolution configuration.

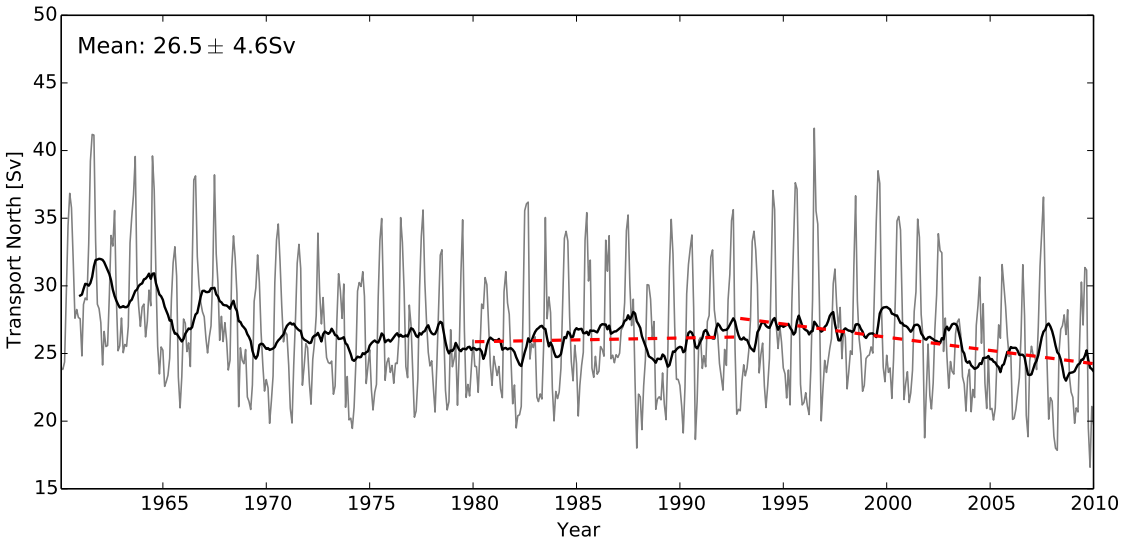

Figure 4.3: Meridional Overturning Circulation component of the transport at 34.5°S. Yearly running mean is overlaid the monthly means form 1960-2009. No trend is seen from 1980-1993. A decreasing trend is seen from 1993-2009. There is a mean tranport of 26.5Sv.

There are no long term observations of the MOC transport in the South Atlantic, although an observational platform is being put in place with the SAMOC project (Ansorge et al., 2014). Dong et al. (2011) found an increasing trend from 1980-1993 in the OFES model (a global ocean general circulation model for the Earth Simulator). A similar trend is not seen in this model. However, the slight decrease in transport that they found from 1993 - 2005 is similar to the slightly decreasing trend that has been found in this model.

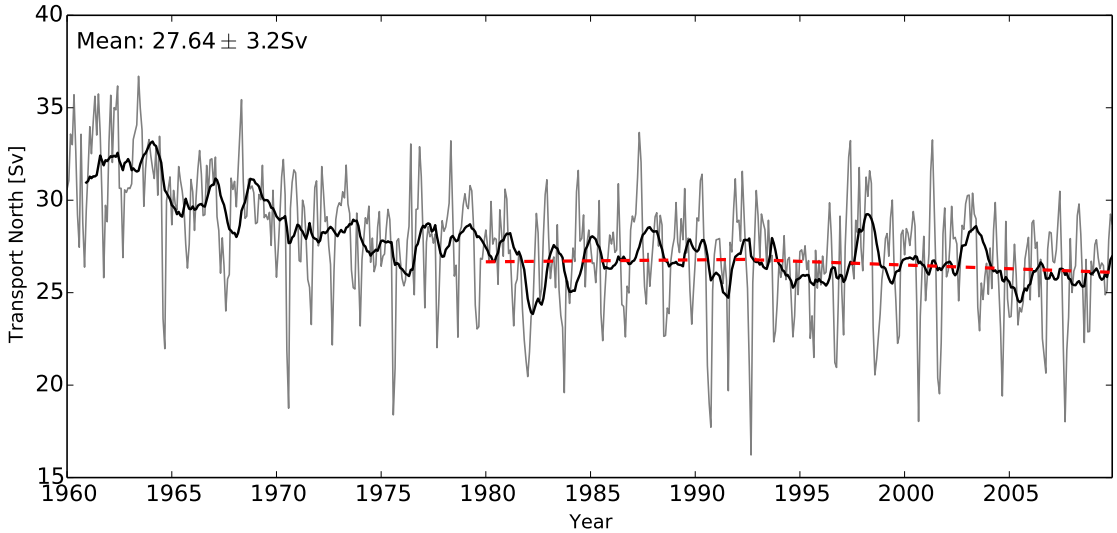

Figure 4.4: Meridional Overturning Circulation component of the transport at 24°S. Yearly running mean is overlaid the monthly means from 1960-2009. A decreasing trend is seen from 1960-1980. No trend is seen from 1980-1993. A slight decrease is seen from 1993-2009. There is mean transport of 27.64Sv for the full timeseries.

4.2 The South Atlantic sub-tropical gyre

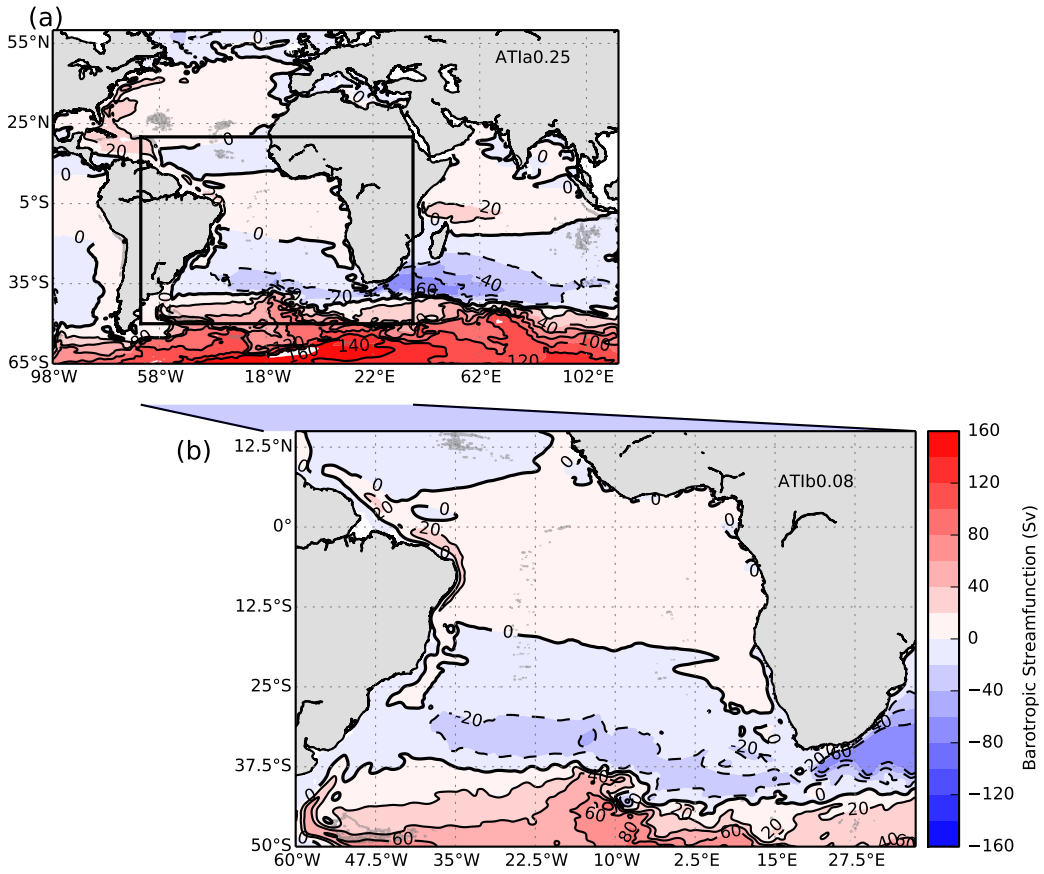

Figure 4.5: Large Scale Circulation represented by the horizontal barotropic streamfunction. (a) ATIa0.25 and (b) ATIb0.08. The 0Sv contour is in bold. Positive flow (north and westward flow) are in shades of red. Negative flow (south and eastward flow) are in shades of blue.

The South Atlantic sub-tropical gyre is located in the Atlantic Ocean, linked to the Pacific, Southern and Indian oceans via the Drake Passage, the Antarctic Circumpolar Current and the Agulhas Leakage. In Figure 4.5, the general circulation as represented by the horizonal barotropic streamfunction in the domains of the base model, ATIa0.25 and the nested model, ATIb0.08 is displayed. Of note in Figure 4.5a, is the southern hemisphere supergyre (De Ruijter, 1982; Gordon, 1986), which can be indentified in shades of blue, within the contours of zero transport, extending across the Indian ocean and into the South Atlantic ocean. The eastward flowing Antarctic Circumpolar Current (Whitworth and Nowlin, 1987), is also visible in shades of red to the south of the supergyre. The northward flow of the Gulf Stream bordering the North American continent (Auer, 1987), is visible in the North Atlantic. Looking at the circulation in the domain of the nested model, ATIb0.08 (Figure 4.5b), the Agulhas System (Lutjeharms, 1996) intruding into the South Atlantic, as part of

the southern hemisphere supergyre is visible south of Africa. Eastward flow south of 40°S can be seen in shades of red, however the ACC is not well resolved, with a large anomaly centered around 10°W, 40°S.

Measurements from satellite altimeters provide reliable information on ocean circulation, currents and eddies over long time periods and at high resolutions (Pascual et al., 2006; Ducet et al., 2000), and thus furnish valuable tools for model comparisons. Figure 4.6 shows the main differences between the model and altimetry in Sea Surface Height (SSH) and SSH variance (Figure 4.6a) and in geostrophic velocity (Figure 4.6b). For a schematic of the currents in the South Atlantic, refer to Figure 1.3.

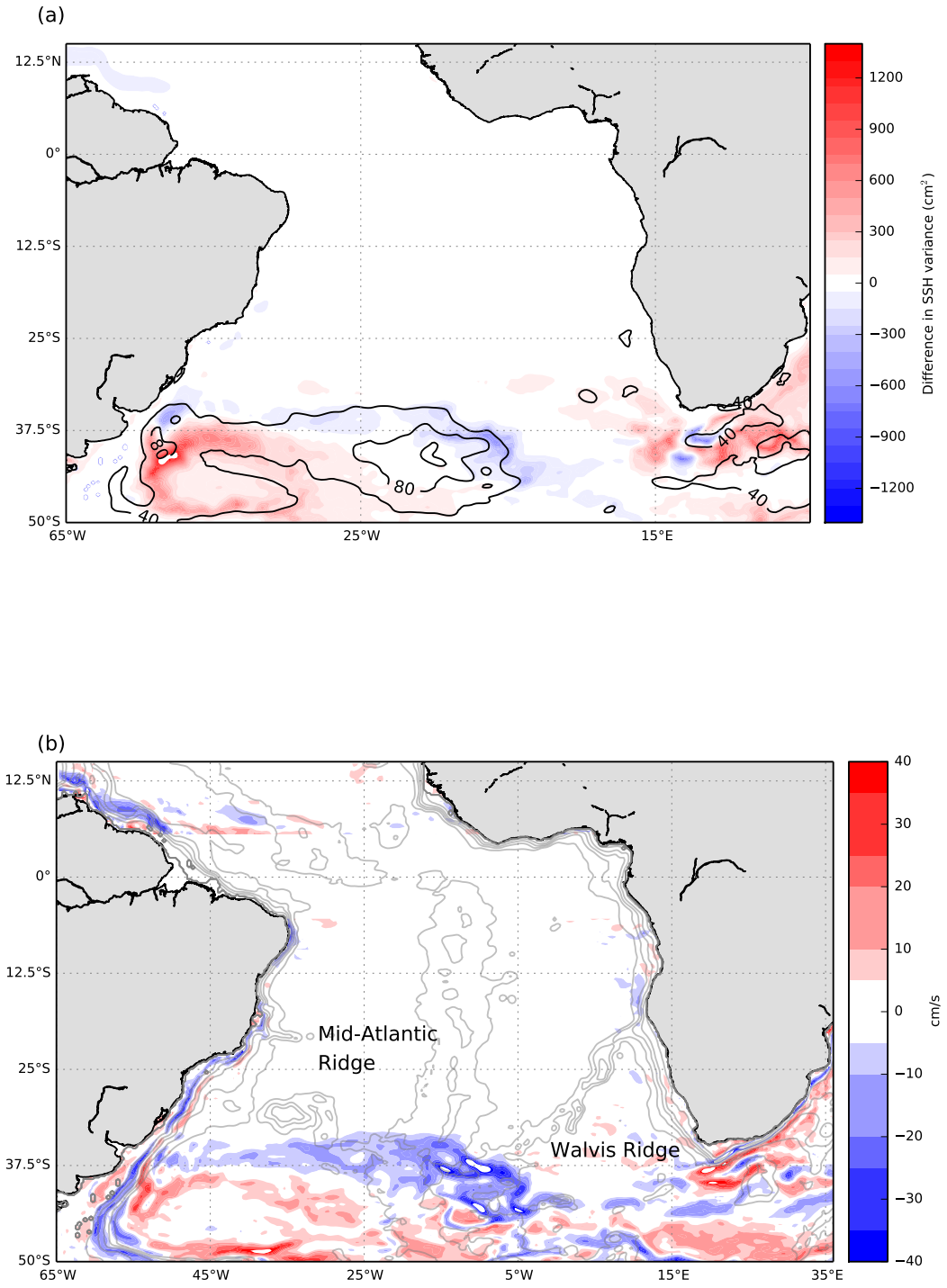

Figure 4.6: Differences between altimetry and ATlb0.08. (a) SSH and SSH variance; (b) Geostrophic velocity with bathymetry at 200m, 1000m, 2000m, 3000m and 4000m in gray contours. Red signifies an underestimation by the model and blue signifies an overestimation by the model. Where the difference is low, there is no shading. The region between 5°N and 5°S is masked.

The model underestimates mesoscale activity south of Africa and in the south western Atlantic from 100 to greater than 1200cm^2. The model overestimates mesoscale activity south of 35°S and between 18°W and 0°W. The model also underestimates SSH by up to 100cm in this region. In terms of geostrophic velocity, the positions of the Agulhas Current and the Agulhas Return Current are shifted to the north by ~2 degrees of latitude. The currents on the western boundary of the South Atlantic are also located closer to the continents than seen in altimetry. The model highly underestimates geostrophic velocity south of 40°S, with greater geostrophic velocity values (30-60cm/s) located around 38°S. Overall, the regions displaying most differences overall are the eastern, western and southern boundaries of the gyre. The regions where the absolute dynamic topography SSH and SSH variance differ from observations correspond with the regions where the geostrophic velocities differ from observations. Each of these regions will now be discussed in further detail. To this end, the South Atlantic is divided into four regions (*see* Figure 4.7).

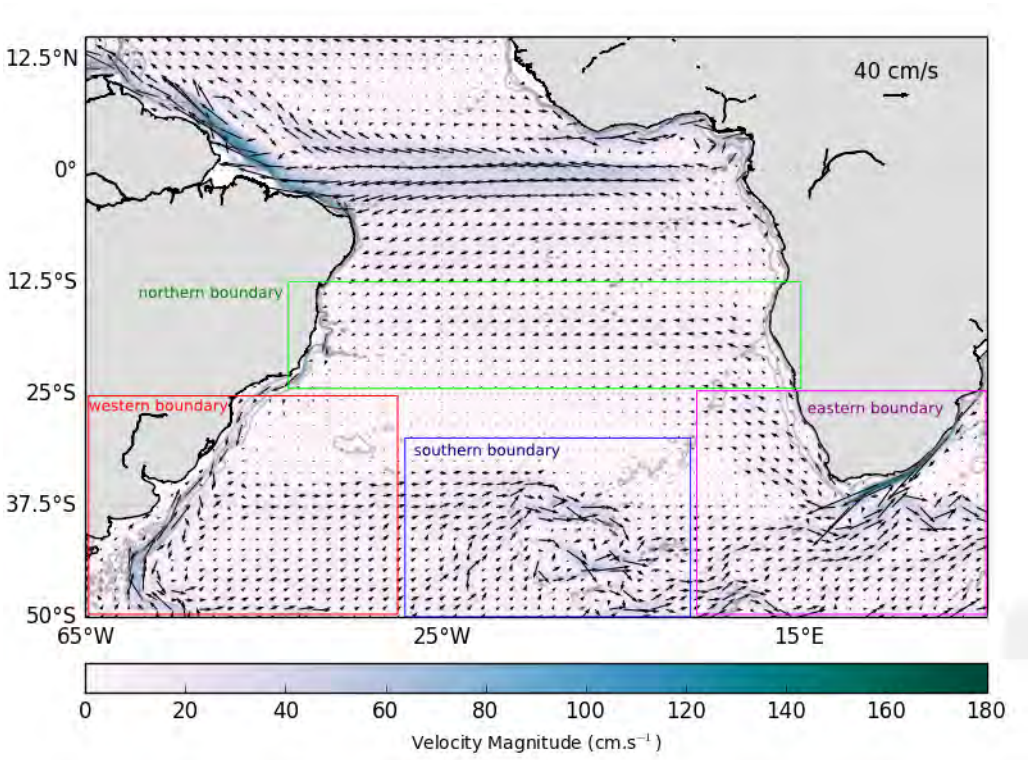

Figure 4.7: Mean surface velocity (1993-2009) in ATIb0.08. Vectors show current direction and magnitude. Shading indicates magnitude. The four domains used for discussion purposes are demarcated.

4.2.1 The Eastern Boundary

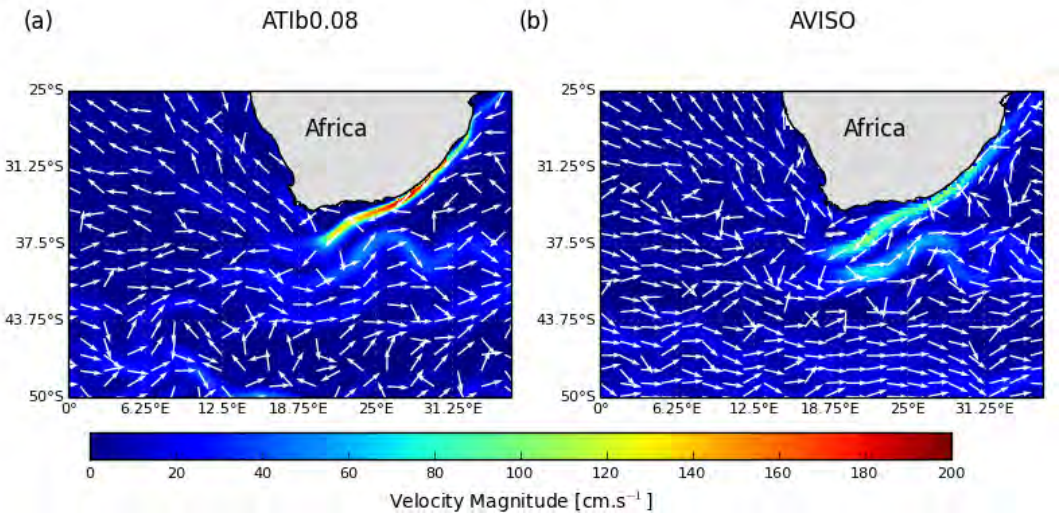

Figure 4.8: Mean (1993-2009) geostrophic velocities in the eastern boundary. (a) ATIb0.08 (b) AVISO altimetry. Current magnitude is shown in color. Vectors show current direction.

The surface flow in the eastern boundary of the South Atlantic as defined in Figure 4.7 is focused on in Figure 4.8 and compared with altimetry. Characteristic of the south-eastern part of the gyre is the inflow of warm and salty water through Agulhas Leakage, derived from the dynamics of the Retroflection Region of the Agulhas System (Stramma and England, 1999). This region is known to be a region of high energy and mixing (Boebel et al., 2003). The Agulhas Current displays typical current speeds of ~180cm/s. This is greater than the mean geostrophic current speed resolved by altimetry, which has a mean of about ~100cm/s at the core of the Agulhas Current. The Agulhas Current in the model is narrower and skirts the continental shelf closer than seen in observations. The Agulhas Return Current (Lutjeharms and Ansorge, 2001) is visible in both model and observations, with the model showing more of a defined meander. The retroflection is located further to the west in the model at ~14°E, while in observations the Agulhas Current retroflects at about 17°E. The weak (~20-40cm/s) northwestward flowing Benguela Current and Benguela Current extension (Peterson and Stramma, 1991; Richardson and Garzoli, 2003) can be identified by the vectors along the western border of southern Africa. The flow of the Antarctic Circumpolar Current (ACC) in the model is more chaotic than the flow in observations, with the model not succeeding in clearly resolving the ACC.

4.2.2 The Northern Boundary

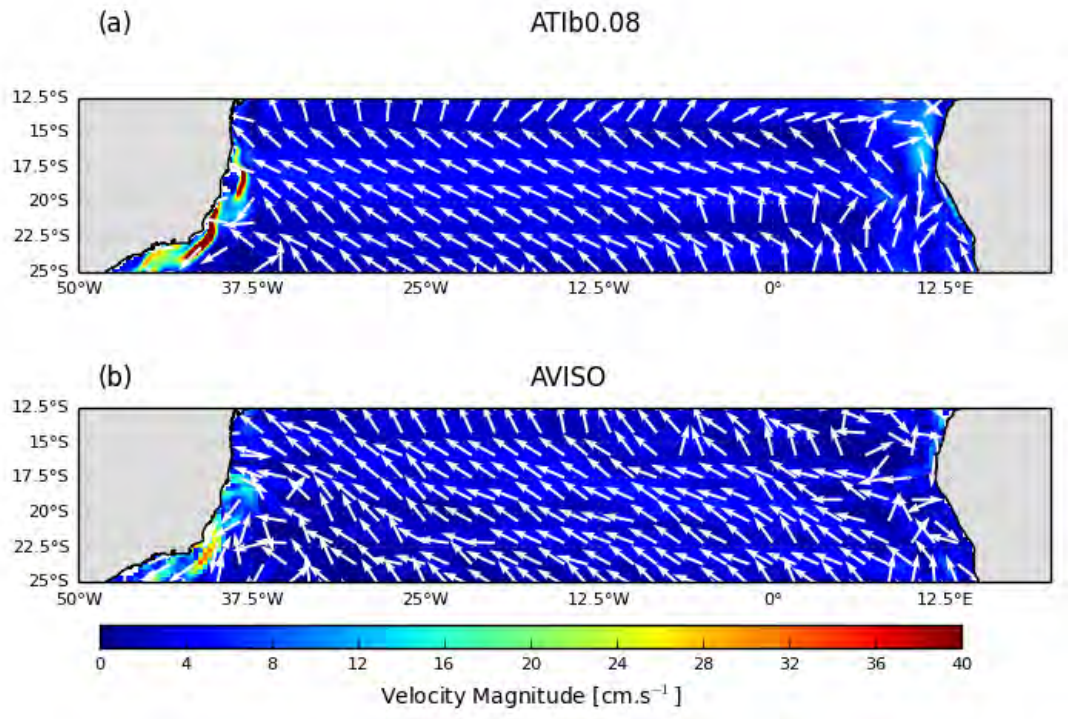

Figure 4.9: Mean (1993-2009) geostrophic velocities in the northern boundary. (a) ATIb0.08 (b) AVISO altimetry. Current magnitude is shown in color. Vectors show current direction.

The South Equatorial Current marks the northern boundary of the subtropical gyre (Stramma and England, 1999) and is composed of recirculated sub-tropical gyre water and additional inflow as a result of Agulhas Leakage (Lutjeharms, 1996). This current flows north-eastwards towards Brazil where it bifurcates at ~18°S (Stramma and England, 1999) and splits into the northwards flowing North Brazil Current and the southwards flowing Brazil Current. This bifurcation occurs at about ~17.5°S in both the model and observations (*see* Figure 4.9). There is little difference between the model and observations in speed of the South Equatorial Current with both having a mean speed of ~10cm/s. The mean speed of the Brazil Current is stronger in the model than in observations reaching speeds greater than 40cm/s while altimetry shows a maximum speed of about 35cm/s.

4.2.3 The Western Boundary

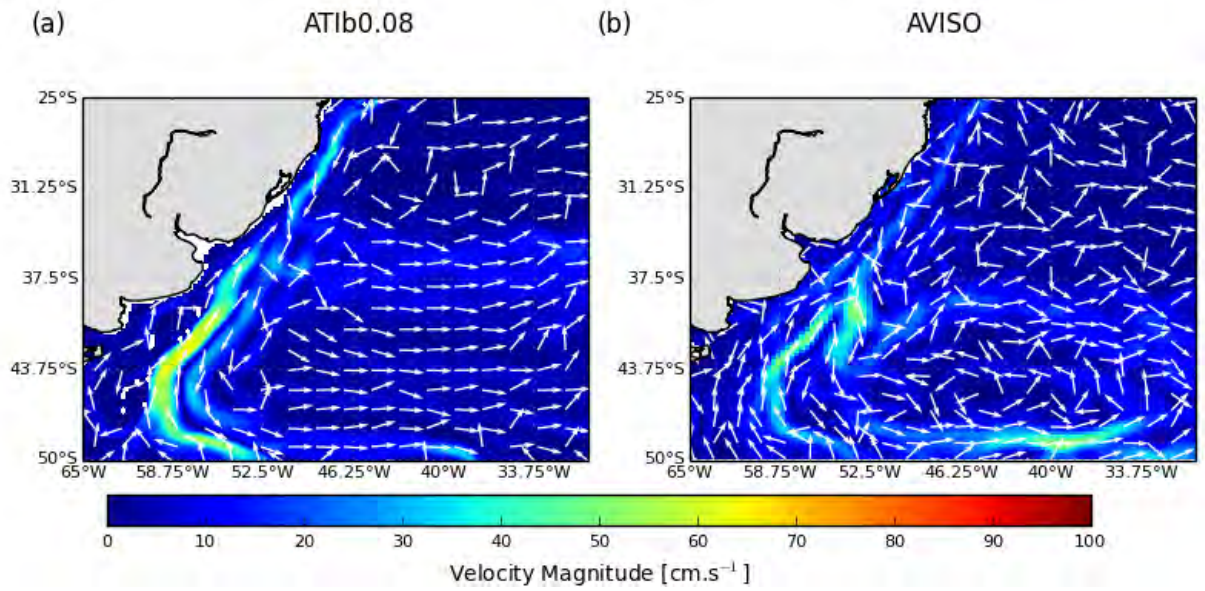

Figure 4.10: Mean (1993-2009) geostrophic velocities in the western boundary. (a) ATIb0.08 (b) AVISO altimetry. Current magnitude is shown in color. Vectors show current direction.

Two major currents compose the flow along the western boundary, namely, the cold Malvinas Current flowing northwards and the warm, weak Brazil Current flowing southwards. The strength of the Brazil Current is expected to increase with increasing latitude, with the Brazil Current having a strength of 9.6Sv at 24°S and 17.5Sv at 33°S (Stramma, 1989). WIth reference to Figure 4.10, this increase in velocity is not clear. The Malvinas Current is stronger than the Brazil Current (Vivier and Provost, 1999), and this is visible in both the model and observations (*see* Figure 4.10). The model does however resolve stronger current speeds than altimetry derived velocities in both the Brazil and Malvinas Currents, with speeds of ~40cm/s and ~70cm/s respectively.

The location of the Brazil/Malvinas Confluence, (Olson et al., 1988), is centered around 36°S in the model, further north than that seen in observations, where it is centered around 40°S.

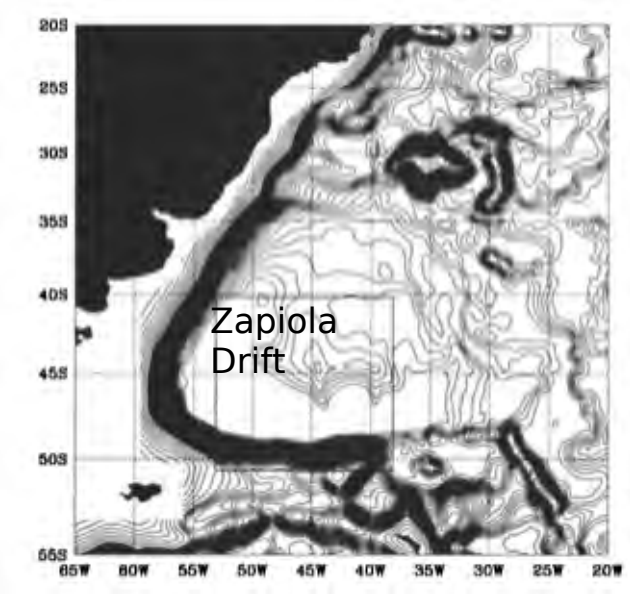

Figure 4.11: The location of the Zapiola Drift, taken from Miranda et al. (1999). The Zapiola drift is the elongated structure centered around 45°W, 45°S.

The general flow in this region, represented through observations, is seen to be very variable. However, in the model, there is a clear eastward flow of water, with the strongest flow of water eastward around 37°S. A similar pattern is not seen in altimetry. A recirculation cell can be seen between 50°S and 40°S. This circulation cell is known as the Zapiola Gyre. The Zapiola Gyre is caused by the bathymetric feature, the Zapiola Drift (*see* Figure 4.11), which is located at about 45°W, 45°S (Saunders and King, 1995; Davis et al., 1996; Miranda et al., 1999). In Figure 4.6b this discrepency is also visible as shown by a circular band of red shading which indicates that the model is under-representing geostrophic flow in this region. The ETOPO5 bathymetry used in the model simulation is contoured in Figure 4.6b. The bathymetric feature, the Zapiola Drift (visible in Figure 4.11) is not resolved by the low resolution bathymetry that is used in the model simulation.

This feature was first realistically simulated by Miranda et al. (1999) in a sigma-coordinate model of 1/3° resolution. The Zapiola Gyre is known to be an important area of water mass transformation in the South Atlantic (Garzoli and Matano, 2011) and its misrepresentation may affect the model's representation of the transfer of water masses within the South Atlantic as well as to the North Atlantic.

4.2.4 The Southern Boundary

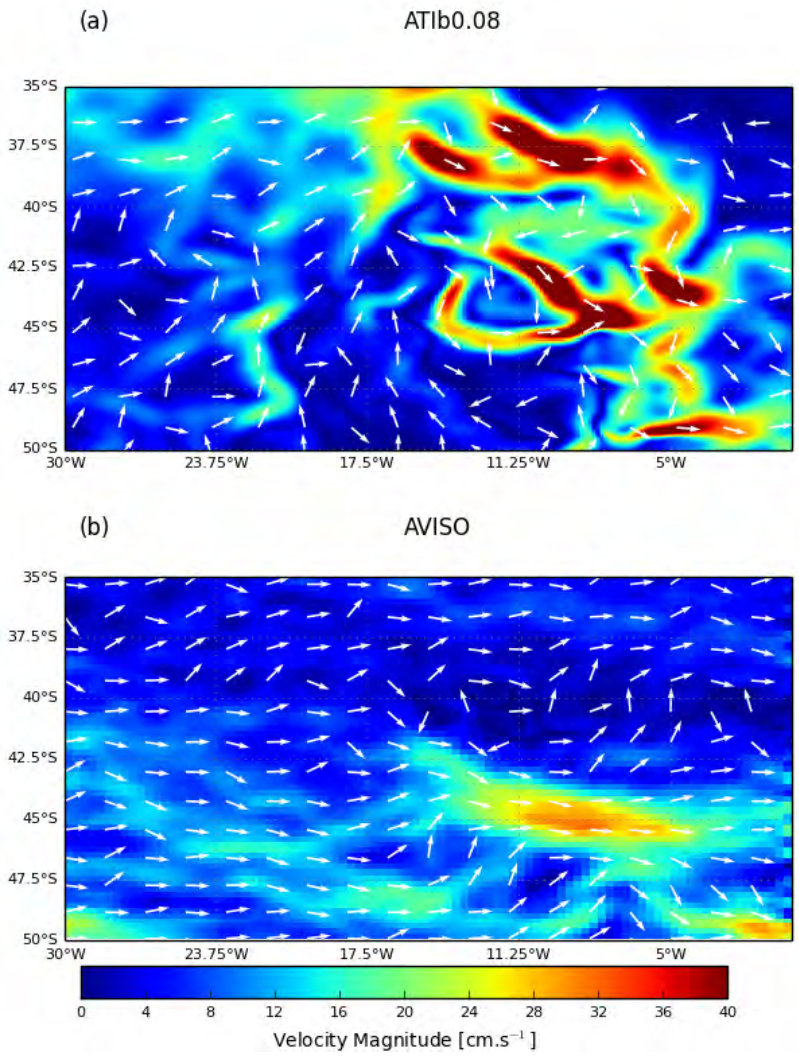

Figure 4.12: Mean (1993-2009) geostrophic velocities in the southern boundary. (a) ATIb0.08 (b) AVISO altimetry. Current magnitude is shown in color. Vectors show current direction.

Large differences between the geostrophic velocity of the model and observations can be clearly seen in Figure 4.12. The model does not resolve this region of the ocean accurately. While observations show an eastward flowing South Atlantic Current at ~37°S north of an eastward flowing Antarctic Circumpolar Current (ACC) at ~45°S, the flow in the model is not coherent. Anomalous current activity is visible over 18°W and 0°W. This is where the mid-atlantic ridge is located. It may be that the model is overreacting to this bathymetric feature. Furthermore, the closed boundary of the low resolution moedl at 65°S in combination with the nesting boundary of the higher resolution ATIb0.08 may contribute to anomalies found here. Together with the barotropic streamfunction (Figure 4.5b), one can see that the ACC is not well resolved.

4.2.5 Summary

To summarise, the surface circulation in South Atlantic sub-tropical gyre is resolved by the $1/12^{\circ}$ model; however, there are some important discrepancies which are listed below. Keeping these differences in mesoscale activity and circulation in mind is essential when using the model as a tool for further studies.

- Meso-scale activity is underestimated in the southwest Atlantic, over the Brazil/Malvinas Confluence and the Zapiola Gyre.
- The Zapiola Gyre is not resolved in the model.
- Mesoscale activity is also underestimated in the Agulhas Region.
- Anomalous meso-scale activity occurs between 18^{0}-0^{0}W and 35^{0}-45^{0}S.
- The current strength at the boundaries of the gyre is, in general, greater in the model than in observations.

4.3 Hydrographic Properties

4.3.1 Sea Surface Temperature (SST)

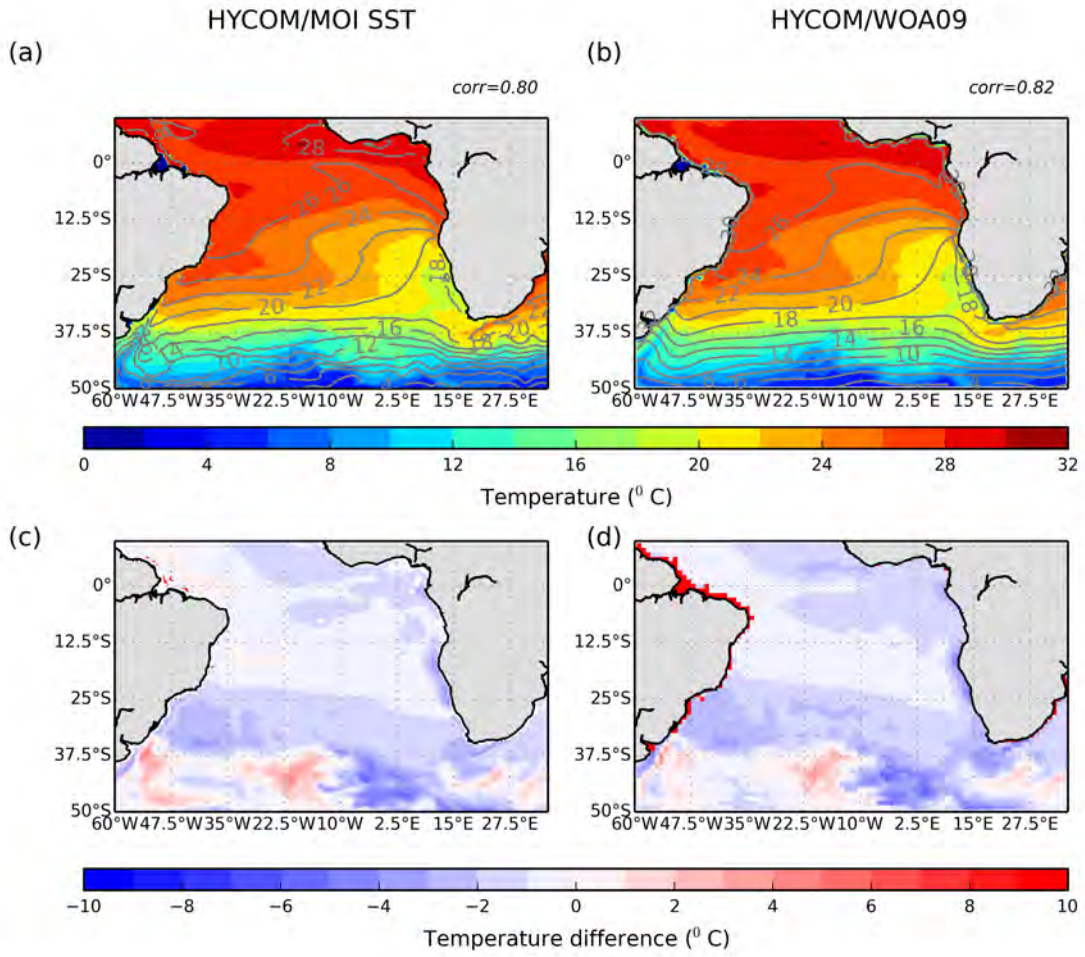

Figure 4.13: Time mean (2002-2009) of Sea Surface Temperature (a) ATIb0.08 in colors with MOI SST contour lines in gray, (b) ATIb0.08 in colors with WOA09 climatology contour lines in gray, (c) SST bias in MOI SST - ATIb0.08 (d) SST bias in WOA09 SST - ATIb0.08

The temperature distribution of the model is similar in the large scale distribution of temperature across the South Atlantic Basin in observations, with warm water in the northern part and cool water in the south, separating the warmer South Atlantic subtropical-gyre from the cooler Southern Ocean (Figure 4.13). The surface temperature field is similar to both that of Microwave Optimally Interpolated SST (MOI SST) and to that of WOA09 in Figure 4.13b with correlation coefficients of 0.80 and 0.82 respectively. The MOI SST is expected to resolve better the temperature distribution than WOA09 due to its higher resolution (1/4° vs 1°).

Warm water in the south of Africa represents the warm Agulhas System. This region is not well resolved by WOA09 which has a resoltuion of 1°, but is clear in the model and in the satellite data. Cold water in the southwest of the gyre is representative of the cool Malvinas Current. Below 38°S, the cold waters of the Southern Ocean are resolved in the model, similar to observations. In the region of the Zapiola Gyre (45°W,45°S), the model is cooler than the satellite data by 4-6°C. This is because the model does not resolve this feature (*see* Section 4.2.3). Between 20°-0°E, the model displays anomalous cool water. To the east, the model then becomes cooler than both observational datasets.

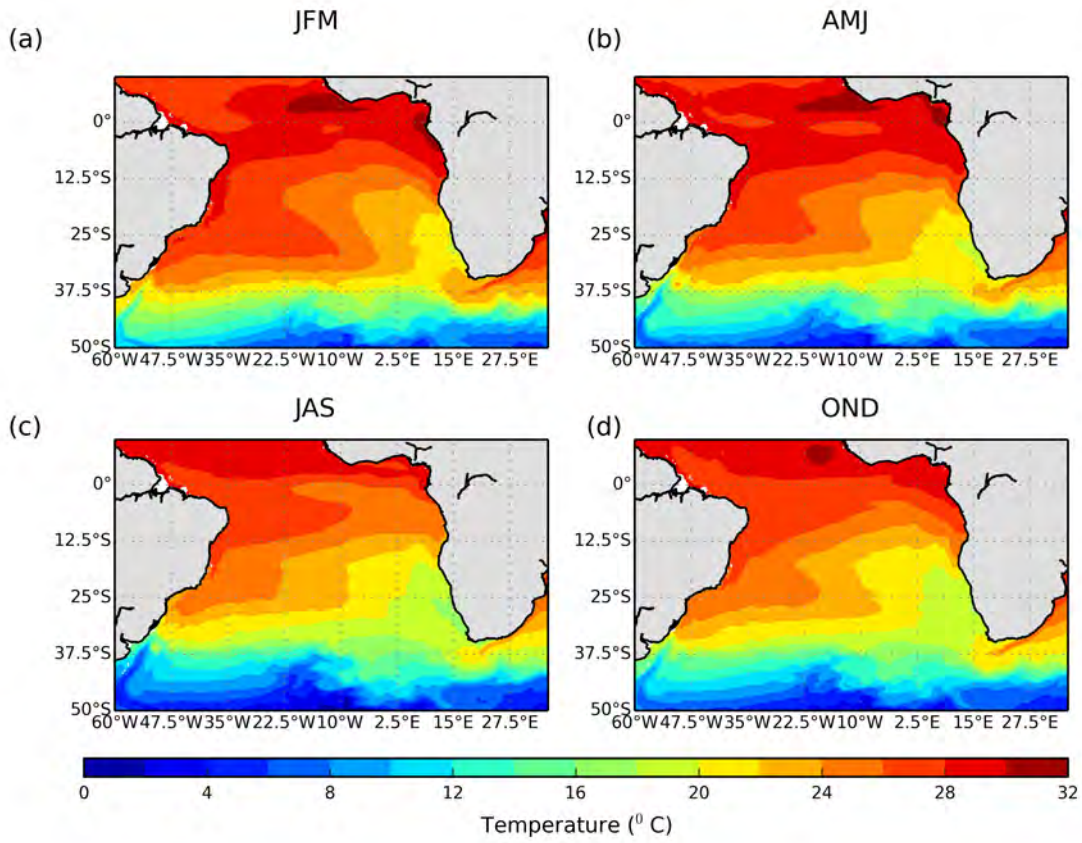

Figure 4.14: Seasonal Means (2002-2009) of SST in ATIb0.08. (a) Summer, JFM, (b) Autumn, AMJ, (c) Winter, JAS and (d) Spring, OND

The seasonality of the South Atlantic due to changes in insolation and surface heat fluxes is visible in the SST signal (Figure 4.14).

4.3.2 Sea Surface Salinity (SSS)

The large scale features in the model simulation and satellite observations are similar, with more saline water located in the sub-tropical gyre and fresher water in the southern, eastern, and north-east sections of the basin (Figure 4.15). The flow of saline water northwards, with the North Brazil Current on the north-western region of the basin is resolved by both model and observations. The fresh water input of the Malvinas Current is also resolved. East of this region, the more saline Zapiola Gyre is again not evident in the salinity field of HYCOM while it is resolved by the Aquarius data. To the east, an intrusion of fresh water northwards is seen in HYCOM at ~20°W, which is not resolved by the Aquarius data. The fresh water feature in the northeast of the basin, in the Gulf of Guinea is resolved by the model and similar to observations. The Sea Surface Salinity (SSS) is very similar to that of the WOA09 climatological dataset (*see* Figure 4.15b) with a correlation coefficient of 0.97. This result was anticipated as the model SSS is relaxed to climatology. However, the anomaly over the mid-Atlantic ridge is nevertheless portrayed in the SSS signal of the model.

SSS has a low correlation coefficient of 0.64 with Aquarius observations. This may be associated with the fact that the model data is relaxed to climatology and so would be expected to be different from observations. Further discrepancies may also be attributed to Aquarius still being in its initial stages with yet unresolved calibration issues especially in the Southern Hemisphere and at higher latitudes (Lagerloef et al., 2013). In general, HYCOM tends to underestimate salinity in the majority of the South Atlantic by about 0.2-0.3. ATIb0.08 overestimates salinity in the anomalous area in the south and also, in comparison to Aquarius, over the equatorial region.

SSS does not show much seasonal variability (Figure 4.16). The sub-tropical gyre is seen to be more saline in the Summer and Autumn months, most likely due to high rates of evaporation. The low salinity off the north west coast of Africa during these months can be attributed to summer rainfall.

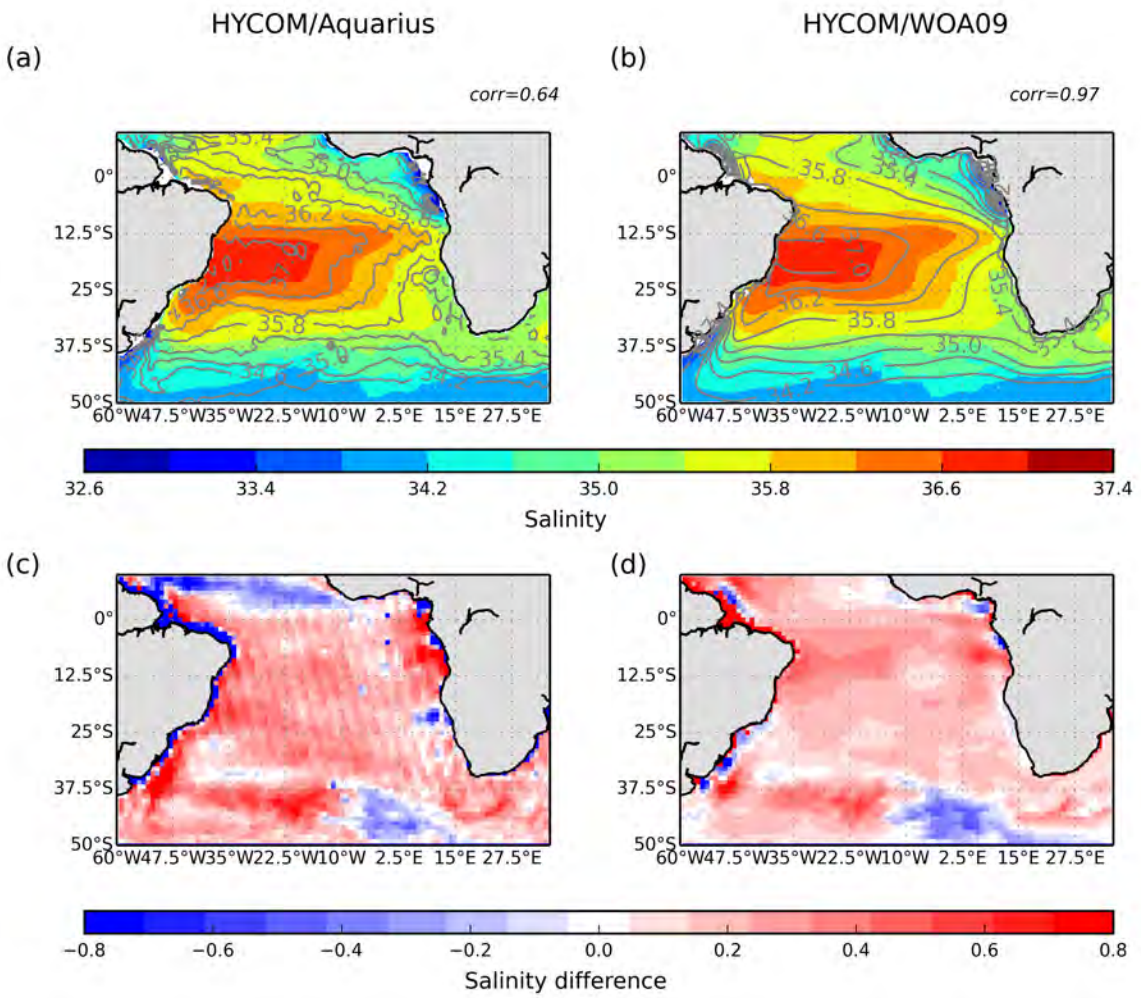

Figure 4.15: Time mean (2002-2009) of Sea Surface Salinity (a) ATIb0.08 in colors with Aquarius (time mean of 2011-2012) contour lines in gray, (b) ATIb0.08 in colors with WOA09 climatology contour lines in gray, (c) SSS bias of Aquarius - ATIb0.08 (d) SSS bias of WOA09 SST - ATIb0.08

4.3.3 The South Atlantic at 34.5°S

4.3.4 Temperature

The ATIb0.08 representation of the vertical sections of temperature and salinity in the upper 2000m across 34.5°S in the South Atlantic are shown and compared with climatologies derived from WOA09 and CARS ARGO-only datasets (Figures 4.17 and 4.18). The stratification of the ocean is well represented by HYCOM in comparison with both the climatological datasets.

In general, the model simulation appears to follow the contours of the CARS dataset more closely than the WOA09 dataset. On the western boundary, the warm water flow of the Brazil Current can

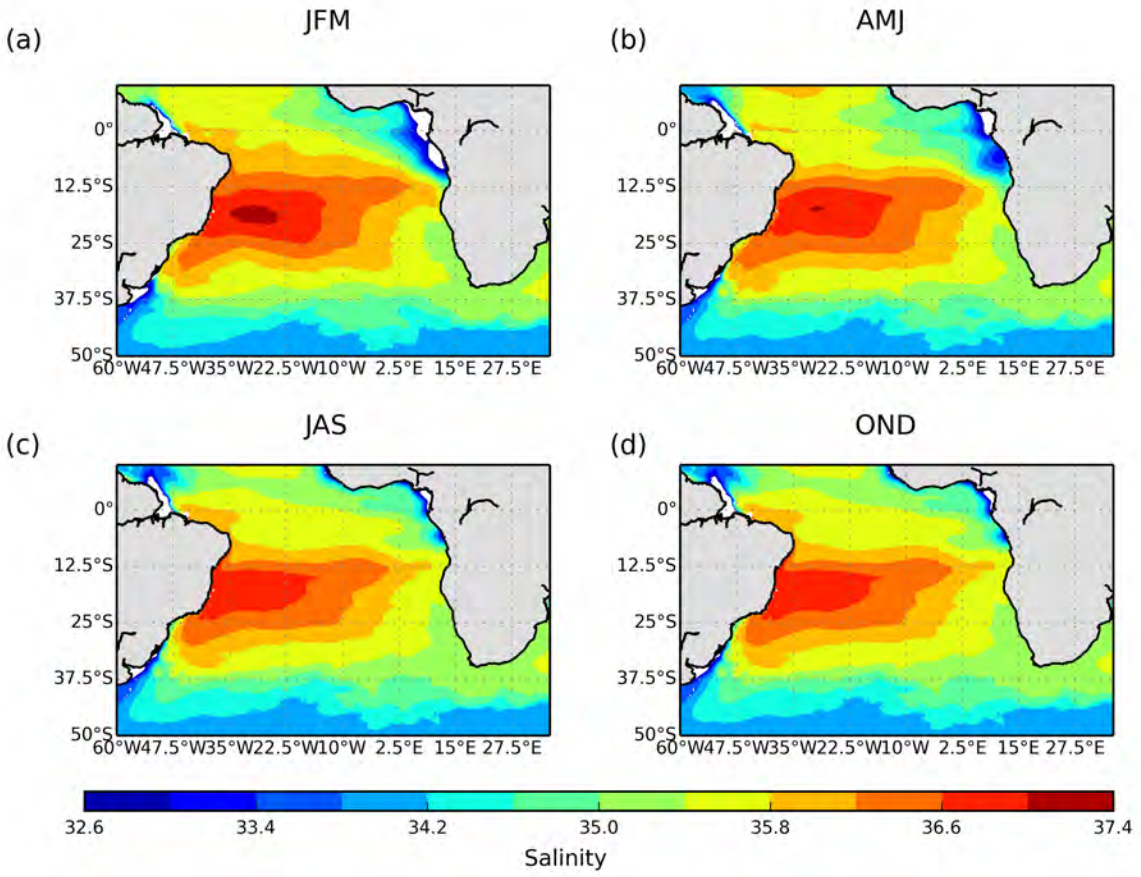

Figure 4.16: Seasonal Means (2002-2009) of SSS in ATIb0.08. (a) Summer, JFM, (b) Autumn, AMJ, (c) Winter, JAS and (d) Spring, OND

be seen in both model and observations, however the model represents water temperatures higher by about 2°C at the surface. On the eastern side of the basin, the warm water intrusion of the Agulhas inflow is seen in both the model and observations. Between 20° and 10°W, an upwelling feature in the model simulation is evident, which is not seen in observations. The major bias seen in ATIb0.08 is emphasised in Figure 4.17c and 4.17d. ATIb0.08 underestimates temperatures in the west between 200 and 800m, and overestimates temperatures mainly in the surface waters above 200m.

4.3.5 Salinity

In terms of salinity, the model simulation is more similar to the CARS ARGO-only dataset than to the WOA09 salinity climatology (Figure 4.18). The saline water of the Brazil Current is resolved on the western boundary of the basin and the saline water of the Agulhas inflow is seen on the

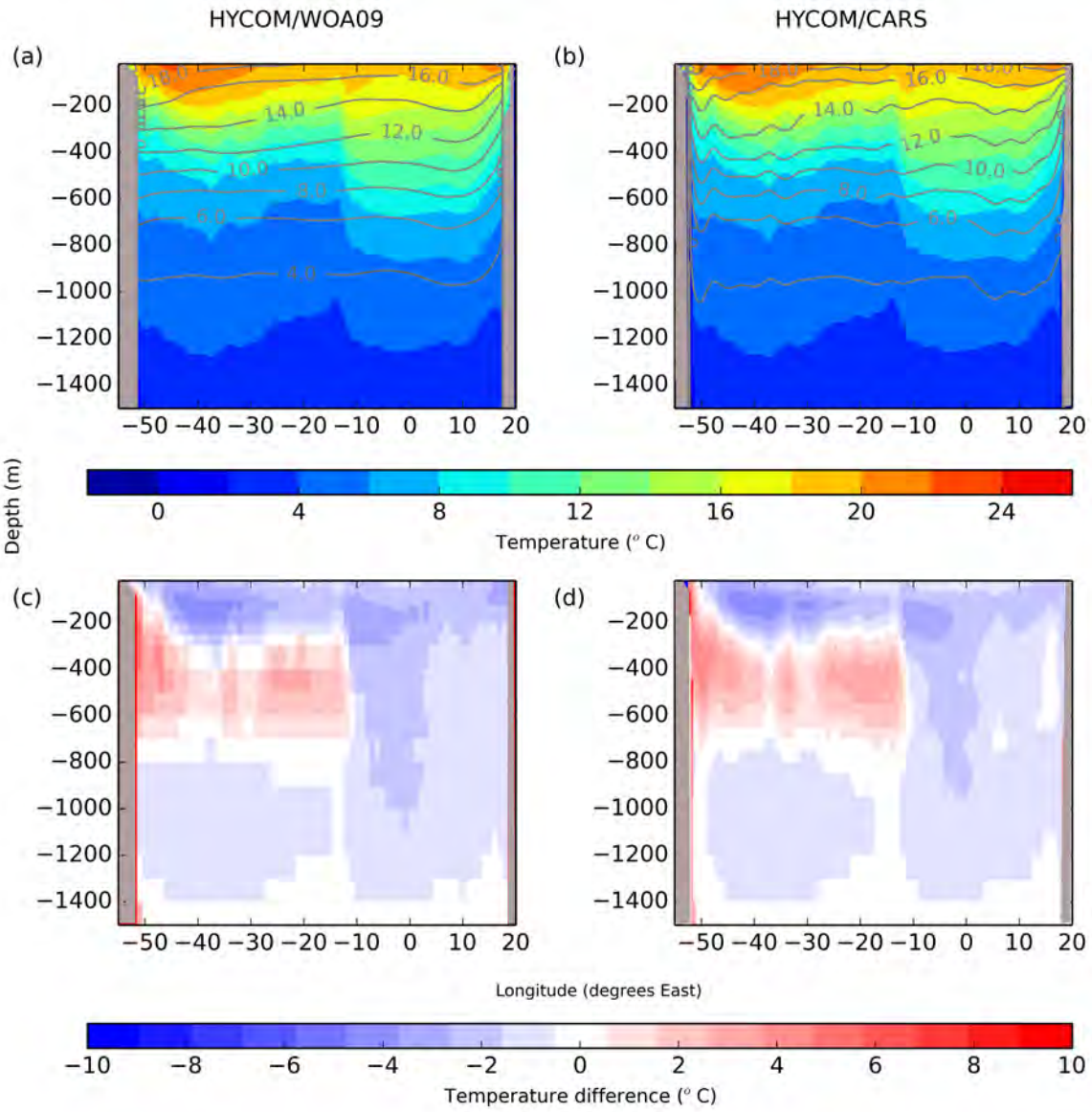

Figure 4.17: Vertical temperature section across 34.5°S in the upper 1500m. (a) HYCOM ATIb0.08 (mean 2002-2009), contours of WOA09 overlaid, (b) HYCOM ATIb0.08 (mean 2002-2009), contours of CARS ARGO-only overlaid, (c) Bias, WOA09-ATIb0.08 and (d) Bias, CARS-ATIb0.08

eastern boundary. The input of fresh water between 800-1000m (where Antarctic Intermediate Water (AAIW) is expected) is not resolved by the model as seen in both observational datasets. AAIW is characterised by the a salinity minimum below the thermocline that is found north of the Subantarctic Front. AAIW of Indian Ocean origin has been observed to enter the South Atlantic at 35°S, 15°E (Schmid and Garzoli, 2009). It may not be resolved in the model because of the Antarctic Circumpolar Current is not well resolved (*see* section 4.2.4). The main bias is again highlighted in Figures 4.18c and 4.18d, with ATIb0.08 underestimating salinity in the surface above 600m throughout the transect, and overestimating salinity below 600m, particularly between 10°W

and 10°E.

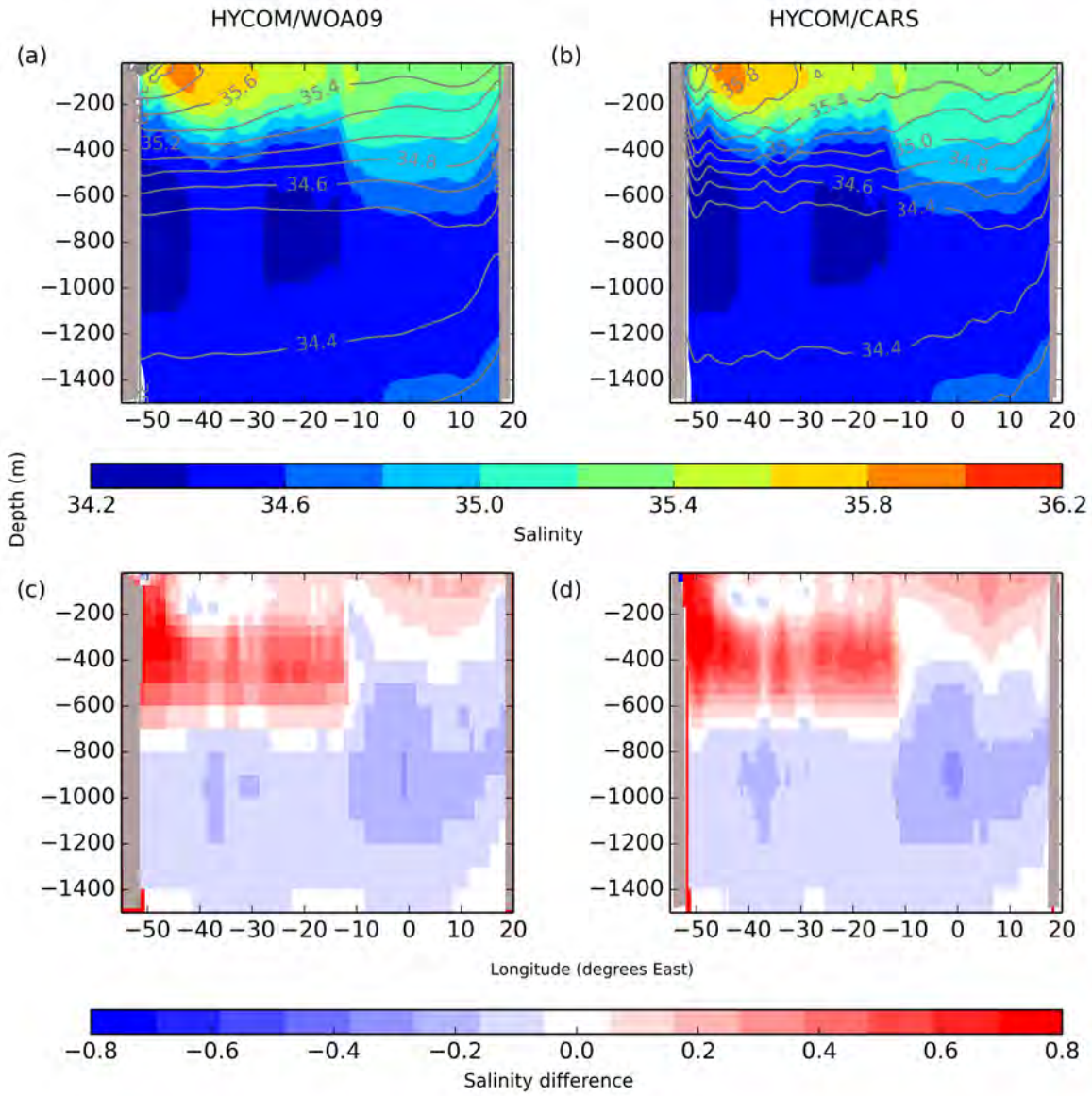

Figure 4.18: Vertical salinity section across 34.5°S in the upper 1500m. (a) HYCOM ATIb0.08 (mean 2002-2009), contours of WOA09 overlaid, (b) HYCOM ATIb0.08 (mean 2002-2009), contours of CARS ARGO-only overlaid, (c) Bias, WOA09-ATIb0.08 and (d) Bias, CARS-ATIb0.08

4.3.6 Summary

The range of temperatures and salinities in each region is summarised in the Table 4.2, below. Throughout almost all regions in the surface, the model is seen to overestimate surface temperature by ~2°C and underestimate surface salinity by ~0.2. With depth (>400m) the model is seen to underestimate temperatures and salinities by ~2-4°C and 0.2-0.4 respectively.

Sea Surface Temperature [^{0}C]			
Region	ATIb0.08 ($1/12^0$)	WOA09 (1^0)	MOI SST ($1/4^0$)
Agulhas	20-28	18-20	18-22
Brazil Current	18-26	20-24	16-24
Malvinas Current	4-16	10-16	8-16
Zonally across the South Atlantic	18-28	18-26	18-26
Southern Ocean	2-12	4-14	4-12
Gulf of Guinea	30-32	26-28	27-30
Sea Surface Salinity			
	ATIb0.08	WOA09 (1^0)	Aquarius (1^0)
Agulhas Region	35-35.4	35-35.6	35.4-35.6
Brazil Current	35.4-37	35.8-37	36-37
Malvinas Current	33-34.2	34.2-35	34.4-35.4
Zonally across the South Atlantic	35-37	35.4-37	35.4-37.4
Southern Ocean	33.8-34.4	34-35	34-35.4
Gulf of Guinea	32-6-34	32.6-34	32.6-34.2
Temperature [^{0}C]			
34.5 S	ATIb0.08	WOA09 (1^0)	CARS09-Argo Only ($1/2^0$)
surface-400m	8-24	10-18	12-20
400-800m	4-8	6-12	6-12
800-1500m	0-6	2-6	2-6
Salinity			
34.5 S	ATIb0.08	WOA09 (1^0)	CARS09-Argo Only ($1/2^0$)
surface-400m	35.4-36	35.2-36.2	35.2-36
400-800m	34.4-34.8	34.4-35.2	34.4-35.2
800-1500m	34.4-34.6	34.2-34.4	34.2-34.4

Table 4.2: Summary of approximate temperatures and salinities in regions of ATIb0.08, WOA09 and satellite observations. The respective resolutions of the data used are shown in brackets. Regions in ATIb0.08 which are warmer (red) / fresher (blue) than observations are highlighted.

4.4 Discussion

The high resolution HYCOM model of the South Atlantic, ATIb0.08, which is nested within the coarser HYCOM model, ATIa0.25, spanning the Atlantic and Indian oceans is analysed. The base

model is forced on its boundaries by Levitus climatology and both models are atmospherically forced by monthly NCEP/NCAR products (*see* Section 2.3, 2.4). This analysis, together with the knowledge of the configuration parameters, furthers the understanding of the South Atlantic in ocean simulations. Moreover, in order to implement this model for further studies, it is of importance to gauge the limitations of the model.

It is found that with the relatively short spin-up time (12 years) of ATIa0.25, the Atlantic Meridional Overturning Circulation (AMOC) is not fully formed. This can be deduced from Figure 4.2, where the Antarctic Bottom Water cell is not defined. However, the mean AMOC transport of 18.35Sv$\pm$8.04Sv at 26.5°N is within range of observations (Cunningham et al., 2007). With these findings, it is assumed that ATIa0.25 partially resolves the AMOC.

The high resolution configuration, ATIb0.08, does not extend to 26.5°N and so the AMOC transport at this latitude could not be computed as in ATIa0.25; however the AMOC in the South Atlantic at 34.5°S and 24°S was computed and compared to existing observational and model studies. At these latitudes, the AMOC was found to be greater than that of observations (see Table 4.1). The AMOC in ATIb0.08 is therefore over-represented.

In terms of surface circulation in ATIb0.08, the major currents in the South Atlantic sub-tropical gyre are resolved, with some biases:

• Boundary currents are closer to the continents than seen in altimetry (Figure 4.6b)

• The geostrophic velocities in ATIb0.08 are generally greater than that derived from altimetry.

• The Zapiola Gyre is not resolved (Figure 4.10, 4.11). This is a region of important water mass transformation in the South Atlantic (Garzoli and Matano, 2011). With its absence in the model, it is likely that this important component of the South Atlantic Circulation is heavily underestimated (Garzoli and Matano, 2011).

• The Antarctic Circumpolar Current is not accurately resolved (Figure 4.5, 4.12). This has implications for the AMOC circulation and the resolution Antarctic Intermediate Water which is transported to the South Atlantic via the cold water route (Speich et al., 2001) and via the warm water route through the Agulhas System (Fine, 1993).

• There is anomalous circulation between 20°-0°W (Figure 4.5). This may have implications for water mass transformation, as the anomaly is seen to extend to deep waters (Figure 4.17, 4.18).

• Mesoscale activity is under-represented in the south west and south east of the gyre (Figure 4.6a). The underestimation of the variability at the Brazil/Malvinas Confluence and the Agulhas Retroflection may contribute to a misrepresentation of the AMOC volume and heat transport as important mesoscale processes that occur in this region are omitted by the simulation. This underrepresentation of variance, even at high resolution, may in part be explained by monthly mean wind products being used, as opposed to daily wind products (Maltrud et al., 1998).

• Mesoscale activity is over-represented over the anomaly between 20°-0°W (Figure 4.6a).

In terms of hydrography, the distribution of sea surface temperature and salinity match well with observations (Figure 4.14, 4.16) and their distributions are seen to vary seasonally (Figure 4.15, 4.17). However, there is a general positive bias of 2°C in temperature and a negative bias of 0.2 in salinity at the surface. With depth (deeper than 400m), the model is seen to have a negative temperature bias of 2-4°C and a positive salinity bias of 0.2-0.5.

While the model is found to well represent the majority of the South Atlantic, of particular interest is the model's representation of the Agulhas Region, and as to whether it succeeds in producing the level of variability and key trends that have been recorded in observational and other model studies. To this end, the Agulhas System is analysed in greater detail in the following chapter. This is a key region, which has downstream effects on the South Atlantic and the Atlantic Meridional Overturning Circulation (Beal et al., 2011). While there are some indications as to the mean transports and seasonal variability of the Agulhas Current (Bryden et al., 2005; Krug and Tournadre, 2012), there are no long term *in situ* observations. Similarly, the *in situ* measurements of Agulhas Leakage are variable ranging from 2 to 15Sv (Gordon et al., 1992; Garzoli et al., 1996; de Ruijter et al., 1999; Richardson, 2007), and no long term *in situ* measurements have been made. Due to this lack of observational data, model simulations over longer time periods become useful platforms for the study of long term variability in the Agulhas and the inter-relationships that exist in the system.

5 The Agulhas System

In support of modelling the Agulhas System, de Ruijter et al. (1999) state:

"To simulate the interocean exchange, numerical models must describe the Agulhas Current and its retroflection, ring shedding and drift, i.e. the leakage of warm water into the Atlantic, in a qualitatively and quantitatively correct way"

The Agulhas Retroflection is a region of high mesoscale activity (Boebel et al., 2003) and has upstream consequences wider afield such as the AMOC (Beal et al., 2011). According to Beal et al. (2011), a model needs to be of a resolution $>1/10^{\circ}$ in order to capture the mesoscale processes associated with the Agulhas System; however, many eddy permitting numerical models (z-coordinate and hybrid) over a large range of resolutions (from $1/4^{\circ}$ to $1/32^{\circ}$) have problems correctly representing the Agulhas Retroflection and subsequent eddy pathways (Barnier et al., 2006; Penven et al., 2011). Common issues revolve around an early (too far to the east) Agulhas Retroflection position and regular eddy pathway. The consistent biases seen across all ranges of model simulations emphasise the lack of process understanding that there is in this region. The following is a discussion of the model's representation of this crucial region in the global circulation. Key regions of focus are the Agulhas Current, the Retroflection Region and the Cape Basin.

An overview of the Agulhas System is shown in Figure 5.1. The $1/12^{\circ}$ simulation is seen within the $1/4^{\circ}$ simulation bordering the eastern and southern boundaries.

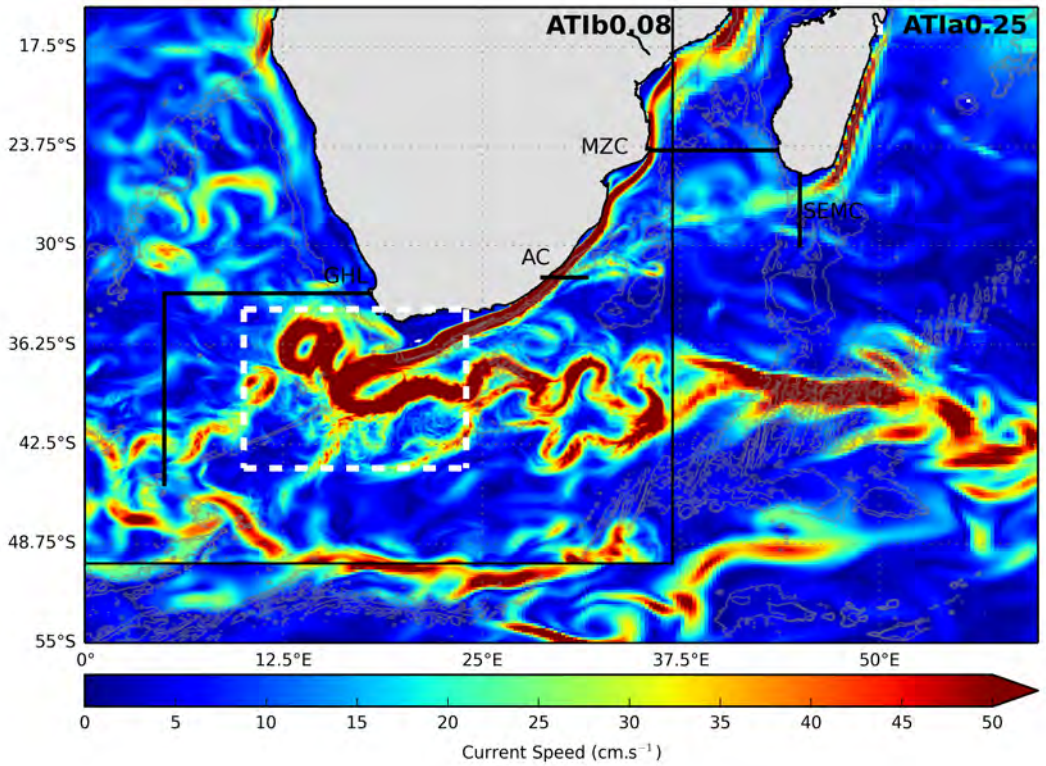

Figure 5.1: Snapshot of the Agulhas System (October 2007) showing current speed (cm.s^{-1}) as represented by ATIb0.08 within ATIa0.25. The boundaries of ATIb0.08 are delineated by the black box. The white dashed lines identify the retroflection region used in analyses which follow. The GoodHope line (GHL), Agulhas Current (AC) transect at 32°S, transect across the Mozambique channel (MZC) and transect across the South East Madagascar Current (SEMC) are identified.

The salient features of the system are identifiable. These comprise of the Mozambique Channel, with a mean southward transport of 11.41Sv (where 1Sv = 1x10^{6}m^3.s^{-1}) at ~23°S , the South East Madagascar Current with a mean westward transport of 56.1Sv (greater than estimates from Nauw et al. (2008) who recorded 32Sv across this line), the Agulhas Current at 32°S with a mean transport of 70.75 $\pm$ 6.43 Sv south, the Agulhas Retroflection, at ~14°E,40°S, Agulhas Rings, eddies and filaments breaking off and moving into the South Atlantic and the Agulhas Return Current meandering eastwards.

5.1 The Agulhas Current

To determine whether the model is representing well the Agulhas Current, a section of the current is extracted from the model and compared to mooring observations available at 32°S. The temperature and salinity along this section is then compared with observational data (Argo floats) and climatological data (WOA09). Finally, the Agulhas Current transport variability and trends are explored, with reference to the available literature.

5.1.1 Structure of the Agulhas Current

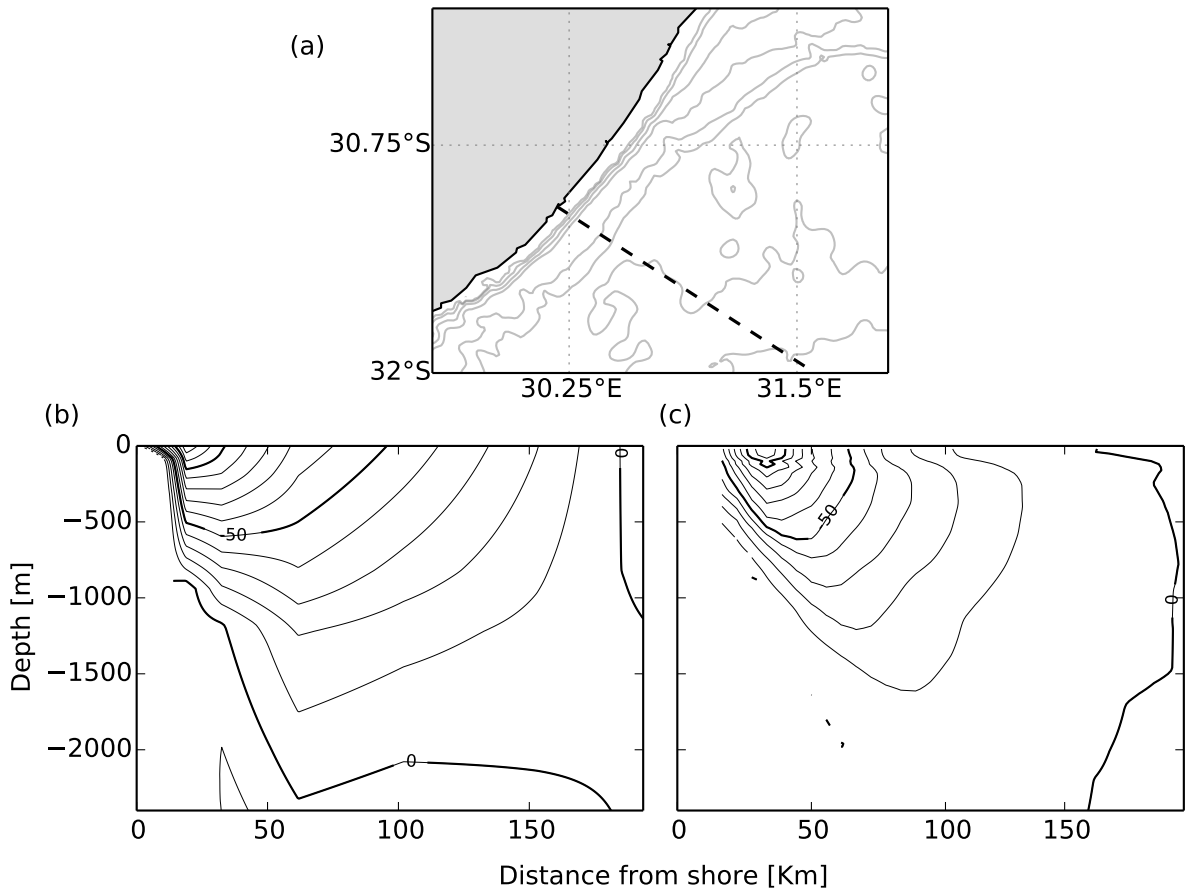

Figure 5.2: Figure showing (a) Location of cross-section of the Agulhas Current (AC) at 32°S, (b) meridional velocity of AC in Bryden et al. (2005) (c) snapshot of meridional velocity of AC in ATIb0.08.

The structure of the Agulhas Current resolved by ATIb0.08 is comparable to observations from a mooring array across 32°S (Bryden et al., 2005; Figure 5.2). The Agulhas Current exhibits the typical characteristic of a Western Boundary Current, with velocity isolines sloping steeply towards the coast coupled with strong poleward velocities. The 50cm/s and 100cm/s isolines are located

at depths of ~600m and ~100m respectively, similar with observations. While the overall structure is similar in ATIb0.08 compared with the structure published by Bryden et al. (2005), the Agulhas Current in ATIb0.08 has a narrower width (~125km) compared to Bryden et al. (2005) where the Agulhas Current has a width of ~160km. In contrast to observations, the model does not simulate the Agulhas Undercurrent (Beal and Bryden, 1997). The mean transport computed by ATIb0.08 in 1995 is 76.24±6.89Sv is comparable to Bryden et al. (2005) who compute a mean of 79.40±17.4Sv. HYCOM has a lower standard deviation than observations, indicating that variability in the current in underrepresented. This is also reflected in the Sea Surface Height (SSH) variance plot (Figure 4.3).

5.1.2 Hydrographics

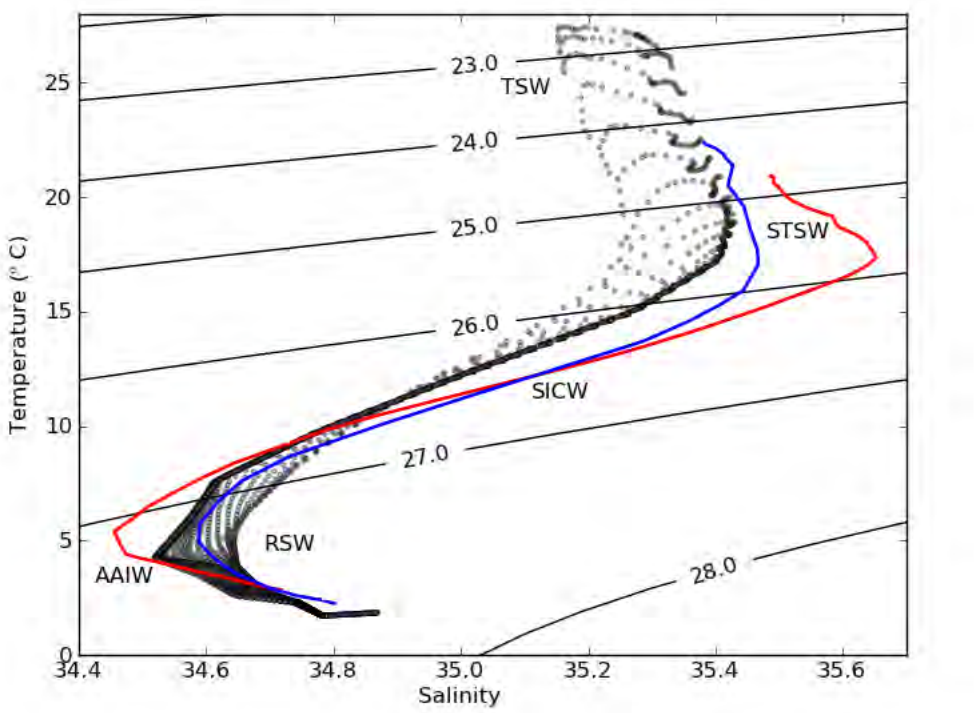

Figure 5.3: T/S plot at 32°S. Gray dots indicate ATIb0.08 along the transect. The blue line is WOA09 and the red line is a mean of Argo floats from 2000-2005.

The water masses located along this transect identified in observations (Beal and Bryden, 1999) are also identified in the model output (Figure 5.3). See Table 1.1 for a summary of the water mass characteristics. Sub-Tropical Surface Water (STSW) and Tropical Surface Water (TSW) make up the surface waters. The thermocline waters are composed mostly of South Indian Central Water

(SICW). Red Sea Water (RSW, identifiable by a high salinity at depth), and Antarctic Intermediate Water (AAIW, identifiable by a salinity minimum at depth) contribute to the intermediate layer depth water mass composition. Neutral densities greater than 28kg/m^3 are characteristic of North Atlantic Deep Water (NADW), which rounds the Cape Agulhas to flow from the southeast Atlantic into the Southwest Indian Ocean at depths greater than 2000m. RSW is commonly found within 100km offshore (Beal and Bryden, 1999), while AAIW and NADW are found between 100-200km offshore and SICW, TSW, STSW are located across the whole current. NADW (T<2; S>34.8; $\gamma > 28.0$.) is not resolved. This may be linked to the AMOC not being fully resolved in the base model (*see* Section 4.1).

There are some differences in the temperatures and salinities of Argo floats and WOA09 in Figure 5.3. The model data is more similar to WOA09 than to Argo. Salinity in the model is very similar to WOA09 although it is slightly less salty at the surface. The model is also less salty at the surface and more salty at depth in comparison with Argo float data. The model is warmer by about 2°C than both WOA09 and Argo.

5.1.3 Agulhas Current Transport

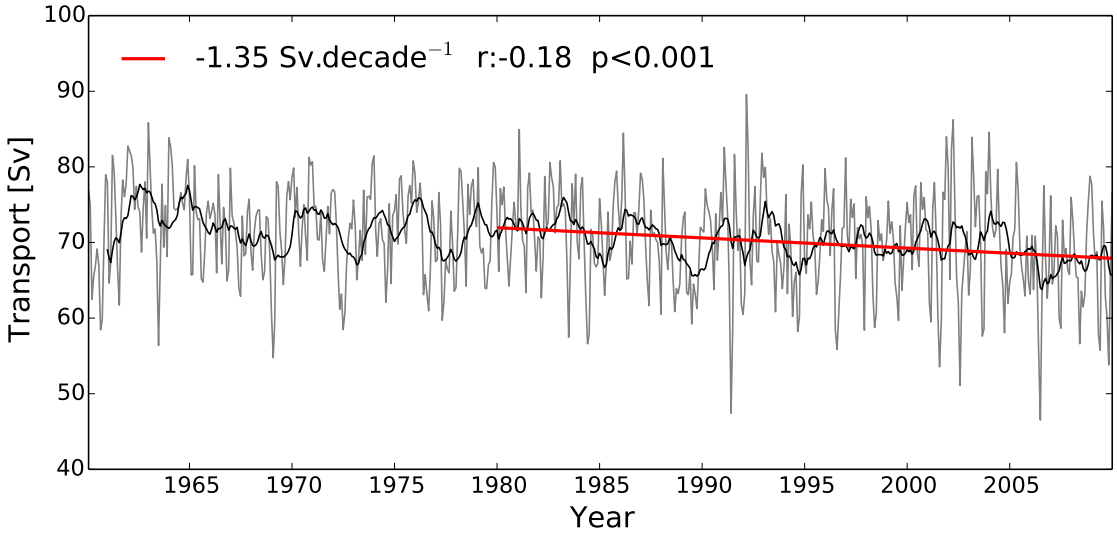

Figure 5.4: Variability of Agulhas Current transport (1960-2009) at 32°S. The annual running mean of the transport are overlayed in black. A trend line is shown for the period 1980-2009.

The interannual and interdecadal variability of the Agulhas Current transport for the full-time period of the model simulation is plotted in Figure 5.4. For the full-time period, there is a mean volume

transport of 70.75 ± 6.43 Sv. There is a significant ($p<0.001$) decrease in Agulhas Current volume transport since the 1980s. Although this contradicts the findings by Rouault et al. (2009) who found an increasing Agulhas Current transport, it is in agreement with the findings by Biastoch et al. (2009), van Sebille et al. (2009) and Loveday et al. (2014) who forced their models with the CORE dataset (Large and Yeager, 2008). In line with the NCEP/NCAR product used in this study, the westerly winds have been found to be increasing since 1980s. This shows that the strength of the Agulhas Current is not entirely Sverdrupian, and other forcing mechanisms play a role as well in determining variability of Agulhas Current transport.

5.1.4 Summary

To summarise, the model simulation shows:

• The Agulhas Current as narrower in width (~130km) compared to observations from Bryden et al. (2005) (~170km).

• The depths (~100m and ~550m) of the 50cm/s and 100cm/s isolines are similar to observations from Bryden et al. (2005).

• The Agulhas Undercurrent is not identified in the model.

• Agulhas Current volume transport (76.24±6.89Sv) is within range of the mean transport reported by Bryden et al. (2005) (79.40±17.4Sv); however the standard deviation in ATIb0.08 is lower, indicating an under-representation of variability in the model.

• Surface and thermocline waters are warmer (~2°C) and fresher (~0.2) than those of observations. This trend is consistent with the trend seen in Section 4.3.

• North Atlantic Deep Water (NADW) is not resolved. This may be related to the model not fully resolving the AMOC as well as the fact that NADW is transported along the Agulhas Undercurrent, which was not identified in the model.

• For the period 1960-2009, Agulhas Current volume transport in ATIb0.08 has a mean of 70.75 ± 6.43 Sv. There is a significantly decreasing trend in the volume transport since the 1980s, in line with the trends found in the simulations of Biastoch et al. (2009), van Sebille et al. (2009) and Loveday et al. (2014).

5.2 The Agulhas Retroflection Region

To determine the model's representation of the Retroflection Region (identified in Figure 5.1.) a number of features are analysed:

• The position of the retroflection is compared to altimetry. This is key to the Agulhas System as, depending on the longitudinal position, the amount of Agulhas leakage can increase (too far west, e.g. Speich et al., 2006) or decrease (too far east, e.g. van Aken et al., 2013).

• The model output along the GoodHope line (*see* Figure 3.3; Swart et al., 2008) is compared to observations.

• The variability and trends in the mesoscale activity are computed using a timeseries (1960-2009) of eddy kinetic energy (EKE) in the Retroflection Region.

• Variability in the inter-ocean exchange (or northwestward transport) is also computed.

5.2.1 Position of the retroflection

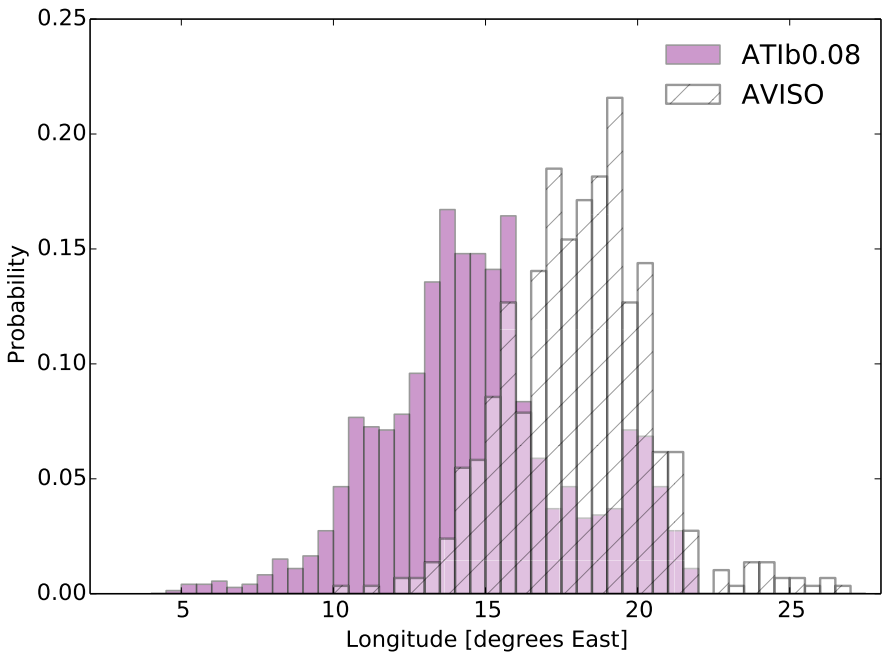

Figure 5.5: Probability distribution of retroflection longitudes for ATIb0.08 (purple bars) and AVISO (grey bars) in the time period 1993-2009.

The position of the Agulhas Retroflection is explicitly tracked in ATIb0.08 and compared with AVISO altimetry (Figure 5.5, refer to the methods in Section 3.2.3). Altimetry show an approximate

Gaussian distribution centred around 18.5°E. This observed pattern is consistent with the findings by Dencausse et al. (2010b). ATIb0.08 does not follow this distribution exactly. The model displays two peaks, with the higher, and more defined peak being centred to the west 13.5°E and the other to the east over 20°E. This is similar to the model findings by Loveday et al. (2014), but in contrast to previous model simulations where the retroflection is positioned too far to the east (Penven et al., 2011). The westward bias of the retroflection is a consequence of overly smoothed topography (Speich et al., 2006), resulting in an overly expressed leakage. Model configurations with more accurate topography succeed better in reproducing the position of the retroflection (Loveday, 2014). In the observations, extreme upstream retroflections have been seen to occur (e.g. the early retroflection in 2001; van Aken et al., 2013) which results in a decrease in Agulhas Leakage; however, from 1993-2009, the model simulation never shifts further east than 22°E.

5.2.2 Hydrographics

Looking at the hydrographics, temperature (Figure 5.6) and salinity (Figure 5.7) vertical profiles from the Bonus GoodHope Cruise (February-March 2008, Speich and Dehairs 2008; *see* track in Figure 3.3) are compared with ATIb0.08 output during the same time period. Because of the high mesoscale variability of the Agulhas Region, direct comparisons of the model output with observational data are not expected to correspond in detail. It was thus anticipated that ATIb0.08 would not resolve the Agulhas Ring that is identifiable in the cruise data at $\pm$44°S. The signal of the Agulhas Current System extends deeper in the model simulation than seen in the cruise data, indicating that the Agulhas Current may be somewhat too barotropic in ATIb0.08.

In the upper 500m, the profiles are the most similar with the 12 degree isotherm extending to about 42°S and to a depth of 400m in both the model and cruise data. Similarly, salinities in the isohaline of 35.2 extend to about 38°S and to 400m. In the salinity profile, it is again seen how ATIb0.08 is under-representing the salinity values by between 0.2-0.4 (also seen in the Agulhas Current in Figure 5.3 and in the South Atlantic in Section 4.3). The model is also not resolving very well the input of less saline water at depth (Antarctic Intermediate Water, AAIW), between 500-1000m, towards the south. The AAIW signal is seen in the cruise data.

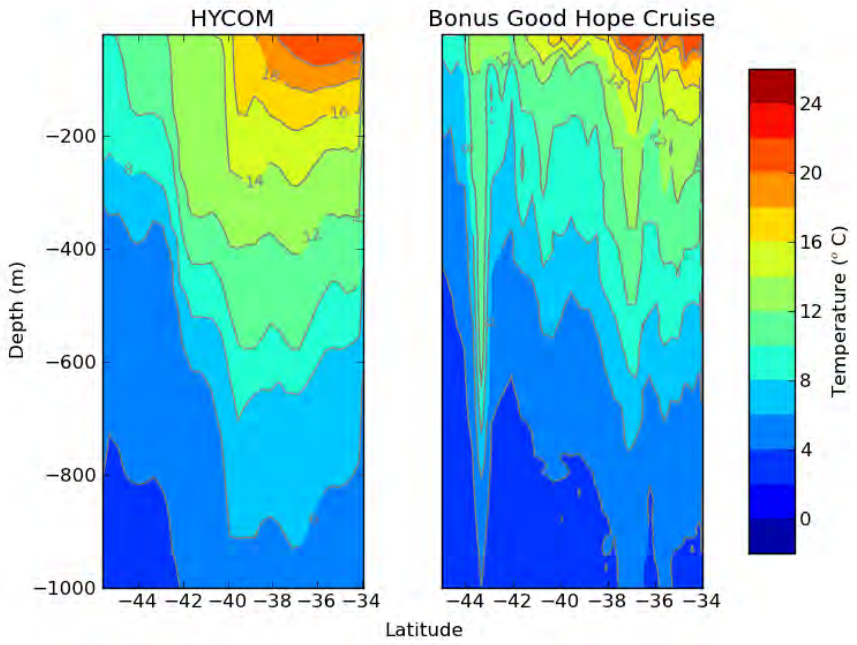

Figure 5.6: Vertical sections of temperature along the GoodHope Line. Left, HYCOM and right, Bonus GoodHope Cruise

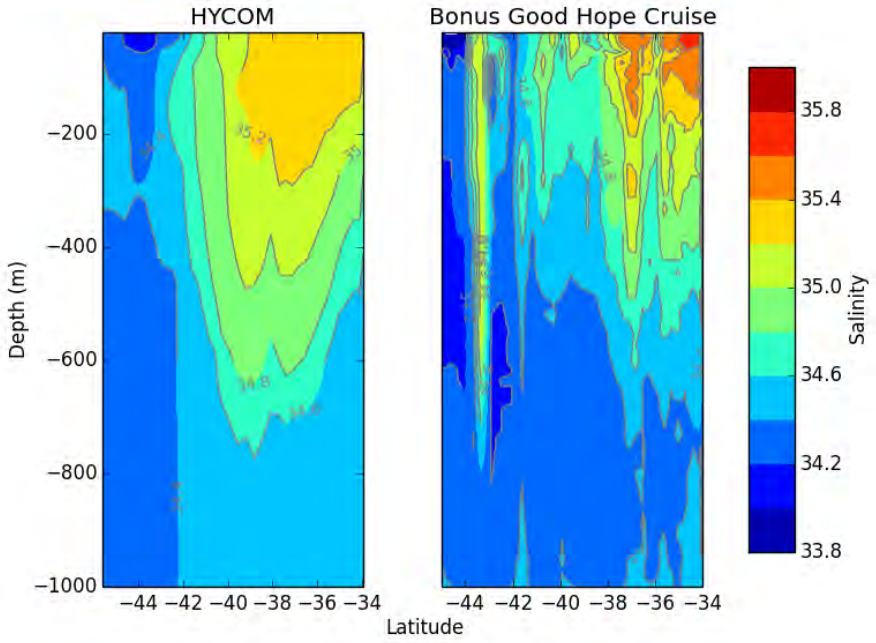

Figure 5.7: Vertical sections of salinity along the GoodHope Line. Left, HYCOM and right, Bonus GoodHope Cruise

5.2.3 Mesoscale variability

Recently, Backeberg et al. (2012), using altimetry data demonstrated an increasing trend (from 1993-2008) in eddy kinetic energy (EKE) over the Agulhas Retroflection region. This was linked to the increasing strength of the Indian Ocean trade winds. The Agulhas region is also known to experience multi-decadal climate variability (Allan et al., 1995; Reason, 2000).

The mesoscale variability is represented in the EKE derived from surface velocities in ATIb0.08. EKE is calculated from surface meridional and zonal velocities in the retroflection region from 1960-2009. The annual means in this region are plotted in Figure 5.8. There is an increasing trend from 1960-1980. While there is interannual variation in mesoscale variability, the mean EKE does not show any increasing or decreasing trends since the 1980s. This result contradicts the trend observed by Backeberg et al. (2012).

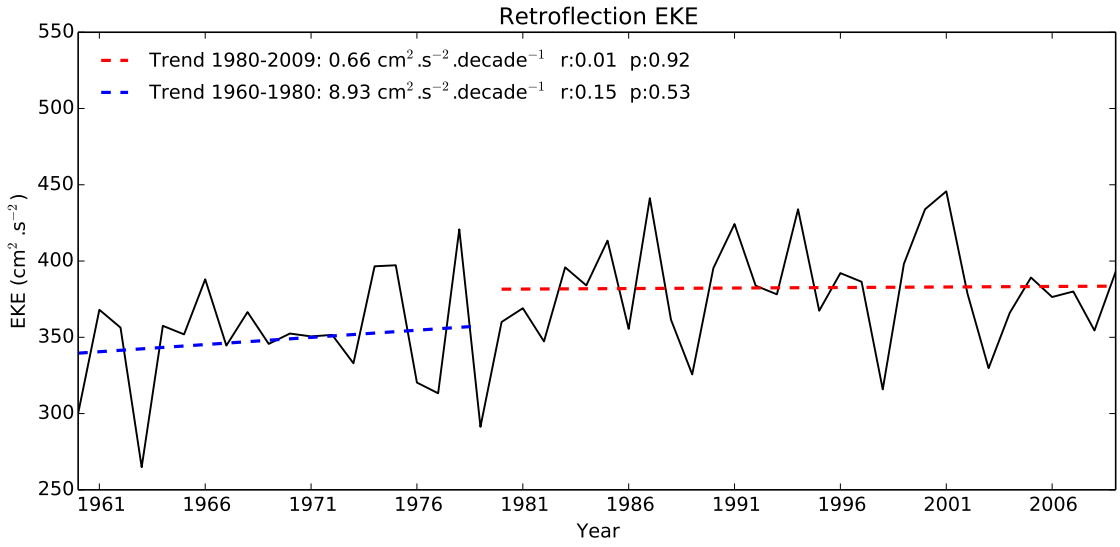

Figure 5.8: Yearly means (1960-2009) of eddy kinteic energy in retroflection region box (identified in Figure 5.1.1). An increasing trend is seen from 1960-1980, however it is not significant. No significant trend is found in the EKE since the 1980s.

5.2.4 Indo-Atlantic Interocean exchange

The Cape Basin (cape cauldron) is a region of turbulent mixing of eddies, rings and filaments (Boebel et al., 2003). There are few direct observations of total Agulhas Leakage and they vary from 4 Sv (Garzoli et al., 1996) to 15Sv (Gordon et al., 1992; Richardson, 2007). The water that enters the South Atlantic through this mechanism substantially changes the hydrography of the region, contributing up to 50% Indian Ocean waters (Garzoli and Goni, 2000). As has been previously highlighted, there is evidence that Agulhas Leakage influenced the Atlantic Meridional Circulation during previous interglacials (Peeters et al., 2004), which makes this exchange of water of key interest in our current changing climate (Beal et al., 2011).

There are four pathways whereby waters enter the South Atlantic through the Agulhas System:

1. Advection inside Agulhas Rings (Gordon, 1986) and in smaller cyclonic and anticyclonic eddies which arise through ring splitting (Schouten et al., 2000; Boebel et al., 2003).
2. Via filaments (Lutjeharms and Cooper, 1996).
3. Through the direct leakage of predominantly intermediate waters (de Ruijter et al., 1999).
4. As a coastal jet at the shelf edge (Bang and Andrews, 1974).

In general, the majority of inter-ocean flux is thought to occur through Agulhas rings, occluded from the retroflection at a rate of 5 ± 1 year^{-1} (Schouten et al., 2002). Contributions from cyclonic eddies (Hall and Lutjeharms, 2011), filaments (Lutjeharms and Cooper, 1996) and through direct flow are thought to be of secondary importance.

Van Sebille et al. (2010) compared Eularian and Lagrangian methods for calculation of Agulhas Leakage in a model simulation. It was found that Eularian methods of leakage calculations underestimate leakage by a factor of 2. A similar result was found by (Loveday, 2014), where only 56% of the leakage was captured by this method. The Lagrangian approach which has been favoured by many recent studies (Speich et al., 2001; Doglioli et al., 2006; Biastoch et al., 2008b, 2009; van Sebille et al., 2009). While flexible, this approach typically excludes diffusive processes, and it is possible that offline calculations decrease precision in turbulent regions. Loveday (2014) utilised a passive tracer methodology as an alternative method for calculation of Agulhas Leakage. Le Bars et al. (2014) have recently computed 20 years of Agulhas Leakage from satellite SSH, and while they

managed to compute the anomalies with good accuracy, their method was not accurate enough for calculations of absolute Agulhas Leakage.

Following the complexity of Agulhas Leakage calculations, no attempt was made to calculate the leakage in this study. A proxy for interocean exchange was computed for this study to extract the variability and trends of all the warm and salty water that moves into the South Atlantic. An Eularian method, similar to that used by van Sebille et al. (2010) was applied, using a threshold of 15°C and salinity of 35.2 for northwestward transport across the GoodHope line (Swart et al., 2008) as indicated in Figure 5.1. The thresholds used were based on those used by Loveday (2014), however the salinity threshold was reduced by 0.2 as ATIb0.08 has been found to underestimate salinity (*see* Figure 5.3). The threshold methodology is graphically illustrated in Figure 5.9, showing the two transects that are masked according to the threshold criteria. The integrated masked zonal velocity (multiplied by -1 to make velocity positive to the west) is added to the integrated masked meridional velocity resulting in an estimate of northwestward transport. It can be seen in Figure 5.9 that the total transport is inevitably underestimated through this technique.

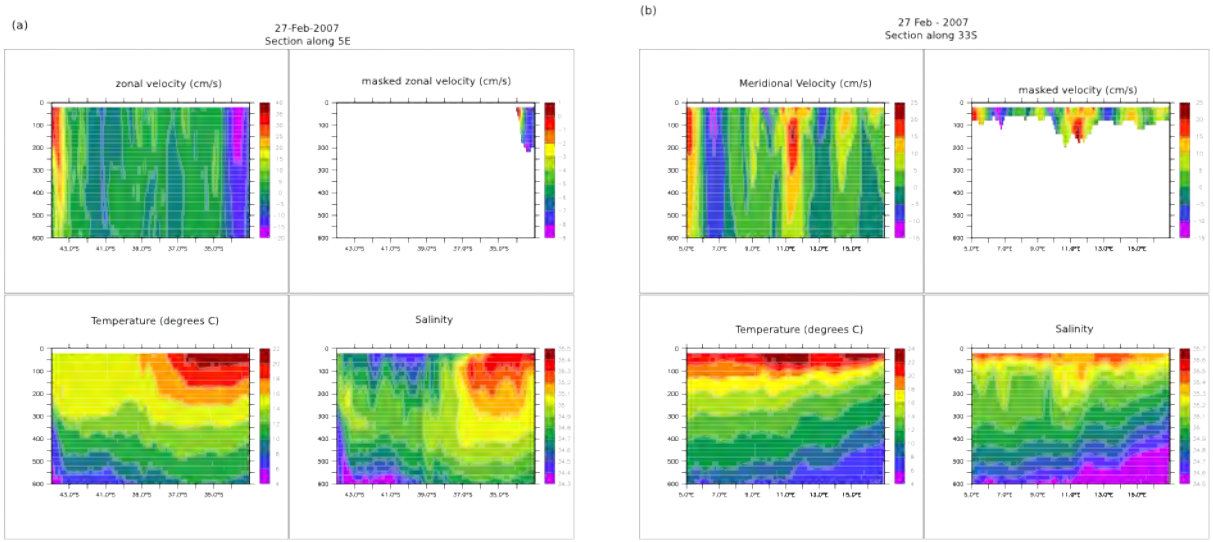

Figure 5.9: (a) Selection of water to integrate along 5E, (b) selection of water to integrate along 33S. The full transect is shown in Figure 5.1

It is found that there is no significant trend at the 5% level of confidence in the northwestward transport of water within the thresholds chosen since the 1980s. This is in contrast to the findings by other studies based on hindcast simulations, where an increasing trend in northwestward transport or Agulhas Leakage has been found (Biastoch et al., 2008a; Rouault et al., 2009; van Sebille et al., 2009; Biastoch et al., 2009; Le Bars et al., 2014).

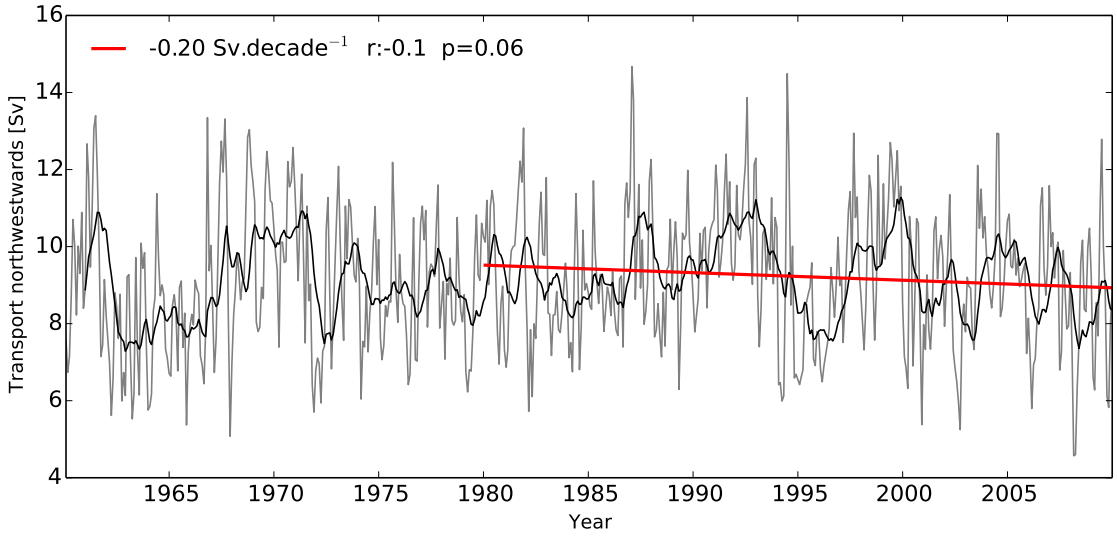

Figure 5.10: Northwestward transport across the GoodHope line marked in Figure 5.1.

5.2.5 Summary

In summary, the retroflection position is also seen to be well represented, although it is shifted to the west. Hydrographically, along the GoodHope Line, ATIb0.08 well represents temperature and salinity in comparison with observations. There are no significant trends in EKE since the 1980s. Similarly, no significant trends are seen in the northwestward transport across the GoodHope line.

5.3 Cape Basin eddies

The Cape Basin is a region of high mesoscale activity (Boebel et al., 2003) and the study of eddy characteristics and flow provides further insight into the dynamics of this region. Eddies are produced all over the world's oceans and in general are associated with the instability of zonal currents and fronts. These currents generate meanders that grow, close in on themselves and pinch off (e.g. Kurushio Rings). The difference between this type of eddy generation and the eddies formed in the Cape basin at the Agulhas retroflection and other similar retroflections, is that these eddies tend to be always produced in the same location and correspond to a primarily zonal protrusion of the source current, suggesting a different formation mechanism.

A number of studies have proposed factors that influence the formation of eddies. It has been shown that eddies are influenced by the flow direction of the jet at the separation from the coast (Ou and de Ruijter, 1986). Boudra and Chassignet (1988), in an isopycnic model, proposed that it is mixed barotropic and baroclinic instability in the strong shear zone of the retroflection loop which results in ring shedding. This suggests that changes in the stability of the system will have an effect on the ring shedding. Furthermore, Boudra and Chassignet (1988) highlighting the importance of the continental configuration within model simulations, found that a triangular landmass produced more rings than its rectangular counterpart. More recently, Nof and Pichevin (1996) introduced the “Retroflection Paradox”, using the North Brazil Current as an example. They describe how the process of a current which turns back from its original direction due to a separation from its guiding wall produces an unbalanced flow force or momentum imbalance. This is compensated for by the shedding of eddies in the current's original direction. They show that without the shedding of the eddies, the retroflection would not exist. This idea was then successfully applied to the Agulhas Retroflection (Pichevin et al., 1999), showing that the production and shedding of eddies is intrinsic to the momentum balance of the system and therefore not the result of any other factor such as transport fluctuations, boundary conditions or instabilities.

The simulation of eddies has been seen to depend on the vertical coordinate system, governing equations, boundary conditions and details of geometry, all of which have direct impacts on the number of model rings formed, their lifetime, and propagation speeds (Chassignet, 1992). The configuration used for ATIb0.08 is discussed in Chapter 2. The SSH variance seen in Figure 4.3

shows the distribution of eddy activity in the model but does not give insight into the individual eddies. In order to quantify this HYCOM configuration's success in reproducing the eddies, an eddy dectection algorithm is used (described in Section 3.2.4). Only eddies with lifetimes longer than 60 days are analysed

Initially, to determine if the scales and paths of simulated Agulhas Rings are consistent with those observed, an eddy tracking algorithm is implemented. These statistics, together with the information on the model setup can also be used to gain further insight into simulating eddies in this region. The results are first compared with altimetry in the period 1993-2009, after which the algorithm is applied to the full-time period of the model simulation from 1960-2009 to look at long term trends.

5.3.1 Eddy distribution

The eddy detection algorithm was implemented first for the entire ATIb0.08 model domain and then concentrated within the retroflection region identified in Figure 5.1 for a more detailed analysis. The focus of this section is on the eddies tracked within the retroflection region.

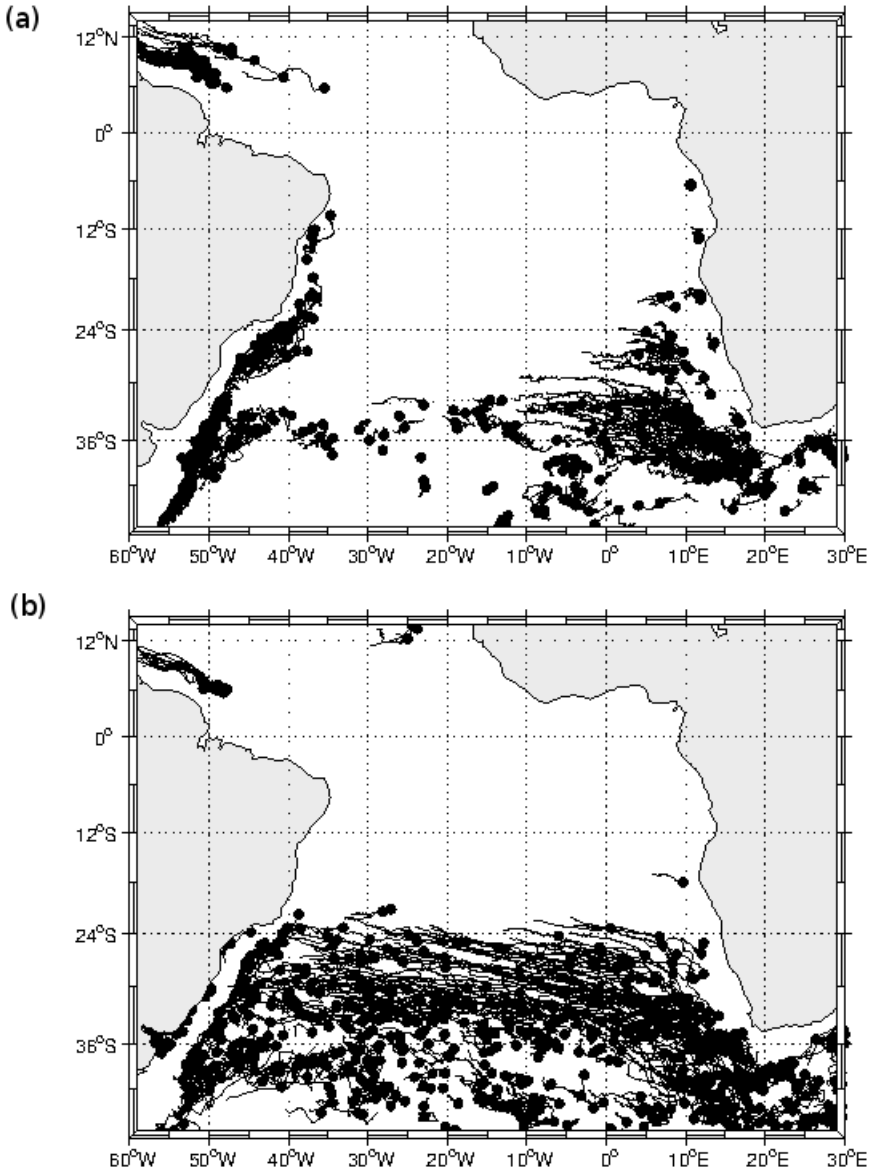

Figure 5.11: Comparison of anticyclonic eddy tracks detected by the eddy detection algorithm in (a) ATIb0.08 and (b) AVISO for the time period 1993-2009. The solid circles indicate where the eddies were initially detected.

Figure 5.11 shows the anticyclonic eddies tracked in (a) ATIb0.08 and (b) AVISO for the period 1993-2009. The regions of eddy occurance in ATIb0.08 and AVISO are in concordance with the distribution of SSH variance seen in Figure 4.6. In ATIb0.08, eddies are identified in the Cape Basin in the southeast of the South Atlantic, in the northwest, at the North Brazil Current, in the west

along the Brazil Current and at the Brazil/Malvinas Confluence (BMC) and in the south between 10-0°W in the erroneous region of the model. In AVISO, eddies are also identifiable in the Cape Basin, at the North Brazil Current, along the Brazil Current and at the Brazil/Malvinas Confluence. Eddy tracks across the South Atlantic along the Agulhas eddy propagation corridor are also identified. This pattern in AVISO altimetry has been previously detected by Souza et al. (2011a), and highlights how in ATIb0.08 the Agulhas eddy tracks do not extend as far west as seen in observations. Many of the anticyclonic eddies in ATIb0.08 that are formed off the Agulhas Retroflection do not remain coherent structures past the Walvis Ridge and are subducted more rapidly than seen in altimetry (*see* Figure 5.13 for the location of the Walvis Ridge).

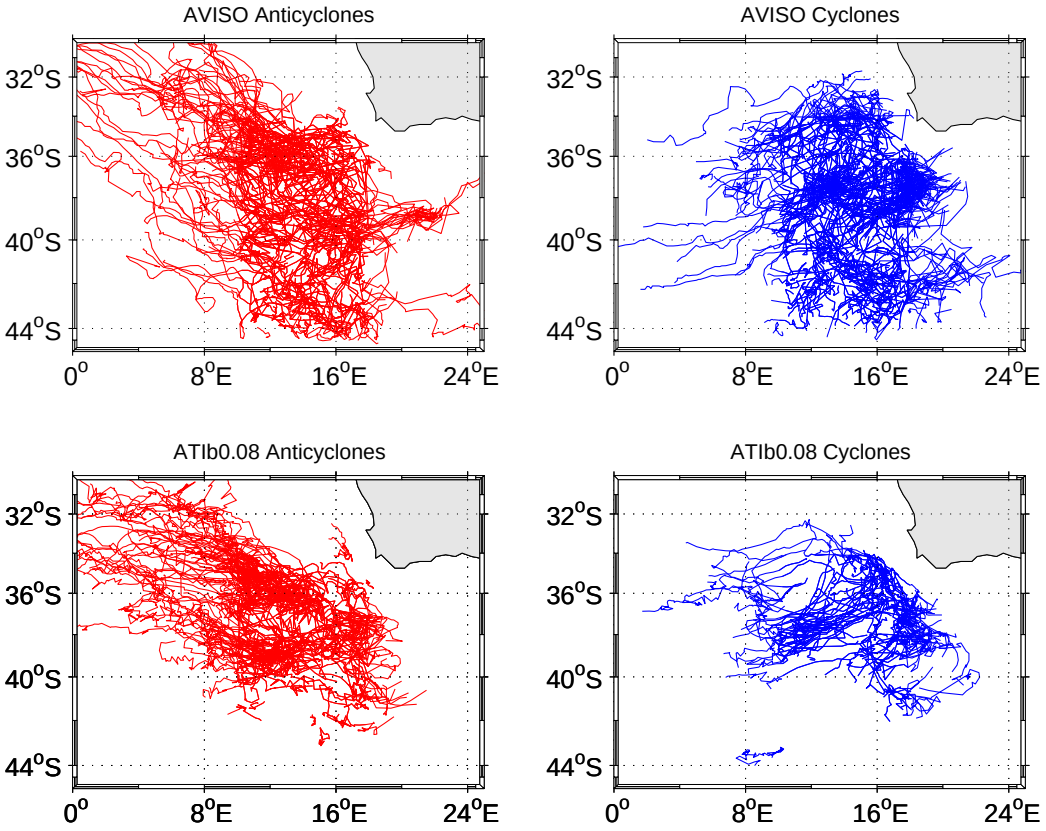

Figure 5.12: Pathways of anticyclonic and cyclonic Agulhas eddies (lifetime > 60 days) into the South Atlantic in ATIb0.08 and AVISO altimetry for the time period 1993-2009. Top Panel: AVISO. Bottom Panel: ATIb0.08. Eddies are tracked which initiated between 10°-24°E and 34°-44°S as identified in Figure 5.1, Anticyclones are depicted in red, cyclones in blue.

Figure 5.12 shows the anticyclonic and cyclonic eddies tracked in the retroflection region in (a) ATIb0.08 and (b) AVISO for the period 1993-2009. The eddies identified in ATIb0.08 are confined further north than those in observations, again in concordance with the SSH variance structure of the region seen in Figure 4.6.

Many model simulations struggle with reproducing a realistic pathway of Agulhas rings into the South Atlantic, tending to produce pathways that are too regular (Barnier et al., 2006; Garzoli and Matano, 2011). Dencausse et al. (2010a), using altimetry data from 1992-2006, defined three routes (South, Central and North) of Agulhas rings into the South Atlantic, delineated by bathymetric features (*see* Figure 5.13).

The southern route is defined as eddies that move south initially and then track over the Agulhas Ridge, the central route is defined as eddies that track between the Agulhas Ridge and the Schmitt-Ott Seamount and Erica Seamount and the northern route is defined as eddies that track north of the Erica Seamount. About half of the rings tracked in their study were observed to follow the central route. They note how Agulhas rings tend to subdivide into rings with diverging northward and southward drift directions, mostly due to interactions with bathymetry (Dencausse et al., 2010a). These bathymetric features are identified in Figure 5.13 below. It can be seen that the low resolution bathymetry used in the model configuration (ETOPO5) does not resolve the details of these important bathymetric features.

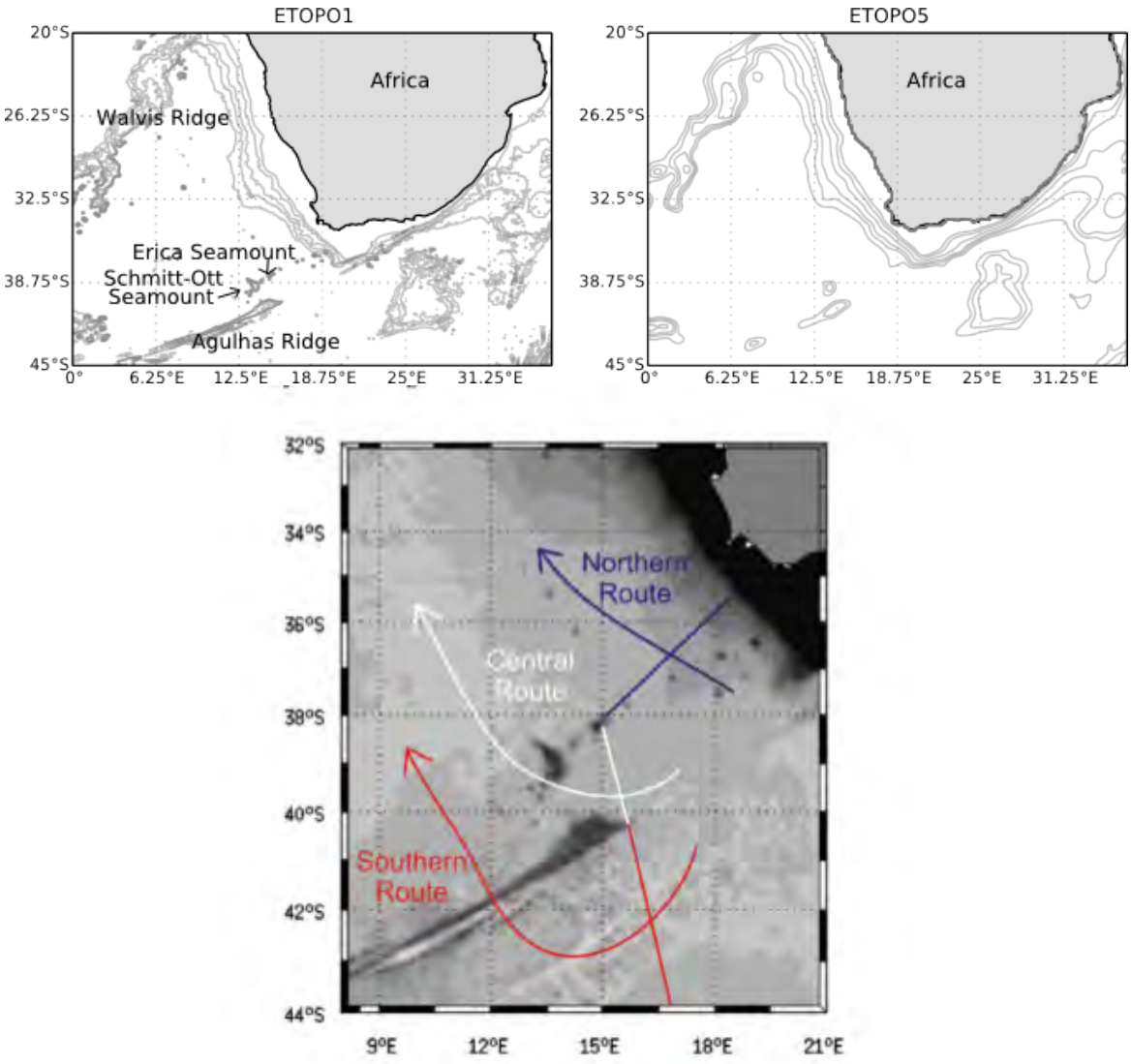

Figure 5.13: Bathymetry in the Agulhas Region resolved by ETOPO1 (left) and ETOPO5 as used by the model (right). The Agulhas Ridge, Schmitt-Ott Seamount and Erica Seamount is identified. The Agulhas Ridge and seamounts are not as well defined in ETOPO5 bathymetry as they are in ETOPO1, which is higher resolution. Bottom panel: The Southern, Central and Northern Routes defined by Dencausse et al. (2010a).

The Agulhas eddy pathways in ATIb0.08 are compared with altimetry in Figure 5.12 and Figure 5.14. Observations show eddy tracks that disperse throughout the Cape Basin (Figure 5.12). Anticyclonic eddies in the observations display a wide distribution of eddies within the Cape Basin, with a high density of eddies covering the regions of the northern, central and southern routes (Figure 5.14). Cyclonic eddies are also seen to have a high density near the African coast as they get trapped become trapped in the region (Hall and Lutjeharms, 2011), as well as a high density further south. These patterns are in concordance with those found by Dencausse et al. (2010a).

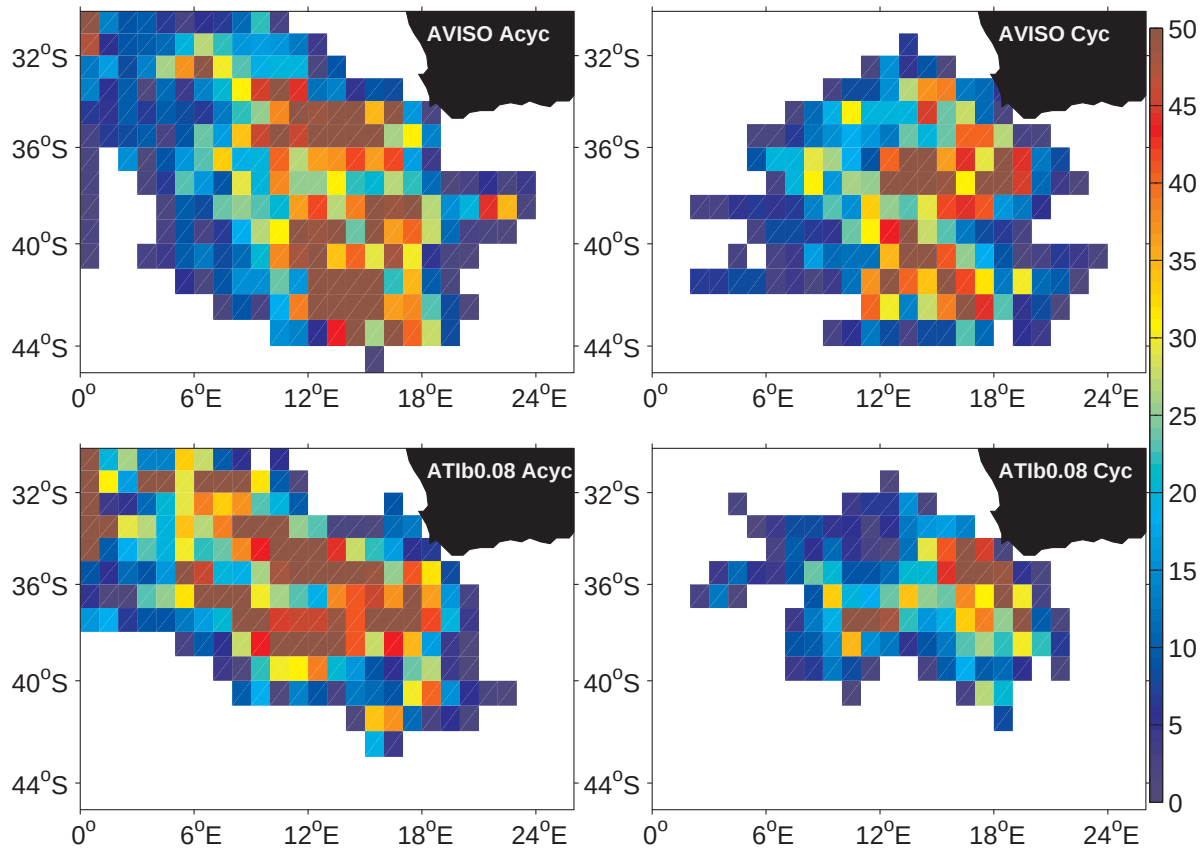

Figure 5.14: Density distribution of anticyclonic and cyclonic eddy pathways. Top Panel: AVISO altimetry. Bottom Panel: ATIb0.08

Extending the same methodology to the model simulation, it is firstly seen that ATIb0.08 produces far fewer eddies than in observations. Secondly, it can be deduced from Figure 5.14 that the anticyclonic eddies in ATIb0.08, diverge from observations distinctly with regards to the southern route. In ATIb0.08 no anticyclonic eddies are seen to be taking this route into the South Atlantic. A contributing factor to eddies not moving southwards may be related to the entire Agulhas System in ATIb0.08 being constrained further north than in reality due to the northward bias of the subtropical front (*see* Figure 4.6). However, the northwestward bias in Agulhas Ring propagation is a common error found in models (Penven et al., 2011).

The effect of eddies that follow the southern route has been discussed by Dencausse et al. (2010a). These eddies enter the sub-antarctic waters of the south of the Subtropical Front (STF), where they undergo modifications through mixing and air-sea exchange (e.g. Arhan et al. (1999)). Because these modifications do not occur to eddies that remain in subtropical waters, they contribute differently to the Indian-Atlantic exchange. Apart from the lack of southern route eddies, ATIb0.08

distinctly shows the central and northern routes, with the bathymetry playing a large role in guiding eddies either south and around the Schmitt-Ott seamount, but above the Agulhas Ridge, or north and around the Erica Seamount.

Moving further into the South Atlantic, once eddies cross the Walvis Ridge their trajectory becomes more westward. Furthermore, it should be remembered that the eddies in ATIb0.08 are quickly subducted , while in AVISO these eddies can be tracked much farther west into the South Atlantic (Figure 5.11).

5.3.2 Eddy characteristics

The surface characteristics of the eddies that initiated within the Agulhas Retroflection region are compared with AVISO for the period 1993-2009. For comparison, the region 10°-24°E and 34°-44°S was chosen, selecting only eddies with lifetimes greater than 8 weeks. The results are summarised in Table 5.1.

Property	ATIb0.08	AVISO
Anticyclones		
Number	9.65 *(±1.85)*	19.06 *(±4.08)*
Radius [km]	72.60 *(±5.54)*	70.21 *(±3.07)*
Amplitude [cm]	24.41 *(±3.84)*	23.40 *(±1.95)*
Meridional Velocity [cm.s^{-1}]	1.43 *(±0.82)*	0.64 *(±0.36)*
Zonal Velocity [cm.s^{-1}]	-2.59 *(±1.04)*	-2.43 *(±0.45)*
Propagation Speed [cm.s^{-1}]	8.83 *(±0.87)*	6.34 *(±0.63)*
Cyclones		
Number	6.35 *(±1.75)*	19.11 *(±3.00)*
Radius [km]	58.90 *(±4.52)*	60.61 *(±2.17)*
Amplitude [cm]	15.98 *(±2.58)*	16.94 *(±1.88)*
Meridional Velocity [cm.s^{-1}]	-1.17 *(±1.04)*	-0.88 *(±0.56)*
Zonal Velocity [cm.s^{-1}]	-2.94 *(±1.17)*	-1.93 *(±0.55)*
Propagation Speed [cm.s^{-1}]	7.83 *(±0.96)*	6.57 *(±0.53)*

Table 5.1: Table showing mean yearly (1993-2009) anticyclonic and cyclonic eddy characteristics in ATIb0.08 and AVISO in the region 10°-24°E and 34°-44°S.

Overall, ATIb0.08 produces fewer eddies than observed in AVISO. Within the region, a mean of 19 anticyclonic eddies and 19 cyclonic eddies are identified per year in AVISO. ATIb0.08 produces a mean of 9 anticyclonic eddies and 6 cyclonic eddies. This is about half the number that is seen in observations. The number of cyclones is also less than the number of anticyclones.

The high number of eddies observed (~19 year^{-1} , which is greater than the average 5 $\pm$ 1 year^{-1} reported by Schouten et al. (2002)) is most likely related to the fact that in this algorithm, eddy splitting is not taken into account and one initial eddy that in the future splits into two, within the retroflection region used for the study would, in this case, be counted as 3 eddies (Arhan et al., 1999). Similarly, with regard to the model output, the under-representation of the number of eddies, seen in the low number of eddies resolved, is emphasised because eddy splitting is not being accounted for.

The radius and amplitudes of both the anticyclonic and cyclonic eddies in ATIb0.08 are similar to those in observations, with ATIb0.08 produced anticyclones slightly larger and cyclones slightly

smaller (radius by ~2km; amplitude by ~1cm; Table 5.1). That Agulhas cyclones have radii smaller than those of Agulhas anticyclones is a characteristic, which has been previously described by Matano and Beier (2003). The mean anticyclonic eddy meridional velocities in ATIb0.08 (1.43±0.82 cm.s^{-1}; Table 5.1) are greater than those in observations (0.64±0.36 cm.s^{-1}; Table 5.1). The anticyclonic zonal velocities in ATIb0.08 are roughly similar to those in observations (ATIb0.08: -2.59±1.04; AVISO: -2.43±0.45 cm.s^{-1}; Table 5.1). The mean cyclonic eddy meridional velocities in ATIb0.08 (-1.17±1.04; Table 5.1) are also greater than those in observations (-0.88±0.56; Table 5.1). Similarly, the mean cyclonic eddy zonal velocities are stronger (-2.94±1.17 cm.s^{-1}; Table 5.1) than those in observations (-1.93±0.55; Table 5.1). While the observations are more similar to the values reported by Boebel et al. (2003) (0.7±0.4 cm.s^{-1} southwards for cyclones and 1.0±0.4 cm.s^{-1} northwards for anticyclones; Table 5.1), ATIb0.08 seems to be consistently producing eddies that move faster. This is again seen in the propagation speeds where anticyclonic eddies in ATIb0.08 propagate ~2 cm.s^{-1} and cyclonic eddies propagate ~1cm.s^{-1} faster than in observations (Table 5.1).

It should be noted that discrepancies within the altimetry data from the values reported by Boebel et al. (2003) are most likely associated with the different altimetry products used, as well as spatial and time scales used in this study. The characteristic of faster propagation speeds reproduced by ATIb0.08 was also found in the study by Loveday (2014) who used the same eddy tracking tool. The same pattern was seen by Doglioli et al. (2007) who tracked eddies using wavelet analysis. The differences may be associated with the model or alternatively may be associated with the difference in time resolutions (ATIb0.08: 4-daily vs AVISO: 7 daily) of the data put into the eddy detection algorithm.

5.3.3 Long term trends of Cape Basin eddies

A number of studies have shown that the Agulhas Leakage has been increasing in strength. Van Sebille et al. (2009) showed that a decrease in the Agulhas Current strength has led to an increase in Agulhas Leakage. While Rouault et al. (2009) found a converse relationship between the Agulhas Current and Agulhas Leakage, they found an increase in Sea Surface Temperature (SST) in the retroflection associated with an increase in Agulhas Leakage. Durgadoo et al. (2013) showed that an increase in westerly wind strength has led to an increase in Agulhas Leakage. Overall, past investigations of this region and its long term trends are inconclusive. In ATIb0.08 some interesting trends have been found since the 1980s:

- The westerly winds that force the model have been significantly increasing in strength (Figure 2.3).
- The Agulhas Current transport at 32^{o}S has been significantly decreasing in strength (Figure 5.4).
- The eddy kinetic energy in the retroflection region of the Cape Basin has shown no significant trends (Fig 5.8).
- The northwestward transport of water warmer than 15^{o}C and more saline than 35.2 does not reflect a significant change in its transport at a 5% level of confidence (Figure 5.9).

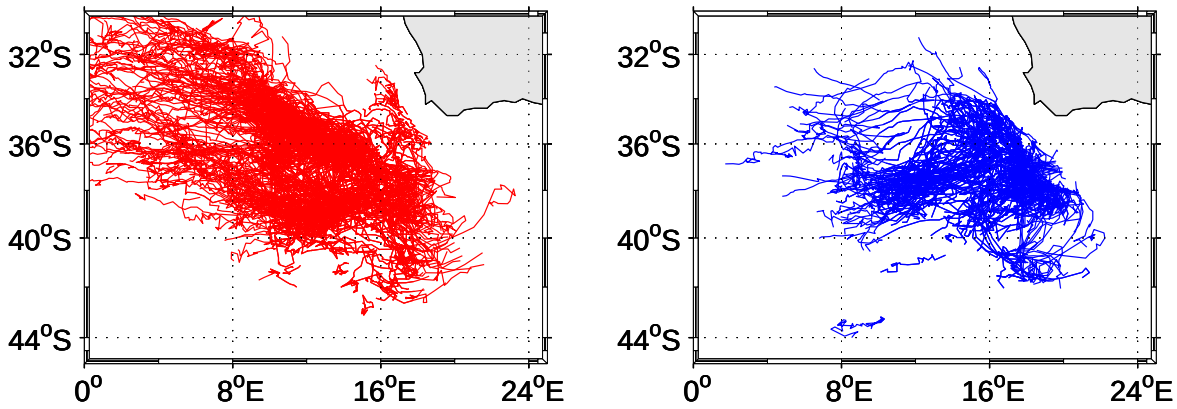

Figure 5.15: Anticyclonic and cyclonic tracks simulated by ATIb0.08 (1960-2009). Anticyclones are in red. Cyclones are in blue.

Alongside these findings, the variability in the eddy component of Indian Atlantic inter-ocean exchange was explored in the model simulation from 1960-2009. Figure 5.15 shows all the eddies

tracked in ATIb0.08 from 1960-2009. This figure is similar to Figure 5.12 where ATIb0.08 was compared with AVISO from 1993-2009.

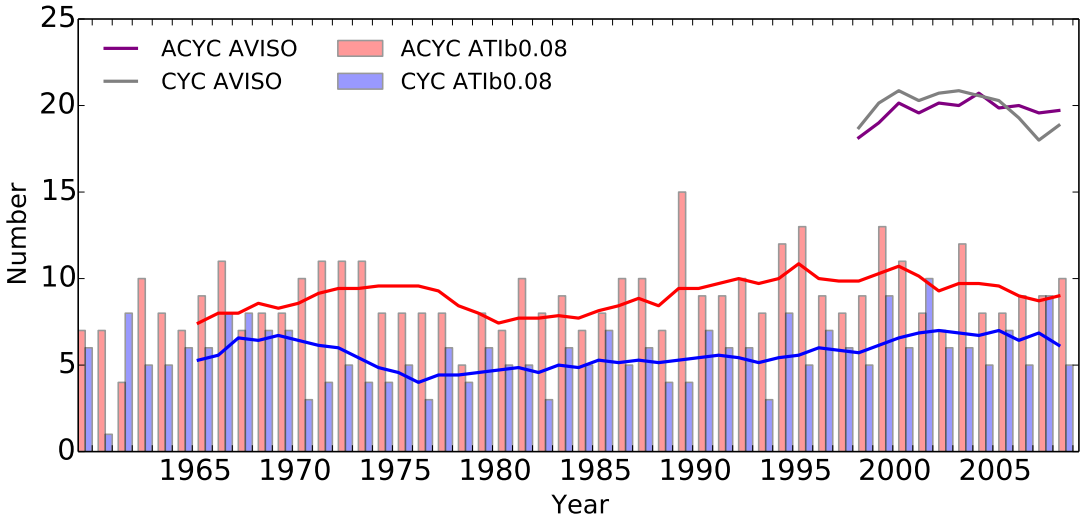

Figure 5.16: Interannual variability in number of anticyclonic and cyclonic eddies tracked in the Retroflection Region of ATIb0.08. 7-year running means are are overlaid in red (anticyclones) and blue (cyclones). 7-year running means of AVISO altimetry output are overlaid in purple (anticyclones) and gray (cyclones).

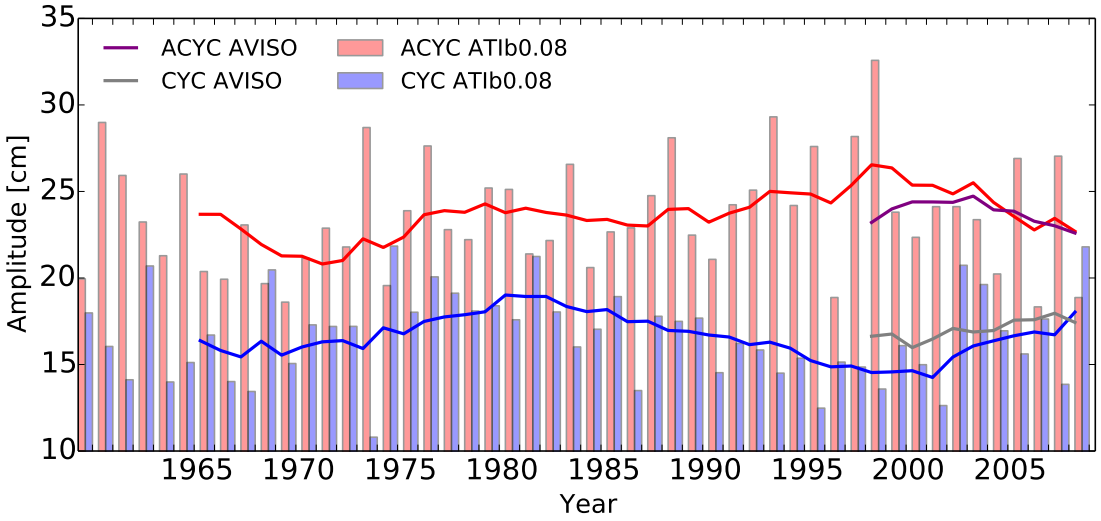

Figure 5.17: Interannual variability in the amplitude of anticyclonic and cyclonic eddies tracked in the Retroflection Region of ATIb0.08. 7-year running means are are overlaid in red (anticyclones) and blue (cyclones). 7-year running means of AVISO altimetry output are overlaid in purple (anticyclones) and gray (cyclones).

Figures 5.16-5.19 summarise the interannual variability in eddy characteristics during the period 1960-2009. Across all variables, eddy number, amplitude, radius and propagation speed, the interannual signal is seen to dominate over decadal signals. No significant decadal trends were found across all eddy properties (*see* Table 5.2); however, there does seem to be decadal variability.

The interannual variability is not consistent across the eddy characteristics indicating that different forcing mechanisms result in the eddies varying in number, amplitude, radius and propagation speed, but that these forcings do not affect aspects of the eddies in the same way. For example, between 1975-1980 the anticylonic eddy speeds increased. The cyclones displayed an inverse reaction, decreasing in speed. At the same time, eddy radii and amplitudes are seen to be slightly increasing. The number of anticyclonic eddies is seen to decrease and the number of cyclonic eddies remains relatively steady. In general the radius and amplitude of the eddies tend to be proportionally related, with the cyclones and anticyclones displaying similar trends. However, this does not always hold for eddy amplitudes. The eddy amplitudes vary more than the eddy radii. From 1960-1985, anticyclonic and cyclonic eddies are seen to vary synchronously but from 1985 to 2000, anticyclonic eddy amplitudes are seen to increase, while cyclonic eddy amplitudes are seen to decrease. At the same time there are only small changes seen in the eddy radii. In terms of eddy propagation speed, the anticyclonic characteristics and the cyclonic characteristics are inversely proportional to each other at times (e.g. 1975-1980), but proportionally related to each other at other times (e.g. 1985-2005). This change in relationship indicates that multiple forcing mechanisms have effects on the eddy propagation speeds and that these vary in dominance.

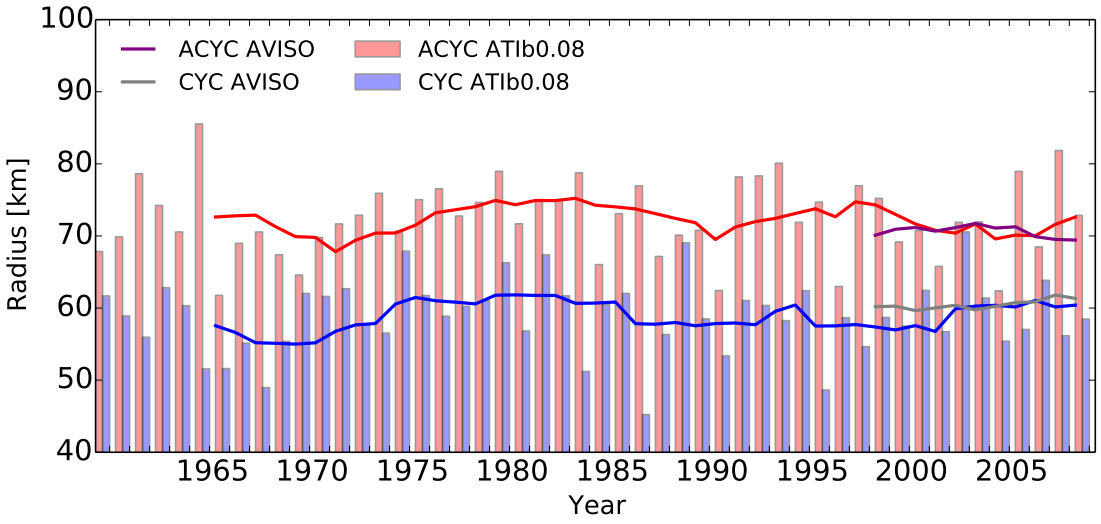

Figure 5.18: Interannual variability in the radius of anticyclonic and cyclonic eddies tracked in the Retroflection Region of ATIb0.08. 7-year running means are are overlaid in red (anticyclones) and blue (cyclones). 7-year running means of AVISO altimetry output are overlaid in purple (anticyclones) and gray (cyclones).

In Figures 5.16 and 5.19 the discrepancy between the model simulation and observations can be clearly seen. The number of eddies formed in ATIb0.08 is less than the number of eddies identified through observations (Figure 5.16) and the propagation speed of eddies is greater in ATIb0.08

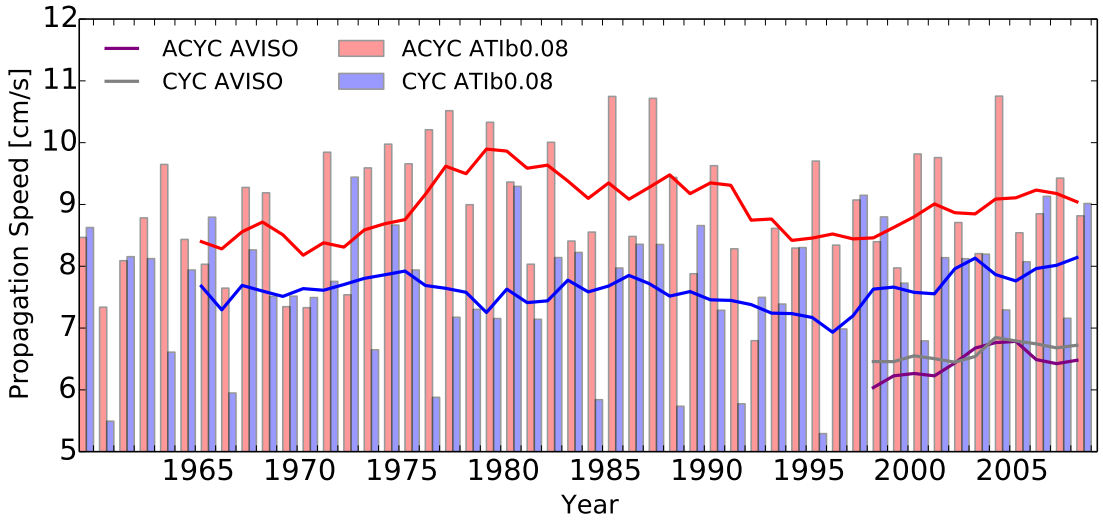

Figure 5.19: Interannual variability in the propagation speed of anticyclonic and cyclonic eddies tracked in the Retroflection Region of ATIb0.08. 7-year running means are are overlaid in red (anticyclones) and blue (cyclones). 7-year running means of AVISO altimetry output are overlaid in purple (anticyclones) and gray (cyclones).

than in observations (Figure 5.19). These differences in the model from observations are similar to the differences found by Loveday (2014) in his ROMS simulation, where the same eddy detection algorithm was applied.

	Mean	Trend	p
Anticyclonic eddies			
Number	8.9	0.39	0.10
Amplitude [cm]	23.6	0.21	0.43
Radius [km]	72.4	0.01	0.97
Propagation Speed [cm/s]	8.9	0.08	0.48
Cyclonic eddies			
Number	5.6	0.27	0.2
Amplitude [cm]	16.7	-0.07	0.8
Radius [km]	58.9	0.20	0.75
Propagation Speed [cm/s]	7.6	0.06	0.28

Table 5.2: Decadal trends in anticyclonic and cyclonic eddies from 1960-2009 in ATIb0.08

From these results, it can be concluded that the eddies in ATIb0.08 are relatively stable, and that the eddy component in ATIb0.08 of the inter-ocean exchange is not showing any significant trends, concurring with the computed eddy kinetic energy (Figure 5.9) and the northwestward transport variability (Figure 5.10).

5.3.4 Summary

The aim of this sub-section was to carry out a detailed analysis of the Cape Basin eddies and their drift. Eddy characteristics and pathways were compared with AVISO altimetry through the period 1993-2009. Overall, the number of eddies is underestimated in ATIb0.08 by ~50% in comparison with observations. Both anticyclonic and cyclonic eddies in ATIb0.08 show similar scales of eddy radii and amplitudes. Eddy velocities and the subsequent eddy propagation speeds are found to be faster in ATIb0.08. With regard to eddy pathways, the eddies in ATIb0.08 are found to differentiate between the central and northern routes described by Dencausse et al. (2010a) but do not show events where eddies follow the southern route. The low resolution bathymetry used in the model may be contributing the eddies not following different tracks. The long term trends in the Cape Basin eddy characteristics were then investigated. While decadal variability is evident in the eddy characteristics, no significant long term trends were found.

5.4 Are trends noticeable in Sea Surface Temperature?

Globally, there has been an increase (0.11°C/decade) in upper ocean temperatures since the 1970s due to enhanced greenhouse gas emission (IPCC AR5, Rhein et al., 2013). The warmer near-surface air temperatures warming the sea surface through surface heat flux changes.

The Sea Surface Temperature (SST) in the retroflection region of the Agulhas System has been increasing since the 1980s at a rate of 0.7°C Rouault et al. (2009). Other than the increase in SST as a result of global warming, the increase here has been linked to an increase in Agulhas Current transport and an increase in westward transport at 18°E. Through paleorecords, Simon et al. (2013) have also shown that, at least in part, temperature and salinity changes seen in the Agulhas corridor might not be neccesarily related to changes in the amount of water being transferred through the Indian-Atlantic Ocean exchange via the Agulhas leakage, but rather a consequence of changes in the hydrographic composition of the Agulhas Current itself.

In ATIb0.08, the mean SSTs have been previously compared to observational data (*see* section 4.3). The model is found to be ~2°C warmer than observational data. This trend is seen again in Figures 5.20 and 5.21; however the variability of the SSTs in ATIb0.08 is highly correlated to that of observational data having correlation coefficients of 0.96 and 0.95 in the Agulhas Current and Agulhas Retroflection respectively.

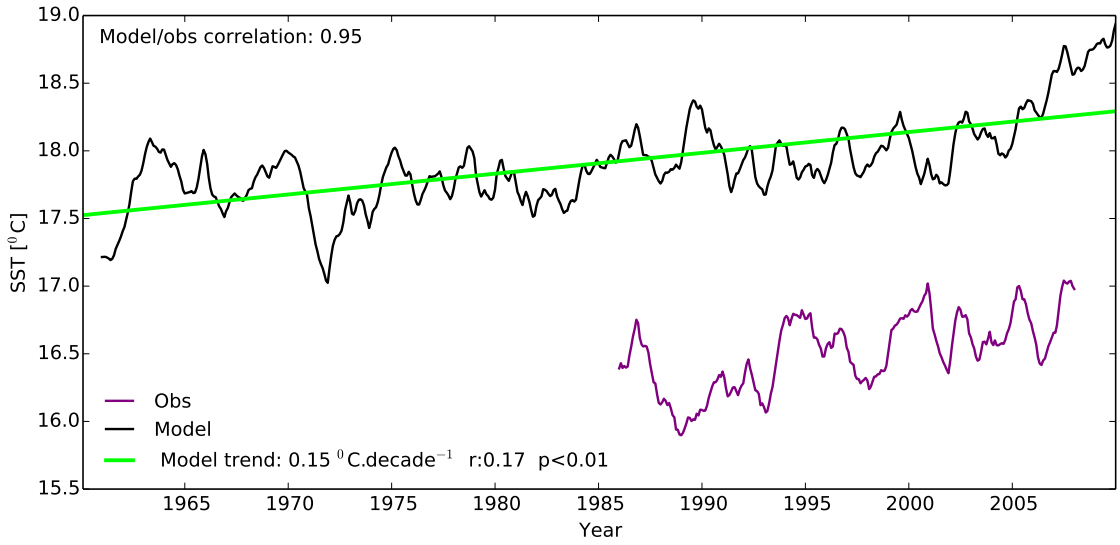

Figure 5.20: 12 month running mean of Sea Surface Temperature (SST) of the Agulhas Retroflection in domain 10°-24°E and 34°-45°S.The black line represents the model output. The purple line represents observational data. An increasing trend in SSTs is found since the 1960s.

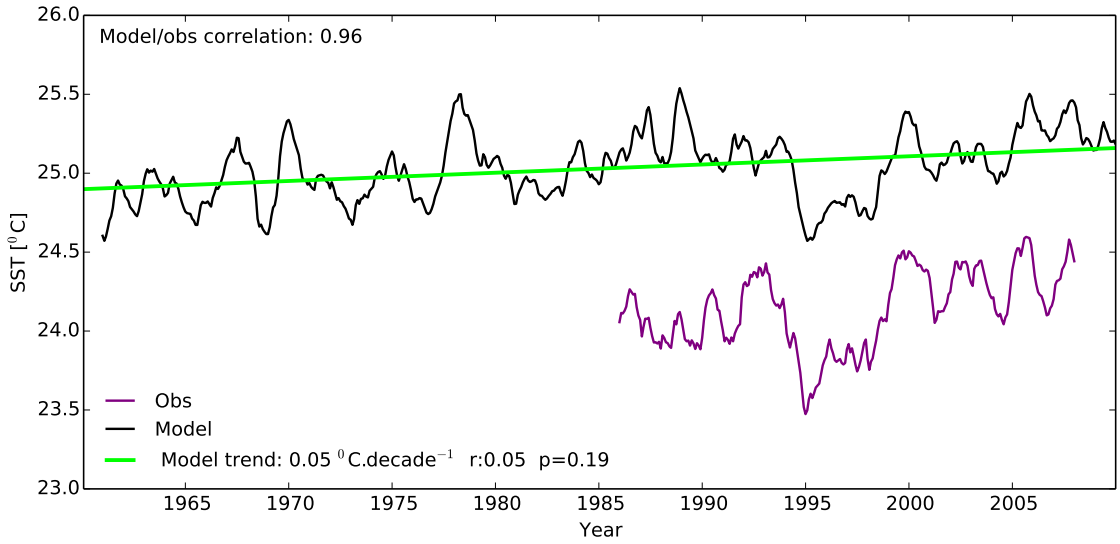

Figure 5.21: 12 month running mean of Sea Surface Temperature (SST) of the Agulhas Current at 32°S.The black line represents the model output. The purple line represents observational data. A slight increasing trend in SSTs is found since the 1960s.

Looking at the SST trend since the 1960s in ATIb0.08, a positively increasing trend is found in the Agulhas Retroflection region (Figure 4.19) and in the Agulhas Current (Figure 4.20). Of note, however, is the difference in the rates of increase at the Agulhas Current and the Agulhas Retroflection. The SSTs in the Agulhas Current have been increasing at a rate of 0.05°C per decade since the 1960s. The SSTs in the Agulhas Retroflection region have been increasing at a rate of 0.15°C per decade since the 1960s. This discrepency in the rates of increase disalign the forcing mechanisms that are causing the increase in surface temperatures in these two regions.

If the only driving force of increased SSTs was atmospheric interactions as a result of global warming, one would expect the rate of increase of SSTs to be similar in these regions, which are within close proximity of each other. Similarly, Simon et al. (2013) have shown how changes in the composition of the water in the Agulhas Current has downstream effects on the water in the Retroflection Region. Once again, this does not fully explain the trends in the Agulhas Retroflection as the rates of changes are different.

Therefore, one suspects another mechanism to be responsible to some extent for the trends seen here. Rouault et al. (2009) linked the increase in SSTs in the Agulhas Retroflection region to an increase in transport of the Agulhas Current. However, such a postulation does not hold in this case as the Agulhas Current transport in ATIb0.08 has shown a decreasing trend (*see* Section 5.1.3). Furthermore, no major trend in the northwestward transport across the GoodHope line has been

identified and concurrently, no significant long term trends were found in mesoscale activity at the retroflection with no significant trends in both eddy kinetic energy and the eddy characteristics. The effects of ENSO and SAM may be another possible cause for the increase in temperatures found at the Agulhas Retroflection region, however, these climatic modes may not be fully resolved in this model simulation as the simulation is closed to the Indonesian Throughflow.

Without the forcing mechanisms proposed by Rouault et al. (2009) and Simon et al. (2013), it is left unclear as to what could be driving the increasing trend in SST anomalies seen in the Retroflection Region in both the model simulation and observations. There is the possibility that the northwestward transport that was computed across the GoodHope line using thresholds is not truely reflecting the actual northwestward transport of Agulhas water, and that possibly this transport is in fact increasing. However, this is unlikely. Similar Eularian methods have been previously implemented in other studies (Rouault et al., 2009; van Sebille et al., 2010; Loveday, 2014), where this Eularian method does reflect multidecadal variability in the transport, although the absolute transport is underestimated by about 50% in comparison to Lagrangian methods.

It can therefore be said that while the SST anomalies are increasing in the retroflection, the primary driving mechanism behind this trend remains undetermined. In part, the positive trend in SST anomalies in the Agulhas Current may be playing a role in increasing the temperature of the water in the retroflection, as found by Simon et al. (2013). However, the temperatures in the Retroflection are increasing at a faster rate than those in the Agulhas Current, implying that another forcing mechanism is at play.

5.5 Discussion

This chapter addressed two key questions:

1. How accurate is the model, ATIb0.08, in representing the Agulhas region in comparison with available observations?

2. How do the trends produced by the model in the Agulhas region compare with the available literature?

At the beginning of the chapter a quote was taken from Weijer et al. (1999), in which they suggest that to simulate interocean exchange, the Agulhas Current, Agulhas Retroflection, the eddies and their drifts need to be quantitively and qualitively represented. These aspects of the Agulhas System were subsequently analysed.

In Section 5.1, the representation of the Agulhas Current in ATIb0.08 as compared to observations was assessed. ATIb0.08 was found to reproduce reported transport values at 32°S with a time mean (1960-2009) of 70.75 $\pm$ 6.43 Sv. Variability of the Agulhas Current transport was found over this time period, with a significant decreasing trend from 1980-2009.

In Section 5.2, the representation of the Agulhas Retroflection in ATIb0.08 in comparison with altimetry observations for the period 1993-2009 and the Bonus GoodHope Cruise in 2008 was assessed. ATIb0.08 was found to reasonably well reproduce the retroflection, with a mean retroflection position of 13.5°E. This is west of that found by observations at 18.5°E, but has avoided the common early retroflection problem experienced by many models (Penven et al., 2011). Hydrographically, salinity and temperature sections along the GoodHope line were found to be similar to observations, with a slight positive temperature bias and negative salinity bias (i.e. warmer and fresher than observations). With regards to the full time period of 1960-2009, no trend was found in the eddy kinetic energy, converse to the findings by Backeberg et al. (2012).

Thereafter, the northwestward transport across the GoodHope line was computed, using temperature and salinity thresholds of 15°C and 35.2 respectively. This was taken as a proxy for interocean exchange via the Agulhas system, from the Indian to the South Atlantic ocean. No significant trend is seen in northwestward transport across the GoodHope line. Possible errors in the Agulhas Leakage

computation may be linked to the methodology used to approximate transport as well as the fact that Agulhas Leakage may be linked to waters that flow through the Indonesian throughflow (Ribbe and Tomczak, 1997), which is closed in the ATIa0.25 configuration - the model that provides the forcing to ATIb0.08 at its boundaries.

In Section 5.3, the Cape Basin eddies and their drift were analysed. Firstly, in comparison with AVISO altimetry from 1993-2009, and secondly only in ATIb0.08 from 1960-2009. ATIb0.08 does not succeed in reproducing eddies that follow the southern route into the South Atlantic; however the model is differentiating between the central and northern routes but low resolution bathymetry may be constricting the model's effectiveness at resolving these pathways. ATIb0.08 under-represents the number of both anticyclonic and cyclonic eddies. These eddies are also seen to propagate faster than those tracked in observations. However, ATIb0.08 reproduces well the eddy radii and amplitudes. Since the 1960s no significant trends were found in the eddy characteristics, although interannual and interdecadal variability is evident.

In Section 5.4, the positive trend seen in SST anomalies in the Retroflection Region is explored. This trend cannot be robustly linked to an increase in Agulhas Current strength as postulated by Rouault et al. (2009), due to the Agulhas Current transport showing a decreasing trend, in contradiction to the findings by Rouault et al. (2009). It also cannot wholely be linked to changes in the composition of the water entering the Retroflection Region from the Agulhas Current as has been found in the paleorecord (Simon et al., 2013).

Drawing all these findings together implies two outstanding points:

1 **Mesoscale variability - reflected in the EKE trend and eddy characteristics - is not linked with changes in transport in the Agulhas System.** The fact that no significant trend in the mesoscale activity was found is in contrast with the trends found in observations by Backeberg et al. (2012). However, this finding supports the "Retroflection Paradox" presented by Pichevin et al. (1999), where it is shown that retroflection eddies are inherent and necessary to the Agulhas Systems momentum balance and are not affected by transport fluctuations, boundary conditions or instabilities.

2 **Changes in the SST at the retroflection region in this simulation are not linked with increasing Agulhas Current strength, in contrast to the findings by Rouault et al. (2009).** This finding demonstrates that the forcing mechanisms behind the warming Agulhas System are still not entirely understood. In part, the warming in the Retroflection Region may be attributed to warming in the Agulhas Current as presented by Simon et al. (2013). However, while the Agulhas Current does show a warming trend, the rate of increase in SST is not the same as the rate of increase in the Retroflection Region.These findings thus indicate that other forcing mechanisms are at play and highlight the need for further study.

6 Conclusions and Perspectives

6.1 Conclusions

Ocean models are tools that can be used in conjunction with observations to further our predictive capabilities and process understanding of the ocean. They become particularly useful in situations where data is lacking or when one wants to exclude or include certain features of the ocean system that is being studied. It is essential to evaluate ocean models in order to improve their ability at reproducing the ocean as well as to gauge to what extent the model deviates from available observations. The closer one gets to accurately reproducing ocean circulation also increases ones understanding of the mechanisms that dominate and drive the ocean. This study contributes to our knowledge base of ocean circulation models, highlighting the limitations of the HYCOM configuration that was used. The deviations that the model has from observations further emphasise the need to use models in conjunction with observations and to continuously improve the available observational database. The study also reveals discrepancies in the long term trends in the model with comparison to available literature on the Agulhas region, accentuating the need for further study and observational platforms.

In conclusion, the HYCOM simulation ATIb0.08 has been thoroughly analysed in the South Atlantic ocean with particular focus on the Agulhas Region.

With regard to the South Atlantic ocean, it is concluded that the combination of the parameterisations and forcings used to configure the HYCOM simulation, ATIb0.08, is successful in reproducing the mean circulation in the South Atlantic, with a few deviations

from observations. ATIb0.08 is seen to under-represent mesoscale variability, specifically at the Brazil/Malvinas Confluence and in the Agulhas System. The temperature and salinity at the surface and with depth are found to differ from observations in being slightly warmer and fresher. The seasonal signals in sea surface temperatures and salinities are reproduced. Anomalous mesoscale activity occurs over the mid-atlantic ridge. This anomaly in seen at the surface and reaches to depth in the temperature and salinity sections.

In the Agulhas System, it is concluded that the HYCOM model, ATIb0.08, resolves the Agulhas Region, although faces similar challenges that are seen in many model simulations (i.e. eddies which consistently follow a similar trajectory into the South Atlantic; Penven et al., 2011). It is felt that the model would benefit from a higher resolution bathymetry product and daily wind forcings due to the system being dominated by mesoscale processes. The main points of difference and similarity are summaried in the following paragraph:

In comparison to observations, the Agulhas Current structure, transport and hydrogaphy is found to be reasonably well reproduced. Similarly to the South Atlantic, the model exhibits warmer and fresher water than in observations in this region. Agulhas Current transport in ATIb0.08 is less variable than in observations. The Agulhas retroflection position is found to be shifted to the west, with a mean of 13.5°E as opposed to 18.5°E seen in observations. Fewer eddies are formed, and these eddies propagate faster than in observations; however, the eddy radii and amplitudes are similar to observations. While there is evidence that anticyclonic eddies follow the central and northern routes into the South Atlantic, they do not follow the southern route into the Cape Basin as seen in observations.

On examination of the trends produced in ATIb0.08 with reference to the available literature two conclusions can be drawn. Firstly, **trends in mesoscale activity are not related to transport changes in the Agulhas Current**. This is due to the fact that while the Agulhas Current transport shows a decreasing trend in contrast to the finding by Rouault et al. (2009), but in agreement with the simulations used by Loveday (2014), Biastoch et al. (2009) and van Sebille et al. (2009), the mesoscale scale activity does not show a similar trend to that of the Agulhas Current. Eddy Kinetic Energy in the retroflection region shows no significant trends conversely to the study by Backeberg et al. (2012) using observations and Loveday (2014) in a ROMS simulation. Furthermore, no

significant trends are found in eddy characteristics since the 1960s.

Secondly, **the trends seen in SST anomalies in the retroflection are not related to transport changes in the Agulhas Current**, in contradiction to Rouault et al. (2009). This trend may, in part, be explained by a warming Agulhas Current but this does not account for the whole story. Other forcing mechanisms must play a role to account for the magnitude of the warming trend seen in the retroflection compared to that of the Agulhas Current.

6.2 Perspectives

In this study an analysis of a $1/12^{\circ}$ resolution HYCOM simulation of the South Atlantic, with particular detail given to the Agulhas Region has been performed.

From the study, a few recommendations have been drawn together for future research. As the spin-up time of 12 years did not allow the model to fully resolve the Atlantic Meridional Overturning Circulation (MOC), it is recommended that longer spin-up times be used in the future however acknowledged that to simulatie the Atlantic MOC requires hundreds of years of spin-up time. Improved observations of the MOC in the South Atlantic with the continuation of the SAMOC project will also contribute to the improvement of simulations in this region. The fact that the model was not nested within a full global model resulted in the exclusion of oceanic teleconnections such as the Indonesion Throughflow. The ocean signal of atmospheric teleconnections such as the Southern Annular Mode and the El Niño-Southern Oscillation would also not be entirely resolved. It is therefore recommended that models be nested within full global models to ensure that the model is able to capture global teleconnections, but to completely resolve these processes requires a coupled ocean-atmosphere model. In terms of the Agulhas Region, which is strongly influenced topographic steering, it is also recommended that higher resolution bathymetry be used in model configurations of this region. Also to be noted is a caveat in the conclusions made in Chapter 5. The uncertainty around the Agulhas Leakage proxy that was computed results in a certain amount of uncertainty in the conclusion. The study could therefore be more robust with the use of a more trusted method for this calculation.

While some conclusions were able to be drawn from the results of this study, some key areas for

further research that were beyond the scope of the study remain outstanding. Of particular interest are the possible driving mechanisms behind the interannual and interdecadal variability in the eddy characteristics. Furthermore, there is scope for research into the question raised pertaining to the forcing mechanisms of the positive sea surface temperature trend simulated in the Retroflection Region of the Cape Basin. These studies would require the use of a model designed specifically to simulate the Agulhas Region, which is nested within a global model and uses a high resolution bathemetry product.

Acknowledgments

This thesis would not have been possible without the funding provided by NRF, the SAMOC-SA programme, the Nansen-Tutu Center and the India-Africa-Brazil Fund and the academic guidance provided by my supervisors, Isabelle Ansorge, Chris Reason, Bjorn Backeberg and Edmo Campos. The support given from Bjorn Backeberg is deeply appreciated. Thanks also goes to Edmo Campos for hosting me at the University of São Paulo. Help from other scientists also deserves acknowledgement; that of Paola Castellanos for her support in São Paulo, Ben Loveday and Jonathan Durgadoo for their insight and Pierrick Penven for making the eddy detection algorithm available. My warm and inviting office at the University of Cape Town that is filled with supportive and helpful fellow students and friends was crucial to the completion of this thesis. I would also like to thank Wizard, for sitting with me throughout the final writing phase of the thesis, my family and friends for supporting me through the difficult times and Paulo for loving me everyday.

Bibliography

Alexander, M., Blade, I., Newman, M., Lanzante, J., Lau, N., and Scott, J. (2002). The Atmospheric Bridge: The Influence of ENSO Teleconnections on Air-Sea Interaction over the Global Oceans. *Journal of Climate*, 15:2205–2231.

Allan, R., Lindesay, J., and Reason, C. (1995). Multidecadal Variability in the Climate System over the Indian Ocean Region during the Austral Summer. *Journal of Climate*, 8:1853–1873.

Ansorge, I. and Lutjeharms, J. (2007). The Cetacean Environment off Southern Africa. In Best, P. and Folkens, P., editors, *Whales and Dolphins of the Southern African subregion*, pages 1–13. Cambridge University Press.

Ansorge, I. J., Baringer, M. O., Campos, E. J. D., Dong, S., Fine, R. A., Garzoli, S. L., Goni, G., Meinen, C. S., Perez, R. C., Piola, A. R., Roberts, M. J., Speich, S., Sprintall, J., Terre, T., and Van den Berg, M. A. (2014). Basin-Wide Oceanographic Array Bridges the South Atlantic. *Eos, Transactions American Geophysical Union*, 95(6):53–54.

Ansorge, I. J., Speich, S., Froneman, P. W., Rouault, M., and Garzoli, S. (2005). Monitoring the oceanic flow between Africa and Antarctica: Report of the first GoodHope cruise. *South African Journal of Science*, 101:29–35.

Antonov, J. I., Seidov, D., Boyer, T. P., Locarnini, R. A., Mishonov, A. V., Garcia, H. E., Baranova, O. K., Zweng, M. M., and Johnson, D. R. (2010). Volume 2: Salinity. In Levitus, S., editor, *World Ocean Atlas 2009*, volume 2, page 184. NOAA Atlas NESDIS 69, U.S. Government Printing Office, Washington,D.C.

Arhan, M., Mercier, H., and Lutjeharms, J. R. E. (1999). The disparate evolution of three Agulhas rings in the South Atlantic Ocean. *Journal of Geophysical Research*, 104(C9):20987.

Auer, S. J. (1987). Five-year climatological survey of the Gulf Stream system and its associated rings. *Journal of Geophysical Research*, 92(C11):11709.

Backeberg, B. C., Penven, P., and Rouault, M. (2012). Impact of intensified Indian Ocean winds on mesoscale variability in the Agulhas system. *Nature Climate Change*, 2(8):608–612.

Bang, N. D. and Andrews, W. R. (1974). Direct current measurements of a shelf edge frontal jet in the southern Benguela system. *Journal of Marine Science*, 32:405–417.

Bard, E. and Rickaby, R. E. M. (2009). Migration of the subtropical front as a modulator of glacial climate. *Nature*, 460(7253):380–3.

Barnier, B., Madec, G., Penduff, T., Molines, J.-M., Treguier, A.-M., Sommer, J., Beckmann, A., Biastoch, A., Böning, C., Dengg, J., Derval, C., Durand, E., Gulev, S., Remy, E., Talandier, C., Theetten, S., Maltrud, M., McClean, J., and Cuevas, B. (2006). Impact of partial steps and momentum advection schemes in a global ocean circulation model at eddy-permitting resolution. *Ocean Dynamics*, 56(5-6):543–567.

Beal, L. and Bryden, H. (1997). Observations of an Agulhas Undercurrent. *Deep Sea Research I: Oceanographic Research Papers*, 44(9):1715–1724.

Beal, L., Chereskin, T., Lenn, Y., and Elipot, D. (2006). The Sources and Mixing Characteristics of the Agulhas Current. *Journal of Physical Oceanography*, 36:2060–2074.

Beal, L. M. and Bryden, H. L. (1999). The velocity and vorticity structure of the Agulhas Current at 32S. *Journal of Geophysical Research*, 104(1998):5151–5176.

Beal, L. M., De Ruijter, W. P. M., Biastoch, A., and Zahn, R. (2011). On the role of the Agulhas system in ocean circulation and climate. *Nature*, 472(7344):429–36.

Beal, L. M., Field, A., and Gordon, A. L. (2000). Spreading of Red Sea overflow waters in the Indian Ocean. *Journal of Geophysical Research*, 105:8549–8564.

Behrens, E., Biastoch, A., and Böning, C. W. (2013). Spurious AMOC trends in global ocean sea-ice models related to subarctic freshwater forcing. *Ocean Modelling*, 69:39–49.

Beron-Vera, F., Wang, Y., Olascoaga, M., Goni, G., and Haller, G. (2013). Objective Detection of Oceanic Eddies and the Agulhas Leakage. *Journal of Physical Oceanography*, 43:1426–1438.

Biastoch, A. and Böning, C. W. (2013). Anthropogenic impact on Agulhas leakage. *Geophysical Research Letters*, 40(6):1138–1143.

Biastoch, a., Böning, C. W., and Lutjeharms, J. R. E. (2008a). Agulhas leakage dynamics affects decadal variability in Atlantic overturning circulation. *Nature*, 456(7221):489–92.

Biastoch, A., Böning, C. W., Schwarzkopf, F. U., and Lutjeharms, J. R. E. (2009). Increase in Agulhas leakage due to poleward shift of Southern Hemisphere westerlies. *Nature*, 462(7272):495–8.

Biastoch, A., Lutjeharms, J. R. E., Böning, C. W., and Scheinert, M. (2008b). Mesoscale perturbations control inter-ocean exchange south of Africa. *Geophysical Research Letters*, 35(20):L20602.

Bleck, R. (2002). An oceanic general circulation model framed in hybrid isopycnic-Cartesian coordinates. *Ocean Modelling*, 37:55–88.

Bleck, R. and Smith, L. T. (1990). A wind-driven isopycnic coordinate model of the north and equatorial Atlantic Ocean: 1. Model development and supporting experiments. *Journal of Geophysical Research*, 95(C3):3273–3285.

Boebel, O., Lutjeharms, J., Schmid, C., Zenk, W., Rossby, T., and Barron, C. (2003). The Cape Cauldron : a regime of turbulent inter-ocean exchange. *Deep-Sea Research II: Topical Studies in Oceanography*, 50:57–86.

Boudra, D. and Chassignet, E. (1988). Dynamics of Agulhas Retroflection and Ring Formation in a Numerical Model. Part 1: The Vorticity Balance. *Journal of Physical Oceanography*, 18:280–303.

Broecker, W. S. (1991). THE GREAT OCEAN CONVEYOR. *Oceanography*, 4(2):79–89.

Bryden, H. L., Beal, L. M., and Louise, M. D. (2005). Structure and Transport of the Agulhas Current and Its Temporal Variability. *Journal of Oceanography*, 61(1980):479–492.

Bryden, H. L., King, B. A., and McCarthy, G. D. (2011). South Atlantic overturning circulation at 24S. *Journal of Marine Research*, 69(1):38–55.

Brydon, D., Sun, S., and Bleck, R. (1999). A New Approximation of the Equation of State for Sea Water, Suitable for Numerical Ocean Models. *Journal of Geophysical Research*, 104:1537–1540.

Cai, W. (2006). Antarctic ozone depletion causes an intensification of the Southern Ocean super-gyre circulation. *Geophysical Research Letters*, 33(3):L03712.

Chassignet, E. (1992). Rings in Numerical Models of Ocean General Circulation: A Statistical Study. *Journal of Geophysical Research*, 97:9479–9492.

Chelton, D. B., Schlax, M. G., and Samelson, R. M. (2011). Global observations of nonlinear mesoscale eddies. *Progress in Oceanography*, 91(2):167–216.

Chelton, D. B., Schlax, M. G., Samelson, R. M., and de Szoeke, R. A. (2007). Global observations of large oceanic eddies. *Geophysical Research Letters*, 34(15):L15606.

Chidichimo, M. P., Kanzow, T., Cunningham, S. A., Johns, W. E., and Marotzke, J. (2010). The contribution of eastern-boundary density variations to the Atlantic meridional overturning circulation at 26.5N. *Ocean Science*, 6:475–490.

Clark, P. U., Pisias, N. G., Stocker, T. F., and Weaver, A. J. (2002). The role of the thermohaline circulation in abrupt climate change. *Nature*, 415:863–869.

Cunningham, S., Kanzow, T., Rayner, D., Baringer, M. O., Johns, W. E., Marotzke, J., Longworth, H. R., Grant, E. M., Hirschi, J. J.-M., Beal, L. M., Meinen, C. S., and Bryden, H. L. (2007). Temporal variability of the Atlantic meridional overturning circulation at 26.5N. *Science*, 317(5840):935–8.

Cunningham, S. and Marsh, R. (2010). Observing and modeling changes in the Atlantic MOC. *Wiley Interdisciplinary Reviews: Climate Change*, 1:180–191.

Davis, R., Killworth, P., and Blundell, J. (1996). Comparison of Autonomous Lagrangian Circulation Explorer. *Journal of Geophysical Research*, 101:855–884.

De Ruijter, W. (1982). Asymptotic Analysis of the Agulhas and Brazil Current Systems. *Journal of Physical Oceanography*, 12:361–373.

de Ruijter, W. P. M., Biastoch, A., Drijfhout, S. S., Lutjeharms, J. R. E., Matano, R. P., Pichevin, T., van Leeuwen, P. J., and Weijer, W. (1999). Indian-Atlantic interocean exchange: Dynamics , estimation and impact. *Journal of Geophysical Research*, 104:20,885–20,910.

de Ruijter, W. P. M., Ridderinkhof, H., Lutjeharms, J. R. E., Schouten, M. W., and Veth, C. (2002). Observations of the flow in the Mozambique Channel. *Geophysical Research Letters*, 29(10):140–1–140–3.

Dencausse, G., Arhan, M., and Speich, S. (2010a). Routes of Agulhas rings in the southeastern Cape Basin. *Deep Sea Research Part I: Oceanographic Research Papers*, 57(11):1406–1421.

Dencausse, G., Arhan, M., and Speich, S. (2010b). Spatio-temporal characteristics of the Agulhas Current retroflection. *Deep Sea Research Part I: Oceanographic Research Papers*, 57(11):1392–1405.

Dijkstra, H. A. and de Ruijter, W. P. M. (2001). On the Physics of the Agulhas Current: Steady Retroflection Regimes. *Journal of Physical Oceanography*, 31(10):2971–2985.

Doglioli, A. M., Blanke, B., Speich, S., and Lapeyre, G. (2007). Tracking coherent structures in a regional ocean model with wavelet analysis: Application to Cape Basin eddies. *Journal of Geophysical Research*, 112(C5):C05043.

Doglioli, A. M., Veneziani, M., Blanke, B., Speich, S., and Griffa, A. (2006). A Lagrangian analysis of the Indian-Atlantic interocean exchange in a regional model. *Geophysical Research Letters*, 33(14):L14611.

Dong, S., Garzoli, S., and Baringer, M. (2011). The Role of Interocean Exchanges on Decadal Variations of the Meridional Heat Transport in the South Atlantic. *Journal of Physical Oceanography*, 41(8):1498–1511.

Dong, S., Garzoli, S., Baringer, M., Meinen, C., and Goni, G. (2009). Interannual variations in the Atlantic meridional overturning circulation and its relationship with the net northward heat transport in the South Atlantic. *Geophysical Research Letters*, 36(20):L20606.

Donohue, K. A. and Toole, J. M. (2003). A near-synoptic survey of the Southwest Indian Ocean. *Deep Sea Research Part II: Topical Studies in Oceanography*, 50(12-13):1893–1931.

Ducet, N., Le Traon, P. Y., and Reverdin, G. (2000). Global high-resolution mapping of ocean circulation from TOPEX/Poseidon and ERS-1 and -2. *Journal of Geophysical Research*, 105(C8):19477.

Durgadoo, J. V., Loveday, B. R., Reason, C. J. C., Penven, P., and Biastoch, A. (2013). Agulhas Leakage Predominantly Responds to the Southern Hemisphere Westerlies. *Journal of Physical Oceanography*, 43(10):2113–2131.

Fine, R. (1993). Circulation Antarctic intermediate water in the South Indian Ocean. *Deep Sea Research I: Oceanographic Research Papers*, 40:2021–2042.

Friocourt, Y., Drifthout, S., Blanke, B., and Speich, S. (2005). Water Mass Export from Drake Passage to the Atlantic, Indian, and Pacific Oceans : A Lagrangian Model Analysis. *Journal of Physical Oceanography*, 35:1206–1222.

Garzoli, S., Speich, S., Piola, A., and Campos, E. (2010). South Atlantic Meridional Overturning Circulation (SAMOC) - Third Workshop. *CLIVAR Exchanges*, (54).

Garzoli, S. L., Baringer, M. O., Dong, S., Perez, R. C., and Yao, Q. (2013). South Atlantic meridional fluxes. *Deep Sea Research Part I: Oceanographic Research Papers*, 71:21–32.

Garzoli, S. L. and Goni, G. J. (2000). Combining altimeter observations and oceanographie data for ocean circulation and climate studies. In *Satellites, oceanograghy and society*, volume 63 of *Elsevier Oceanography Series*, pages 79–97. Elsevier Oceanography Series.

Garzoli, S. L., Gordon, A. L., Kamenkovich, V., Pillsbury, D., and Duncombe-Rae, C. (1996). Variability and sources of the southeastern Atlantic circulation. *Journal of Marine Research*, 54:1039–1071.

Garzoli, S. L. and Matano, R. (2011). The South Atlantic and the Atlantic Meridional Overturning Circulation. *Deep Sea Research Part II: Topical Studies in Oceanography*, 58(17-18):1837–1847.

Gillett, N. P. and Thompson, D. W. J. (2003). Simulation of recent southern hemisphere climate change. *Science*, 302(5643):273–5.

Gordon, A. L. (1986). Interocean exchange of thermocline water. *Journal of Geophysical Research*, 91(C4):5037.

Gordon, A. L. (2003). The brawniest retroflection. *Nature*, 421:904–905.

Gordon, A. L., Bosley, K. T., and Aikman, F. (1995). Tropical atlantic water within the Benguela upwelling system at 27S. *Deep Sea Research Part I: Oceanographic Research Papers*, 42(1):1–12.

Gordon, A. L., Weiss, R. A. Y. F., Smethie, W. M., and Warner, M. J. (1992). Thermocline and Intermediate Water Communication Between the South Atlantic and Indian Oceans. *Journal of Geophysical Research*, 97:7223–7240.

Gregory, J. M. (2005). A model intercomparison of changes in the Atlantic thermohaline circulation in response to increasing atmospheric CO2 concentration. *Geophysical Research Letters*, 32(12):L12703.

Gründlingh, M., Carter, R., and Stanton, R. (1991). Circulation and water properties of the southwest Indian Ocean. *Progress In Oceanography*, 28:305–342.

Hall, C. and Lutjeharms, J. (2011). Cyclonic eddies identified in the Cape Basin of the South Atlantic Ocean. *Journal of Marine Systems*, 85(1-2):1–10.

Halo, I., Backeberg, B., Penven, P., Ansorge, I., Reason, C., and Ullgren, J. (2013). Eddy properties in the Mozambique Channel: A comparison between observations and two numerical ocean circulation models. *Deep Sea Research Part II: Topical Studies in Oceanography*.

Hermes, J. C. and Reason, C. (2005). Ocean Model Diagnosis of Interannual Coevolving SST Variability in the South Indian and South Atlantic Oceans. *Journal of Climate*, 18:2864–2882.

Hu, A., Meehl, G. A., Han, W., and Yin, J. (2009). Transient response of the MOC and climate to potential melting of the Greenland Ice Sheet in the 21st century. *Geophysical Research Letters*, 36(10):L10707.

Hurrell, J. W., Kushnir, Y., Ottersen, G., and Visbeck, M. (2003). An Overview of the North Atlantic Oscillation. *Geophysical Monograph*, 134:1–35.

Kanzow, T., Cunningham, S. a., Johns, W. E., Hirschi, J. J.-M., Marotzke, J., Baringer, M. O., Meinen, C. S., Chidichimo, M. P., Atkinson, C., Beal, L. M., Bryden, H. L., and Collins, J. (2010). Seasonal Variability of the Atlantic Meridional Overturning Circulation at 26.5N. *Journal of Climate*, 23(21):5678–5698.

Knorr, G. and Lohmann, G. (2003). Southern Ocean origin for the resumption of Atlantic thermohaline circulation during deglaciation. *Nature*, 424:532–536.

Krug, M. and Tournadre, J. (2012). Satellite observations of an annual cycle in the Agulhas Current. *Geophysical Research Letters*, 39:L15607.

Lagerloef, G., Kao, H., Melnichenko, O., Kacker, P., Hackert, E., Chao, Y., Hilburn, K., Meissner, T., Yueh, S., Hong, L., and Lee, T. (2013). Aquarius Salinity Validation Analysis. Technical Report February, Aqurius/SAC-D.

Large, W. G., Danabasoglu, G., Doney, S. C., and McWilliams, J. C. (1997). Sensitivity to Surface Forcing and Boundary Layer Mixing in a Global Ocean Model: Annual-Mean Climatology. *Journal of Physical Oceanography*, 27:2418–2447.

Large, W. G. and Yeager, S. G. (2008). The global climatology of an interannually varying air-sea flux data set. *Climate Dynamics*, 33(2-3):341–364.

Le Bars, D., De Ruijter, W. P. M., and Dijkstra, H. A. (2012). A New Regime of the Agulhas Current Retroflection: Turbulent Choking of Indian-Atlantic leakage. *Journal of Physical Oceanography*, 42(7):1158–1172.

Le Bars, D., Dijkstra, H. A., and De Ruijter, W. P. M. (2013). Impact of the Indonesian Throughflow on Agulhas leakage. *Ocean Science*, 9(5):773–785.

Le Bars, D., Durgadoo, J. V., Dijkstra, H. A., Biastoch, A., and De Ruijter, W. P. M. (2014). An observed 20-year time series of Agulhas leakage. *Ocean Science*, 10(4):601–609.

Lee, T., Lagerloef, G., Gierach, M. M., Kao, H.-Y., Yueh, S., and Dohan, K. (2012). Aquarius reveals salinity structure of tropical instability waves. *Geophysical Research Letters*, 39(12):n/a–n/a.

Locarnini, R., Mishonov, A., Antonov, J., Boyer, T., Garcia, H., and Levitus, S. (2006). World Ocean Atlas 2005 Volume 1: Temperature. In *NOAA Atlas NESDIS*, page 182.

Locarnini, R. A., Mishonov, A. V., Antonov, J. I., Boyer, T. P., Garcia, H. E., Baranova, O. K., Zweng, M. M., and Johnson, D. R. (2010). Volume 1: Temperature. In Levitus, S., editor, *World Ocean Atlas 2009*, volume 1, page 184. NOAA Atlas NESDIS 69, U.S. Government Printing Office, Washington,D.C.

Loveday, B. (2014). *Modelling wind-driven inter-ocean exchange in the greater Agulhas with the Regional Ocean Modelling System*. PhD thesis, University of Cape Town.

Loveday, B. R., Durgadoo, J. V., Reason, C. J. C., Biastoch, A., and Penven, P. (2014). Decoupling of the Agulhas Leakage from the Agulhas Current. *Journal of Physical Oceanography*, 44(7):1776–1797.

Lozier, M. S. (2010). Deconstructing the conveyor belt. *Science*, 328(5985):1507–11.

Lumpkin, R. and Speer, K. (2003). Large-Scale Vertical and Horizontal Circulation in the North Atlantic Ocean. *Journal of Physical Oceanography*, 33:1902–1920.

Lumpkin, R. and Speer, K. (2007). Global Ocean Meridional Overturning. *Journal of Physical Oceanography*, 37(2003):2550–2562.

Lutjeharms, J. (1996). The exchange of water between the South Indian and the South Atlantic. In Wefer, G., Berger, W., Siedler, G., and Webb, D., editors, *The South Atlantic: Present and Past Circulation*, pages 125–162. Springer, Berlin.

Lutjeharms, J. and Ansorge, I. (2001). The Agulhas Return Current. *Journal of Marine Systems*, 30(1-2):115–138.

Lutjeharms, J. and Cooper, J. (1996). Interbasin leakage through Agulhas current filaments. *Deep Sea Research Part I: Oceanographic Research Papers*, 43(2):213–238.

Lutjeharms, J. R. E. (2006). The Agulhas Current. *African Journal of Marine Science*, 28(3-4):729–732.

Lutjeharms, L. R. E. and Van Ballegooyen, R. (1988). The Retroflection of the Agulhas Current. *Journal of Physical Oceanography*, 18:1570–1583.

Macdonald, A. and Wunsch, C. (1996). An estimate of global ocean circulation and heat fluxes. *Nature*, 382:436–439.

Maltrud, M. E., Smith, R. D., Semtner, A. J., and Malone, R. C. (1998). Global eddy-resolving ocean simulations driven by 1985-1995 atmospheric winds. *Journal of Geophysical Research*, 103:30,825–30,853.

Marshall, G. J. (2003). Trends in the Southern Annular Mode from Observations and Reanalyses. *Journal of Climate*, 16:4134–4143.

Martínez-Méndez, G., Zahn, R., Hall, I. R., Peeters, F. J. C., Pena, L. D., Cacho, I., and Negre, C. (2010). Contrasting multiproxy reconstructions of surface ocean hydrography in the Agulhas Corridor and implications for the Agulhas Leakage during the last 345,000 years. *Paleoceanography*, 25(4):PA4227.

Matano, R. and Beier, E. (2003). A kinematic analysis of the Indian/Atlantic interocean exchange. *Deep Sea Research Part II: Topical Studies in Oceanography*, 50(1):229–249.

McCarthy, G., Frajka-Williams, E., Johns, W. E., Baringer, M. O., Meinen, C. S., Bryden, H. L., Rayner, D., Duchez, A., Roberts, C., and Cunningham, S. A. (2012). Observed interannual variability of the Atlantic meridional overturning circulation at 26.5N. *Geophysical Research Letters*, 39(19):n/a–n/a.

Meinen, C. S., Speich, S., Perez, R. C., Dong, S., Piola, A. R., Garzoli, S. L., Baringer, M. O., Gladyshev, S., and Campos, E. J. D. (2013). Temporal variability of the meridional overturning circulation at 34.5Â°S: Results from two pilot boundary arrays in the South Atlantic. *Journal of Geophysical Research: Oceans*, 118(12):6461–6478.

Miranda, A. P., Barnier, B., and Dewar, W. K. (1999). On the dynamics of the Zapiola Anticyclone. *Journal of Geophysical Research*, 104(C9):21137.

Morioka, Y., Tozuka, T., Masson, S., Terray, P., Luo, J.-J., and Yamagata, T. (2012). Subtropical Dipole Modes Simulated in a Coupled General Circulation Model. *Journal of Climate*, 25(12):4029–4047.

Munk, W. (1950). On the wind-driven ocean circulation. *Journal of Meteorology*, 7:79–93.

Nof, D. and Pichevin, T. (1996). The Retroflection Paradox. *Journal of Physical Oceanography*, 26:2344–2358.

Okubo, A. (1970). Horizontal dispersion of floatable particles in the vicinity of velocity singularities such as convergences. *Deep Sea Research*, 17:445–454.

Olson, D., Podesta, G., Evans, R., and Brown, O. (1988). Temporal variations in the separation of Brazil and Malvinas Currents. *Deep Sea Research I: Oceanographic Research Papers*, 35:1971–1990.

Ou, H. W. and de Ruijter, W. P. (1986). Separation of an Inertial Boundary Current from a Curved Coastline. *Journal of Physical Oceanography*, 16:280–289.

Pascual, A., Faugère, Y., Larnicol, G., and Le Traon, P.-Y. (2006). Improved description of the ocean mesoscale variability by combining four satellite altimeters. *Geophysical Research Letters*, 33(2):L02611.

Peeters, F. J. C., Acheson, R., Brummer, G.-J. A., De Ruijter, W. P. M., Schneider, R. R., Ganssen, G. M., Ufkes, E., and Kroon, D. (2004). Vigorous exchange between the Indian and Atlantic oceans at the end of the past five glacial periods. *Nature*, 430(7000):661–5.

Penven, P., Echevin, V., Pasapera, J., Colas, F., and Tam, J. (2005). Average circulation, seasonal cycle, and mesoscale dynamics of the Peru Current System: A modeling approach. *Journal of Geophysical Research*, 110(C10):C10021.

Penven, P., Herbette, S., and Rouault, M. (2011). Ocean Modelling in the Agulhas Current System. In *Proceedings of the Joint Nansen-Tutu Scientific Opening Symposium and OceansAfrica Meeting*, pages 17–19.

Peterson, R. and Stramma, L. (1991). Upper-level circulation in the South Atlantic Ocean. *Progress In Oceanography*, 26:1–73.

Philander, S. G. H. (1985). El Nino and La Nina. *Journal of the Atmospheric Sciences*, 42:2652–2662.

Pichevin, T., Nof, D., and Lutjeharms, J. (1999). Why Are There Agulhas Rings? *Journal of Physical Oceanography*, 29:693–707.

Reason, C. J. C. (2000). Multidecadal climate variability in the subtropics / mid-latitudes of the Southern Hemisphere oceans. *Tellus*, 52:203–223.

Renault, A., Provost, C., Sennéchael, N., Barré, N., and Kartavtseff, A. (2011). Two full-depth velocity sections in the Drake Passage in 2006-Transport estimates. *Deep Sea Research Part II: Topical Studies in Oceanography*, 58(25-26):2572–2591.

Rhein, M., Rintoul, S., Aoki, S., Campoe, E., Chambers, D., Feely, R., S., G., Johnson, G., Josey, S., Kostianoy, A., Mauritzen, C., Roemmich, D., Talley, L., and Wang, F. (2013). Observations: Ocean. In Stocker, T., Qin, D., Plattner, G.-K., Tignor, M., Allen, S., Boschung, J., Nauels, A., Xia, Y., Bex, V., and Midgley, P., editors, *Climate Change 2013: The Physical Science Basis. Contribution of Working Group I to the Fifth Assessment Report of the Intergovernmental Panel on Climate Change*. Cambridge University Press, Cambridge, United Kingdom and New York, NY, USA.

Ribbe, J. and Tomczak, M. (1997). Effect of the Missing Indonesian Throughflow in the Fine Resolution Antarctic Model. *Journal of Physical Oceanography*, 27:445–455.

Richardson, P. and Garzoli, S. (2003). Characteristics of intermediate water flow in the Benguela current as measured with RAFOS floats. *Deep Sea Research Part II: Topical Studies in Oceanography*, 50(1):87–118.

Richardson, P., Lutjeharms, J., and Boebel, O. (2003). Introduction to the "Inter-ocean exchange around southern Africa". *Deep Sea Research Part II: Topical Studies in Oceanography*, 50(1):1–12.

Richardson, P. L. (2007). Agulhas leakage into the Atlantic estimated with subsurface floats and surface drifters. *Deep Sea Research Part I: Oceanographic Research Papers*, 54(8):1361–1389.

Ridgway, K., Dunn, J., and Wilkin, J. (2002). Ocean Interpolation by Four-Dimensional Weighted Least Squares - Application to the Waters around Australasia. *Journal of Atmospheric and Oceanic Technology*, 19:1357–1376.

Ridgway, K. R. and Dunn, J. R. (2007). Observational evidence for a Southern Hemisphere oceanic supergyre. *Geophysical Research Letters*, 34(13):n/a–n/a.

Rintoul, S., Balmeseda, M., Cunningham, S., Dushaw, B., Garzoli, S., Gordon, A., Heimbach, P., Hood, M., Johnson, G., Latif, M., Send, U., Shum, C., Speich, S., and D. Stammer (2010). Deep circulation and meridional overturning: recent progress and a strategy for sustained observations. In Hall., J., Harrison, D., and Stammer, D., editors, *Proceedings of OceanObs'09: Sustained Ocean Observation and Information for Society*, number 1, Italy. ESA Publications WPP-306.

Rintoul, S. R. (1991). South Atlantic interbasin exchange. *Journal of Geophysical Research*, 96(C2):2675.

Rio, M. H., Guinehut, S., and Larnicol, G. (2011). New CNES-CLS09 global mean dynamic topography computed from the combination of GRACE data, altimetry, and in situ measurements. *Journal of Geophysical Research*, 116(C7):C07018.

Rouault, M., Penven, P., and Pohl, B. (2009). Warming in the Agulhas Current system since the 1980's. *Geophysical Research Letters*, 36(12):L12602.

Rühs, S., Durgadoo, J. V., Behrens, E., and Biastoch, A. (2013). Advective timescales and pathways of Agulhas leakage. *Geophysical Research Letters*, 40(15):3997–4000.

Saekno, O., Weaver, A., and Gregory, J. (2003). On the Link between the Two Modes of the Ocean Thermohaline Circulation and the Formation of Global-Scale Water Masses. *Journal of Climate*, 16:2797–2801.

Saha, S., Moorthi, S., Pan, H.-L., Wu, X., Wang, J., Nadiga, S., Tripp, P., Kistler, R., Woollen, J., Behringer, D., Liu, H., Stokes, D., Grumbine, R., Gayno, G., Wang, J., Hou, Y.-T., Chuang, H.-Y., Juang, H.-M. H., Sela, J., Iredell, M., Treadon, R., Kleist, D., Van Delst, P., Keyser, D., Derber, J., Ek, M., Meng, J., Wei, H., Yang, R., Lord, S., Van Den Dool, H., Kumar, A., Wang, W., Long, C., Chelliah, M., Xue, Y., Huang, B., Schemm, J.-K., Ebisuzaki, W., Lin, R., Xie, P., Chen, M., Zhou, S., Higgins, W., Zou, C.-Z., Liu, Q., Chen, Y., Han, Y., Cucurull, L., Reynolds, R. W., Rutledge, G., and Goldberg, M. (2010). The NCEP Climate Forecast System Reanalysis. *Bulletin of the American Meteorological Society*, 91(8):1015–1057.

Saunders, P. M. and King, B. A. (1995). Oceanic Fluxes on the WOCE A11 Section*. *Journal of Physical Oceanography*, pages 1942–1957.

Schiermeier, Q. (2013). Oceans under surveillance. *Nature*, 497(7448):167–8.

Schmid, C., Boebel, O., Zenk, W., Lutjeharms, J., Garzoli, S., Richardson, P., and Barron, C. (2003). Early evolution of an Agulhas Ring. *Deep Sea Research Part II: Topical Studies in Oceanography*, 50(1):141–166.

Schmid, C. and Garzoli, S. L. (2009). New observations of the spreading and variability of the Antarctic Intermediate Water in the Atlantic. *Journal of Marine Research*, 67(6):815–843.

Schmitz, W. J. (1995). On the Interbasin-scale Thermohaline Circulation. *Reviews of Geophysics*, 33:151–173.

Schouten, M., Ruijter, W. P. M. D., Leeuwen, P. J. V., and Lutjeharms, J. R. E. (2000). Translation, decay and splitting of Agulhas rings in the southeastern Atlantic Ocean. *Journal of Geophysical Research*, 105:21,913–21,925.

Schouten, M. W., Ruijter, W. P. M. D., and Leeuwen, P. J. V. (2002). Upstream control of Agulhas Ring shedding. *Journal of Geophysical Research*, 107.

Siegel, A. and Weiss, J. (1997). A wavelet-packet census algorithm for calculating vortex statistics. *Physics of Fluids*, 9:1988–1999.

Sigman, D. M., Hain, M. P., and Haug, G. H. (2010). The polar ocean and glacial cycles in atmospheric CO2 concentration. *Nature*, 466(7302):47–55.

Simon, M. H., Arthur, K. L., Hall, I. R., Peeters, F. J., Loveday, B. R., Barker, S., Ziegler, M., and Zahn, R. (2013). Millennial-scale Agulhas Current variability and its implications for salt-leakage through the Indian-Atlantic Ocean Gateway. *Earth and Planetary Science Letters*, 383:101–112.

Smeed, D. A., McCarthy, G. D., Cunningham, S. A., Frajka-Williams, E., Rayner, D., Johns, W. E., Meinen, C. S., Baringer, M. O., Moat, B. I., Duchez, A., and Bryden, H. L. (2014). Observed decline of the Atlantic meridional overturning circulation 2004-2012. *Ocean Science*, 10(1):29–38.

Smith, S. R., Legler, D. M., and Verzone, K. V. (2001). Quantifying Uncertainties in NCEP Reanalyses Using High-Quality Research Vessel Observations. *Journal of Climate*, 14:4062–4073.

Souza, J. M. A. C., de Boyer Montégut, C., Cabanes, C., and Klein, P. (2011a). Estimation of the Agulhas ring impacts on meridional heat fluxes and transport using ARGO floats and satellite data. *Geophysical Research Letters*, 38(21):n/a–n/a.

Souza, J. M. A. C., Montegut, C. d. B., and Traon, P. Y. L. (2011b). Comparison between three implementations of automatic identification algorithms for the quantification and characterization of mesoscale eddies in the South Atlantic Ocean. *Ocean Science*, 7:317–334.

Speich, S., Blanke, B., and Cai, W. (2007). Atlantic meridional overturning circulation and the Southern Hemisphere supergyre. *Geophysical Research Letters*, 34(23):n/a–n/a.

Speich, S., Blanke, B., and Madec, G. (2001). Warm and cold water routes of an O.G.C.M thermohaline Conveyor Belt. *Geophysical Research Letters*, 28(2):311–314.

Speich, S., Blanke, B., Vries, P. D., Drijfhouté, S., Döös, K., Ganachaud, A., and Marsh, R. (2002). Tasman leakage: A new route in the global ocean conveyor belt. *Geophysical Research Letters*, 29(10):55–1–55–4.

Speich, S. and Dehairs, F. (2008). Cruise report MD 166 bonus-goodhope. Technical Report March, Laboratoire de Physique des Oceans.

Speich, S., Garzoli, S. L., Piola, A., Baehr, J., Baringer, M., Barreiro, M., Biastoch, A., Budillon, G., Byrne, D., Campos, E., Chereskin, T., den Tom, M., Dijstra, H., Donohue, K., Gladyshev, S., Goni, G., Gordon, A., Guerrero, R., King, B., Macrander, A., Mata, M. M., Matano, R. P., McDonagh, E., Meinen, C., Meredith, M., Nof, D., Ollitrault, M., Owens, B., Reynaud, T., Rupolo, V., Shuckburgh, E., Sokov, A., Troisi, A., Watts, R., Wimbush, M., and Zahn, R. (2010). A monitoring system for the South Atlantic as a component of the MOC. In Hall., J., Harrison, D., and Stammer, D., editors, *Proceedings of OceanObs'09: Sustained Ocean Observation and Information for Society*, number 1, Venice, Italy. ESA Publications WPP-306.

Speich, S., Lutjeharms, J. R. E., Penven, P., and Blanke, B. (2006). Role of bathymetry in Agulhas Current configuration and behaviour. *Geophysical Research Letters*, 33(23):L23611.

Sprintall, J., Wijffels, S. E., Molcard, R., and Jaya, I. (2009). Direct estimates of the Indonesian Throughflow entering the Indian Ocean: 2004-2006. *Journal of Geophysical Research*, 114(C7):C07001.

Stammer, D. (2008). Response of the global ocean to Greenland and Antarctic ice melting. *Journal of Geophysical Research*, 113(C6):C06022.

Stammer, D., Tokmakian, R., Semtner, A., and Wunsch, C. (1996). How well does a 1/4 global circulation model simulate large-scale oceanic observations? *Journal of Geophysical Research*, 101:25,779–25,811.

Sterl, A. and Hazeleger, W. (2003). Coupled variability and air-sea interaction in the South Atlantic Ocean. *Climate Dynamics*, 21(7-8):559–571.

Stramma, L. (1989). The Brazil current transport south of 23S. *Deep Sea Research I: Oceanographic Research Papers*, 36:639–646.

Stramma, L. and England, M. (1999). On the water masses and mean circulation of the South Atlantic Ocean. *Journal of geophysical Research*, 104:20,863–20,883.

Swart, N. C. and Fyfe, J. C. (2012). Observed and simulated changes in the Southern Hemisphere surface westerly wind-stress. *Geophysical Research Letters*, 39(16):L16711.

Swart, S., Speich, S., Ansorge, I. J., Goni, G. J., Gladyshev, S., and Lutjeharms, J. R. E. (2008). Transport and variability of the Antarctic Circumpolar Current south of Africa. *Journal of Geophysical Research*, 113:C09014.

Talley, L. D. (2003). Shallow, Intermediate, and Deep Overturning Components of the Global Heat Budget. *Journal of Physical Oceanography*, 33:530–560.

Thompson, D. W. J. and Solomon, S. (2002). Interpretation of recent Southern Hemisphere climate change. *Science*, 296(5569):895–9.

Thompson, D. W. J. and Wallace, J. M. (2000). Annular Modes in the Extratropical Circulation . Part I : Month-to-Month Variability *. *Journal of Climate*, 13:1000–1016.

Thompson, D. W. J., Wallace, J. M., and Hegerl, G. C. (2000). Annular Modes in the Extratropical Circulation. Part II : Trends *. *Journal of Climate*, 13(689):1018–1036.

Toggweiler, J. R. (2009). Shifting Westerlies. *Science*, 323:1434–1435.

van Aken, H., Lutjeharms, J., Rouault, M., Whittle, C., and de Ruijter, W. (2013). Observations of an early Agulhas current retroflection event in 2001: A temporary cessation of inter-ocean exchange south of Africa? *Deep Sea Research Part I: Oceanographic Research Papers*, 72:1–8.

van Sebille, E., Beal, L. M., and Johns, W. E. (2011). Advective Time Scales of Agulhas Leakage to the North Atlantic in Surface Drifter Observations and the 3D OFES Model. *Journal of Physical Oceanography*, 41:1026–1034.

van Sebille, E., Biastoch, a., van Leeuwen, P. J., and de Ruijter, W. P. M. (2009). A weaker Agulhas Current leads to more Agulhas leakage. *Geophysical Research Letters*, 36(3):L03601.

van Sebille, E., Sprintall, J., Schwarzkopf, F., Sen Gupta, A., Santoso, A., England, M., Biastoch, A., and Boning, C. (2014). Pacific-to-Indian Ocean connectivity: Tasman leakage, Indonesian Throughflow, and the role of ENSO. *Journal of Geophysical Research*, 119:1365–1382.

van Sebille, E., van Leeuwen, P. J., Biastoch, A., and de Ruijter, W. P. (2010). Flux comparison of Eulerian and Lagrangian estimates of Agulhas leakage: A case study using a numerical model. *Deep Sea Research Part I: Oceanographic Research Papers*, 57(3):319–327.

Venegas, S. A., Mysak, L. A., and Straub, D. N. (1997). Atmosphere-Ocean Coupled Variability in the South Atlantic. *Journal of Climate*, 10:2904–2920.

Vivier, F. and Provost, C. (1999). Direct velocity measurements in the Malvinas Current. *Journal of Geophysical Research*, 104(C9):21083.

Weijer, W., de Ruijter, P. M., Dijkstra, A., and Jan Van Leeuwen, P. (1999). Impact of Interbasin Exchange on the Atlantic Overturning Circulation. *Journal of Phyysical Oceanography*, 29:2266–2284.

Weijer, W., Ruijter, W. P. M. D., Sterl, A., and Drijfhout, S. S. (2002). Response of the Atlantic overturning circulation to South Atlantic sources of buoyancy. *Global and Plantetary Change*, 34:293–311.

Weiss, J. (1991). The dynamics of enstophy transfer in two-dimensional hydrodynamics. *Physica D*, 48:273–294.

Whitworth, T. and Nowlin, W. D. (1987). Water masses and currents of the Southern Ocean at the Greenwich Meridian. *Journal of Geophysical Research*, 92(7):6462–6476.

Wunsch, C. (2002). What is the Thermohaline Circulation. *Science*, 298:64–65.

You, Y. (1997). Seasonal variations of thermocline circulation and ventilation in the Indian Ocean. *Journal of Geophysical Research*, 102(C5):10391.

Zahn, R. (2009). Beyond the CO2 connection. *Nature Climate Change*, 24(2):335–336.